Complex equilibria in strongly alkaline aqueous solutions containing Ca(II), Nd(III) and gluconate ions

Ph.D. Dissertation

Éva Böszörményi

Supervisor: Prof. Pál Sipos

Consultants: Dr. Bence Kutus

Dr. Gábor Peintler

Doctoral School of Chemistry

Department of Inorganic, Organic and Analytical Chemistry

Faculty of Science and Informatics

University of Szeged

Szeged

2023

Table of contents

1. Introduction

Sugar acids are formed in biological processes through the oxidation of D-glucose and are found in large quantities in our environment. Apart from their important role in nature, they are essential to various industrial processes. One example for this is gluconic acid, which has many applications in food[1], pharmaceutical[2,3], textile[4] and building industries[5–9]. To supply this industrial demand, up to 100,000 tons of gluconic acid are produced per annum, mainly through biotechnological processes[10] (although chemical methods are also available[11,12]).

The main use of gluconate roots in its complexing ability; it prevents drinks from clouding by binding Ca(II) and Fe(II) in drinks, and also inhibits the precipitation of calcium salts in dairy products. It is often used as a delivering agent in clinical practice; Ca(II) and Fe(II) gluconate are applied as mineral supplements[2,3,9]. Sodium gluconate is also utilized in large quantities as an additive in the construction industry[5–9,13]. It is added to cement to improve certain properties, i.e. setting time[5] and mechanical strength[13]. Being a cement additive, gluconate has potential environmental impact, too, concerning low- and intermediate-level (LL/IL) radioactive waste repositories. Here, the containers are filled with cement to prevent leakage; and the mobility of actinides can be enhanced in an alkaline pore water due to the complexation of metal ions by gluconate [14,15]. The possibility of these complexing processes in LL/IL waste deposits have been excessively studied in the past decades.

Recent publications show that gluconate is not only an efficient complexing agent for divalent alkaline earth (Ca(II)[16,17], Mg(II)[17]) and transition (Cu(II)[18], Co(II)[19], Ni(II)[19], Mn(II)[20], Zn(II)[20]) metal ions, but it is also capable of enhancing the solubility of tri-, and tetravalent actinides and lanthanides in alkaline media[21,22]. Anoxic conditions are typical in radioactive waste repositories[23] ensuring that reduced oxidation states of actinides prevail under these conditions (Cm(III), Am(III), Pu(III) and Pu(IV))[24]. Organic ligands, produced by the decomposition of contaminated cellulosic materials (e.g. isosaccharinate[25], Isa^-) or dissolving from concrete (e.g. gluconate[5–8] ($Gluc^-$) are also present in these repositories.

To reveal their capability to increase the solubility of actinide ions is essential [21], since the calculation of the maximum degree of mobilization of these metal ions is crucial for the associated risk assessment of disposal[24]. As for the purposes of thermodynamic modeling, tri- and tetravalent actinides can be replaced by less elaborate lanthanide ions[26] due to the pronounced chemical analogies between f-block metal ions of the same oxidation state[27].

To obtain a relevant model of possible complexation processes in radioactive waste repositories, neodymium (Nd(III)) and $Gluc^-$ have been employed previously as model ions in measurements carried out in aqueous solutions[28,29] but data acquired in alkaline equilibria is scarce[30,31].

2. Literature review

2.1. Characteristics of gluconic acid in aqueous media

Gluconic acid is a weak polyhydroxy carboxylic acid which belongs to the group of aldonic acids. It is produced from β–D-glucose by the oxidation of the C1 formyl to a carboxyl group[9] (depicted in Figure 1).

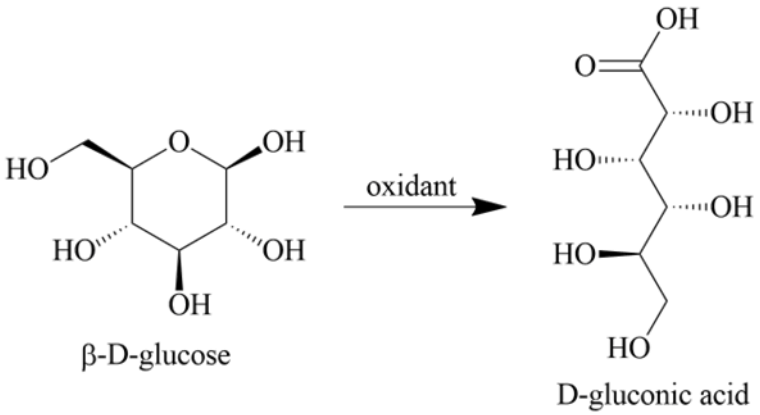

Figure 1. Oxidation of β–D-glucose to D-gluconic acid

As for industrial scale production, biotechnological methods prevail because of their selectivity and efficiency. For the industry, the use of chemical oxidation methods is hindered by high costs and deactivation of the catalysts. Fermentation methods are promising because the application of selective membranes can help achieve the cost-effective and eco-friendly production of high-purity gluconic acid[32].

2.1.1. Lactonization of gluconic acid

Due to their structure, sugar acids can undergo lactonization in acidic aqueous solutions. Lactones are cyclic esters of hydroxy carboxylic acids, containing a 1-oxacycloalkan-2-one structure, or analogs having unsaturation or heteroatoms replacing one or more carbon atoms of the ring[33]. The smallest compounds of the class are α–, β–, γ–, δ–lactones which contain 3-, 4-, 5-, and 6-membered rings[34], respectively. In nature, the most abundant of them are γ–, and δ–rings because of the high stability due to the reduced angular strain[35]. Lactonization

is an acid-catalyzed process, during which the sugar acid molecule forms an intramolecular ester, accompanied by the loss of a water molecule.

Depending on which hydroxyl group is involved in the formation of the ester bond, different constitutional isomers (i.e. γ, δ) can be formed. Due to their different ring stabilities, lactones also differ in their stability and the associated equilibrium constant describing their formation[36]. As for gluconic acid (HGluc), the more stable isomer is D-glucono-1,5-lactone (δ–lactone, Figure 2) forming readily at pH = 5 and reaching equilibrium almost one hundred times faster than D-glucono-1,4-lactone (γ–lactone, Figure 2)[37], which is observed in larger amounts only at pH < 2 [36].

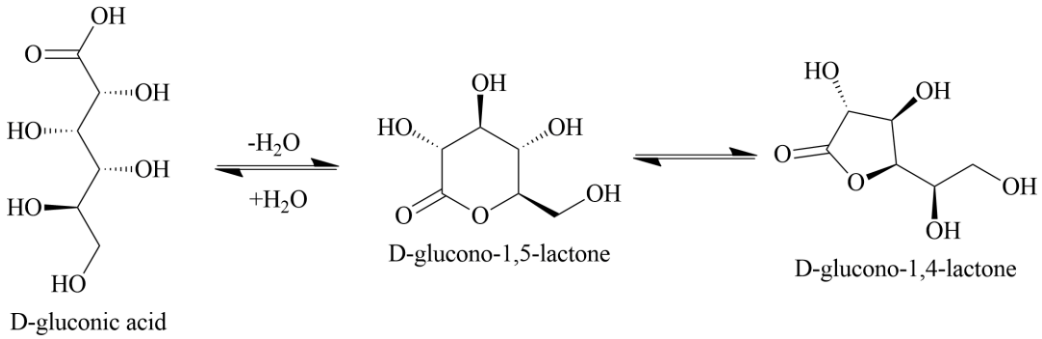

Figure 2. δ– and γ–lactones of D-gluconic acid

Jermyn suggested in his publication[38] that the γ–lactone is generated only from the δ–lactone and not from the acidic form. This corroborates the results of Takahashi et al. who also suggested that direct interconversion between δ– and γ–lactone takes place reversibly and spontaneously, but γ–lactone cannot be directly hydrolyzed. They also reported that lactonization cannot be detected in the studied pH range of 6.0–8.6, therefore lactonization can be disregarded in solutions with pH higher than 6[39].

2.1.2. Deprotonation of gluconic acid

Compared to sorbitol, which has a pK_a of 13.6[40], D-gluconic acid is a much stronger acid which can be ascribed to the more acidic OH function of the carboxylate group in HGluc. Due to the presence of adjacent OH groups with negative inductive effect, HGluc is a stronger acid than hexanoic acid (pK_a = 4.88[41]). (Structure of above mentioned ligands are shown in Figure 3.)

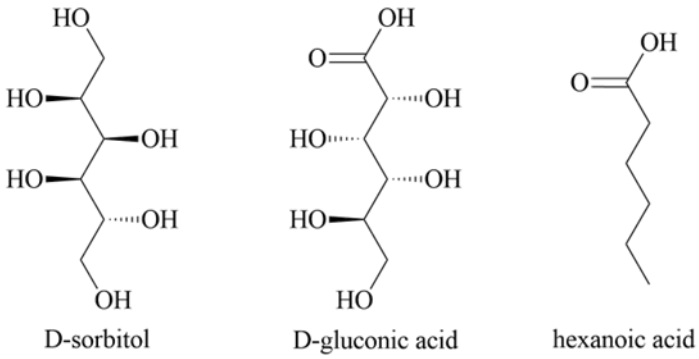

Figure 3. Structure of D-sorbitol, D-gluconic and hexanoic acid

The corresponding deprotonation constant of HGluc is written as:

$$HGluc + H_2O = Gluc^- + H_3O^+ \quad (1)$$

$$K_{a1} = \frac{1}{K_{p2}} = \frac{[Gluc^-] \cdot [H_3O^+]}{[HGluc] \cdot c^{\ominus}} \quad (2)$$

where K_{a1} is the acid dissociation constant of HGluc and K_{p2} is the protonation constant of $Gluc^-$ and $c^{\ominus}$ means the standard molar concentration, 1 mol·dm^{-3}. Note that the activity of water, a_w (equals unity at infinite dilution), is already included in K_{a1}.

The protonation constant of $Gluc^-$ have been determined by several independent research groups and different methods. According to Eq. 2, the pK_{a1} of HGluc is equal to the lg K_{p2} of $Gluc^-$ and in some cases only the K_{a1} or K_{p2} was given in the article; to compare the data, the values have been converted to pK_{a1} and are shown in Table 1. Depending on the ionic strength (I) and the method of measurement, the value of pK_a falls between 3.2–3.9.

Zubiaur et al. published their results in 1998, reporting that the protonation constant of $Gluc^-$ depends on the ionic strength, and has a minimum value at around I = 0.5 M $NaClO_4$ (albeit that may be different for another background electrolyte)[42]. Their results are in good agreement with the published data of Bretti et al., who determined the pK_a at various ionic strengths and temperatures and reported a pK_a value of 3.763 at 4.4 M ionic strength (NaCl)[43]. At pH > 6 only the deprotonated $Gluc^-$ is present in solution, and at pH = 11 hydroxyl groups start to deprotonate, and the $Gluc^{2-}$ form dominates acid-base equilibria over pH = 13[36].

Table 1. Deprotonation constants, pK_{a1}, of HGluc in aqueous media, at different ionic strengths and temperatures, determined by various methods. Abbreviations mean the following: POL: polarimetry, POT: potentiometry, NMR: nuclear magnetic resonance, CAL: calorimetry

Ionic strength and background electrolyte	pK_a	Method	Temperature (°C)	Year of publication
I → 0	3.85[37]	POL/POT	25±0.20	1970
I → 0	3.77[44]	POL/POT	25±0.04	1973
I → 0	3.92[42]	POT	25±0.10	1998
0.1 M $NaClO_4$	3.70[42]			
0.5 M $NaClO_4$	3.60[42]			
1 M $NaClO_4$	3.63[42]			
3 M $NaClO_4$	3.84[42]			
0.1 M $NaNO_3$	3.40[45]	POT	20±0.10	1992
0.1 M NaCl	3.46[46]	POT	25	1994
0.1 M $NaClO_4$	3.50[18]	POT	25	1998
0.1 M $NaClO_4$	3.472[47]	POT	25±0.10	2000
0.1 M $NaClO_4$	3.30[36]	^{13}C NMR/POT	22±1	2007
0.15 M $NaClO_4$	3.572[20]	POT	37	1977
0.2 M KCl	3.36[48]	POT	25±0.10	2008
1 M NaCl	3.23[49]	^{1}H NMR/POT	25±1	2010
1 M NaCl	3.24[49]	^{13}C NMR/POT	25±1	2010
1 M $NaClO_4$	3.48[50]	POT	25±0.05	1978
1 M $NaClO_4$	3.30[51]	POT	25	2006
I → 0	3.709[43]	POT/CAL	25	2016
1.031 M NaCl	3.428[43]			
1.021 M $NaNO_3$	3.363[43]			
4.436 M NaCl	3.763[43]			

Zhang et al. observed that chemical shifts on the ^{13}C NMR spectra of $Gluc^-$ show a tendency similar to an inflection point at pH = 13. They speculated that this could occur because a second deprotonation takes place and $Gluc^{2-}$ forms by deprotonation of an alcoholic hydroxyl group. Because of limited number of data points they determined the

constant with high uncertainty and estimated a value of $pK_a = -13 \pm 1$ for the following reaction[36]:

$$Gluc^{2-} + H_3O^+ = Gluc^- + H_2O \quad (3)$$

$$K_{a2} = \frac{1}{K_{p1}} = \frac{[Gluc^{2-}] \cdot [H_3O^+]}{[Gluc^-] \cdot c^{\ominus}} \quad (4)$$

Later, this theory was supported by Pallagi et al., who carried out accurate measurements in alkaline media and calculated the value of $pK_{a2} = -13.68$ (I = 1 M)[52]. Buckó et al. determined the pK_{a2} value to be –14.08 (by potentiometry) and –13.90 (by NMR spectroscopy) at I = 4 M[53].

2.2. Complexing properties of gluconate

Carbohydrates are able to form relatively weak complexes with metal cations since the coordination occurs through alcoholic hydroxyl functions. However, when an anchoring group, such as carboxylate, is introduced, it is able to promote the coordination and induce deprotonation of the alcoholic hydroxyl functions of the ligand, thereby enhancing its complexing ability significantly[54]. In a strongly alkaline medium, the deprotonation of hydroxyl functions can further improve the ligand's efficacy in coordination. In turn, the metal ion also facilitates proton displacement from the O-bearing donor group, which is known as metal ion promoted deprotonation, and was studied in detail by van Duin and coworkers[55]. They proposed that as pH increases, a proton dissociates from the carboxylate group of the sugar acids and the second deprotonation takes place at the α–OH group in every case. A third proton could be displaced from the remaining hydroxyl functions upon further increasing the pH, yielding complexes forming mostly by the coordination of an alcoholate and a hydroxyl function. The stability of the complexes strongly depends on the conformation of ligands, especially in the case of sugars[55]. While Ca(II) is sequestered through the carboxylate and the α–hydroxyl function and is able to promote the deprotonation of the latter only at pH = 10–11, they predicted that for La(III) this reaction would take place at a pH as low as 6, which was experimentally supported by them later. Moreover, they proposed that cations with a higher charge density and a larger polarization ability, such as lanthanides, would be bound by even two deprotonated hydroxyl functions at high enough pH [55].

In a review article published by Sawyer in 1964, the stability constants of alkaline earth metal (Mg(II), Ca(II), Sr(II), and Ba(II)) and Zn(II)–$Gluc^-$ complexes were analyzed. It was suggested that $Gluc^-$ coordinates only through its carboxylate group and the stoichiometry of the complexes were assumed to be 1:1. In more alkaline aqueous solutions, in which an alcoholic hydroxyl function can undergo deprotonation, chelate rings and more stable complexes of $Gluc^{2-}$ are possible to be formed. For the three studied trivalent metal ions, i.e. Fe(III), Al(III) and Cr(III), it was suggested that beyond the carboxylate group, the ligand coordinates through the oxygen atoms of the α–, β–, γ–, and δ–hydroxyl functions. For Ca(II) and Fe(III) ions, the formation of complexes with a metal to ligand ratio of 2:1 was suggested[56].

Escandar et al. studied the $Gluc^-$ complexes of several transition metals. In 1992 they published their results on studying the systems Cu(II)-D-gluconic, -D-galactonic and -D-ribonic acids, and proved the similar behaviour of these aldonic acids when complexing Cu(II)[45]. Regarding the Cu(II)–$Gluc^-$ system, they carried out potentiometric titration in the pH range of 4.5–10.5, and reported the formation of $CuGluc^+$, $Cu_2Gluc_2H_{-3}^-$ and $CuGlucH_{-2}^-$ complexes in solutions with a metal to ligand ratio of 1:1, and $CuGluc_2^0$, $CuGluc_2H_{-1}^-$, $CuGluc_2H_{-2}^{2-}$ and $CuGlucH_{-3}^{2-}$ when the ratio was 1:2. Based on their potentiometric results, the $Cu_2Gluc_2H_{-3}^-$ complex is formed over a wide range of pH = 5.0–10.0 but as pH increases, the deprotonated form of a 1:1 complex, $CuGlucH_{-2}^-$ becomes predominant; even at twofold ligand excess, $CuGlucH_{-3}^{2-}$ is present in significant concentrations at pH > 10.0[45].

In more alkaline systems, Pecsok and Juvet reported the formation of $Cu_2Gluc_2H_{-3}^-$, $Cu_2Gluc_2H_{-4}^{2-}$ and $Cu_2Gluc_2H_{-5}^{3-}$ [57]. While they assumed that the binary Cu(II)–$Gluc^-$ complexes form through oxygen bridging, Escandar et al. proposed two other possible structure for binary complexes (displayed in Figure 4). They also highlighted that based on the dissociation constant, which is lg K = 3.02 for $CuGluc^+$, i.e. one unit higher than lg K of 1.83 of Cu(II)-acetate complexes, coordination must take place via involving the α–hydroxyl group[45].

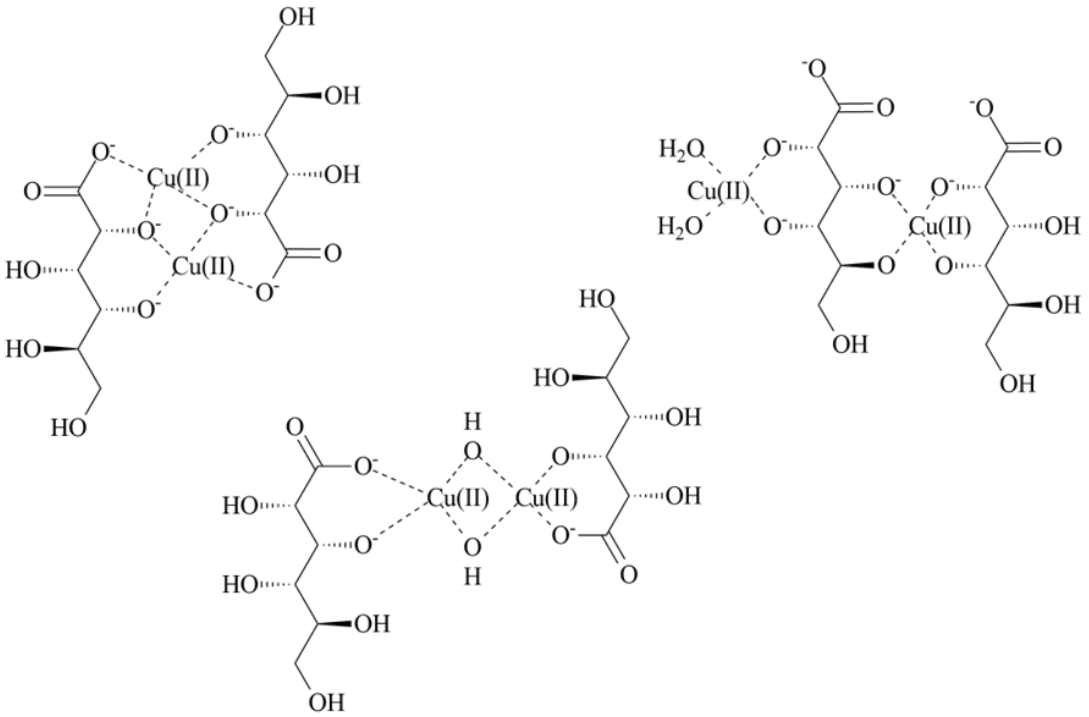

Figure 4. Suggested structures of binuclear Cu(II)–$Gluc^-$ complexes

Later, they published their results on the Co(II)–, and Ni(II)–$Gluc^-$ systems[19]. They carried out potentiometric measurements at pH = 3–11 and found that at pH = 8 and 1:1 metal to ligand ratio, a precipitate appeared. They concluded that $CoGluc^+$ is the main species in solution before the neutral $CoGlucH_{-1}^0$ complex precipitates. At sufficient excess of NaOH, this precipitate redissolves in the form of $CoGlucH_{-2}^-$. They stated that this model provides a relatively good fit of the potentiometric data at 1:1 and 1:2 metal to ligand ratios. Furthermore, precipitation did not occur at 1:3 ratio in alkaline media. Therefore, they proposed that in this regime, complexes of 1:3 metal to ligand ratio are formed. As for the associated equilibria, they suggested the binary complex $Co_2Gluc_2H_{-3}^-$ to form at pH = 8 and is present at the highest amount (28%) at pH = 10.

$$Co(II) + 3Gluc^- = CoH_{-1}Gluc_3^{2-} + H^+ \quad (5)$$

$$CoH_{-1}Gluc_3^{2-} = CoH_{-2}Gluc_3^{3-} + H^+ \quad (6)$$

$$2Co(II) + 2Gluc^- = Co_2H_{-3}Gluc_2^- \quad (7)$$

Based on potentiometric measurements, complex formation is insignificant in the 1:1 Ni(II):$Gluc^-$ system, and precipitation takes place at pH = 8. At metal to ligand molar ratio of 2, the $NiGluc_2H_{-2}^{2-}$ and the binuclear $Ni_2Gluc_2H_{-3}^-$ complexes are present. At a metal to

ligand molar ratio of 3, the $NiH_{-2}Gluc_3^{3-}$ complex was found to be formed in the higher pH range[19].

In a later work of Escandar et al. $Gluc^-$ complexes of Mn(II), Cd(II), Hg(II) and Pb(II)[58] were reported. The Mn(II)–$Gluc^-$ system could only be studied at pH < 7 owing to precipitation; the complexes in acidic media proved not to be stable enough to determine their stability constants. Cd(II) forms two simple $CdGluc^+$ and $CdGlucH_{-2}^-$ complexes which satisfactorily simulate the potentiometric titration curves up to the onset of precipitation, and the presence of hydrolytic Cd(II) species was negligible. However, the low concentration of the complexes in the soluble region causes considerable uncertainty in their stability constants. Conversely, in the Hg(II)–$Gluc^-$ system, the formation of $HgOH^+$ was considered, and with other two species $HgGlucH_{-1}^0$ and $HgGlucH_{-2}^-$ the model adequately described the measured data.

Similarly to Cu(II), Pb(II) also forms a binuclear complex in neutral-alkaline media. In acidic solutions, $PbGluc^+$ is predominant, $Pb_2Gluc_2H_{-3}^-$ forms in the highest proportion between pH 7 and 9, and interestingly, $PbGlucH_{-3}^{2-}$ is the only complex present at pH > 11[58].

Stoichiometry of the solid complexes was deduced to be $MGluc_2 \cdot 3H_2O$, where M = Mn(II), Co(II), Ni(II), Cu(II); and $MGluc_2$, where M = Cd(II), Pb(II) and HgGlucOH. Ni(II) and Co(II) form octahedral complexes, with the coordination of water molecules. For $MnGluc_2 \cdot 3H_2O$, trigonal bipyramidal symmetry was suggested with the participation of three water molecules and one coordination site of each $Gluc^-$ [58].

Upon forming Cu(II), Ni(II) and Co(II) complexes, $Gluc^-$ coordinates mainly through C1– and C2–OH functions, but a weak interaction was suggested in the case of Co(II) between metal ion and C–OH functions, based on the broadening and shifting of the NMR signal. While based on potentiometry, the stoichiometry of forming Mn(II)–$Gluc^-$ complexes could not be determined, NMR spectra of the system suggest that coordination takes place at C1, C2, C3, and C4 hydroxyls. For Cd(II) and Hg(II), a structure of „nesting" metal ions in a cavity formed with the participation of the C1, C2 and C4 hydroxyls of $Gluc^-$ is suggested. At pH = 5, the $PbGlucH_{-1}^0$ complex forms through coordination of the carboxylate and C2–OH group, but as pH increases, the NMR signals of C3 and C4 chemical variation indicate that a binary complex similar to that of Cu(II) forms. Based on their experimental data, they suggested that this cavity, formed by $Gluc^-$ coordinating through its carboxylate as well as the C2 and C4 hydroxyl functions, is responsible for the coordination of the ligand[58].

Gajda et al. published their results on the Cu(II)–$Gluc^-$ system with the intention to study how coordination is affected by the OH functions. Their findings also supported previous publications, suggesting that while at acidic and neutral pH mainly $CuGluc^+$, $CuGluc_2^0$ and $CuGluc_2H_{-1}^-$ complexes are present, at pH > 6 binuclear species $Cu_2Gluc_2H_{-3}^-$ and $Cu_2Gluc_2H_{-4}^-$ prevail, while complexes $CuGluc_2H_{-2}^{2-}$ and $CuGlucH_{-3}^{2-}$ form in smaller amount, although the latter shows a tendency to increase in concentration in strongly alkaline media[18]. They also mentioned that the formation constants of CuL^+ and CuL_2^0 complexes compared to those of the analogous acetate complexes are significantly higher in slightly acidic pH, indicating the coordination of OH groups. CD spectra suggested the involvement of C2–, C3– and C4–OH functions in the formation of binary complexes. They suggested that above pH = 8, OH groups have a cooperative effect in coordination[18].

In the Al(III)–$Gluc^-$ system, pH-potentiometric measurements were carried out between pH = 2 and 10, and the stoichiometries of forming complexes are suggested as follows: $AlGluc^{2+}$, $AlGlucH_{-1}^+$, $AlGlucH_{-2}^0$, $AlGlucH_{-3}^-$, $AlGluc_2H_{-1}^0$, and $AlGluc_2H_{-2}^-$ [48]. When Al(III) is bound by two $Gluc^-$, the plausible structure of the complex forming is likely one ligand coordinating through its carboxylate, C2–OH and C4–OH functions while the other interacts with Al(III) by the first two above-mentioned moieties. A water molecule coordinates to Al(III) in the sixth position of its octahedral coordination sphere and as it deprotonates, the $AlGluc_2H_{-2}^-$ complex forms. However, this well-defined structure only describes the complexes in the solid phase based on Molecular Force Field calculations, whereas in aqueous media, variations of metal ion binding by the C2, C3 and C4 hydroxyl functions can be assumed based on NMR observations[48]. Differences in stability constants suggest that in the 1:1 Al(III):$Gluc^-$ complex the coordination of the carboxylate group and two protonated alcoholic functions are very likely to be present. While the hydroxyl functions lose their protons upon coordination to the metal ion, further deprotonation of a coordinated water molecule happens as pH increases, resulting in the formation of the complex $AlGlucH_{-3}^-$ [48].

Szorcsik et al. performed reverse titrations in the $Me_2Sn(IV)$-D-gluconic acid 1:3 system. They found that while 1:2 $Me_2Sn(IV)$:$Gluc^-$ complexes form in acidic and neutral solution, alkaline pH is dominated by the $Me_2Sn(IV)H_{-2}Gluc^-$, which further deprotonates at pH > 10. They suggested that in parallel to the deprotonation of the carboxyl group of HGluc, metal ion induced deprotonation of a hydroxyl function can take place at pH as low as 5.5. The complex $Me_2Sn(IV)H_{-2}Gluc^-$ is predominant in the pH region of 8–10. Based on

^{13}C NMR spectra, the two most likely alkoxy groups to take part in coordination are the ones in the α– and in δ– position[59].

Based on solubility measurements, Kobayashi et al. suggested that in the Zr(IV):$Gluc^-$ system, the $Zr(OH)_4Gluc_2^{2-}$ and $Zr(OH)_4H_{-1}Gluc_2^{3-}$ are the predominant complexes in the pH range 4.0–12.5[60].

2.2.1. Hydrolysis of Ca(II) and its gluconate complexes

In acidic and neutral media, the extent of hydrolysis of Ca(II) is negligible, therefore it was often disregarded (lg K values reported for $CaOH^+$ fall between the range 1.2–1.3)[61]. Several authors published results on the solubility of $Ca(OH)_2$ in alkaline aqueous solutions with a reduced solubility at elevated temperatures[62]. Also, they found that the solubility constant shows a maximum as a function of ionic strength[63]. The stability constant of $CaOH^+$ however, increases with increasing temperature, and a study carried out with acetate suggests that organic acids can increase the solubility significantly, especially when alcoholic hydroxyls are involved[64]. Nevertheless, the low values of carbohydrate complexes' stability constants impede their exact determination[65].

The earliest publications concerning the Ca(II)–$Gluc^-$ system reported the formation of one simple $CaGluc^+$ complex in acidic (lg K = 1.21)[66] and neutral (lg K = 1.22)[67] media. Haas reported that the coordination of $Gluc^-$ is stronger compared to sugars and carboxylates with less possibly coordinating OH functions, and the formation constant for their only forming 1:1 complex at pH = 8.1 (I = 0.70 M KNO_3) is 20.4 (lg K = 1.31), still relatively high compared to other hydroxycarboxylates[68]. Van Loon et al. published that in solution, $CaGluc_2^0$ complex forms and increases the solubility of Ca(II)[69]. Pallagi et al. studied the complexes formed in the Ca(II)–$Gluc^-$ system in neutral and in alkaline media. They found that at pH = 6–11, the C2– and C3–OH moieties coordinate to Ca(II) resulting in five- and six-membered chelate rings, while their molecular modelling calculations suggested that these two hydroxyls are able to take part simultaneously in coordination[49].

Compared to a protonated OH function, a deprotonated alcoholate group is far more efficient in coordination. Pallagi et al. also investigated how this process prevails in strongly alkaline media. In addition to the $CaGluc^+$ and $CaGluc_2^0$, they proved the formation of $CaGluc(OH)^0$ and two polynuclear $Ca_2Gluc(OH)_3^0$ and $Ca_3Gluc_2(OH)_4^0$ complexes, which are present in the system above pH > 12 in a dominant proportion[52]. These results have been recently affirmed by Bouzouaid et al.[70].

Pallagi et al. identified the binding sites of $Gluc^-$ in alkaline media by multinuclear NMR measurements. Besides the carboxylate moiety, $Gluc^-$ can coordinate to Ca(II) via oxygens of the C2−OH and C3−OH groups. Ab initio calculations for the $Ca_3Gluc_2(OH)_4^0$ complex suggest that one Ca(II) is bound through coordination of oxygens of C1 and C2 carbon atoms of both $Gluc^-$ while the other two Ca(II) are sequestered by $Gluc^-$ through forming six membered chelate rings via the oxygens of the carboxylate and the C3 carbon atom. The presence of these polynuclear species is significant because they can serve as precursors for the formation of actinide-containing ternary complexes formed in radioactive waste repositories[52].

2.2.2. Hydrolysis of Nd(III)

Ionic radii show only slight changes for Nd(III), Pu(III), Am(III), and Cm(III)[14,71], ensuring comparable charge densities and resulting in similar chemical properties for the corresponding coordination compounds[72]. This enables the use of Nd(III) as a proxy of actinides, the use of which in laboratory practice is limited[73]. Its availability, safe usage, and the sensitivity of its visible spectrum to coordination explain why Nd(III) is often used as a substitute[14].

Conditions typical for LL and IL radioactive repositories (concrete backfill environments) ensure that actinide ions are mainly present as hydroxides, hydroxycarbonates and carbonates. To understand how they affect the solubility in surface and near-surface aqueous solutions and whether they exist in stable phases in this extreme environment, Diakonov et al. studied La(III) and Nd(III) speciation and proposed an adequate model for actinide and lanthanide systems based on the solubility of these species[26]. Dissolution of the solid $Nd(OH)_3$ phase can be written as:

$$Nd(OH)_3(s) + 3H^+ = Nd(III) + 3H_2O \quad (8)$$

The solubility product of $Nd(OH)_3$ is written as follows, and values published by independent research groups are shown in Table 2.

$$pK_s = -log \frac{[Nd(III)]}{[H_3O^+]^3} \quad (9)$$

where [Nd(III)] and $[H_3O^+]$ are the equilibrium concentration of the respective ions.

Table 2. Solubility products of $Nd(OH)_3$ at different ionic strengths

Temp. (°C)	I	pKs	solid phase
21.5	1	–19.4[74]	crystalline
20	I → 0	–18.58[75]	amorphous
25	I → 0	–17.61[26]	crystalline
		–14.96[76]	crystalline
	0.1	–18.94[77]	crystalline

Lanthanides and actinides do not have a well-defined coordination or hydration number, both can be as high as 8 or even 9. This results in the formation of various hydroxido complexes of Nd(III) in aqueous systems:

$$p\mathrm{Nd(III)} + q\mathrm{H_2O} = \mathrm{Nd_pH_{-q}^{(3p-q)}} + \mathrm{qH_3O^+} \quad (10)$$

The corresponding stability constants can be written as:

$$\beta_{p-r} = \frac{\left[Nd_pH_{-q}^{(3p-q)}\right] \times [H_3O^+]^q}{[Nd(III)]^p \times c^{o\,1-p+q}} \quad (11)$$

(with a_w again merged into β).

Tobias et al. published their results stating that $Nd(OH)_3$ shows a slight tendency to dissolve in concentrated base solutions but low solubility interferes with the accurate identification of the species present[77].

Kragten et al. found that the predominant species in equilibrium with the precipitate are $Nd_2(OH)_2^{4+}$ and $Nd(OH)_3$, while $Nd(OH)_2^+$ and $Nd(OH)^{2+}$ form in negligible amounts. Determined via solubility measurements (T = 22 °C at I = 1 M), $\log\beta_{2-2}$, $\log\beta_{1-3}$ $\log\beta_{1-2}$ and $\log\beta_{1-1}$ are −11.6, −24.3, −16.2, and −8.1, respectively[74], $\log\beta_{1-1}$ and $\log\beta_{2-2}$ were calculated to be –8.51 and –14.03[78] based on potentiometric titrations (T = 25 °C). In addition, Ciavatta et al. published values of $\log\beta_{2-2} = -13.73 \pm 0.03$ and $\log\beta_{1-1} = 8.96 \pm 0.15$[79] as derived from coulometric measurements.

Rabung et al. identified ternary Ca(II)−Cm(III)−OH mixed hydroxide species and proved experimentally that the interaction between Ca(II) and Cm(III)-hydroxydes is strong enough to increase the solubility of the latter at pH = 11–12 resulting in the formation of positively charged ternary hydroxide complexes[80]. Based on their extensive study of

Am(III), Cm(III) and Nd(III), they suggested the formation of the following ternary hydroxydes in the Ca(II)−Nd(III)−OH^- system: $Ca[Nd(OH)_3]^{2+}$, $Ca_2[Nd(OH)_4]^{3+}$, and $Ca_3[Nd(OH)_6]^{3+}$ [14].

2.2.3. Complexes of Ln(III) and gluconate

When studying Ln(III) complexes in a more alkaline pH range, occurrence of a precipitate at around pH = 8 is often described[31,47,81]. This precipitate is usually referred to as $Ln(OH)_3$, because of its low solubility at higher pH [76,82,83]. It is also mentioned in these publications that increasing ligand excess would shift the precipitation to higher pH[81] or the precipitate would appear after longer time periods than compared to the instantaneous formation of $Ln(OH)_3$[47]. However, the described precipitate only appears at ligand to metal ratios lower than 2:1, and the predominant species in these systems is a neutral MLH_{-2}^0 complex, which can also precipitate. However, the solid phase have not been thoroughly investigated[31,47].

Zanonato et al. found that Nd(III) forms reasonably simple stoichiometric complexes with acetate (NdL_x, where L: ligand, x = 1, 2, 3) and the stability of the complexes increases with increasing temperature[84]. Kostromina et al. extensively studied the La(III)–$Gluc^-$ system[85–87] and proposed that while in acidic and neutral media stoichiometry varies and the metal to ligand ratio can reach up to 1:6, in alkaline aqueous solutions the 1:2 ratio is favored by La(III) and similar lanthanides, like Nd(III), Sm(III) and Ce(III)[86]. Presumably, this is the effect of how increasing pH promotes the coordination of alcoholic hydroxyl groups through deprotonation of the ligand. They proposed that the two main coordination sites of $Gluc^-$ are its carboxylate and α–OH functions, but in alkaline media the γ– and δ–hydroxyl functions also take part in coordination[56]. Both Kostromina et al.[88] and Zhang et al.[29] determined the stability constant of complexes forming with relatively simple stoichiometry in acidic and neutral Nd(III)–$Gluc^-$ solutions; the published stability constants are shown in Table 3.

Giroux et al. investigated the complexation of lanthanide ions by $Gluc^-$ mainly by potentiometric titrations carried out between pH = 2–12. They reported the appearance of a precipitate in several Ln(III)–$Gluc^-$ system (Ln(III): La(III), Eu(III), Dy(III), Er(III), Lu(III)) around pH = 8[31]. With a few exceptions, the composition of the complexes formed was the same for the entire lanthanide series: $LnGluc^{2+}$, $LnGlucH_{-1}^+$, $LnGlucH_{-2}^0$, $LnGluc_2^+$, $LnGluc_2H_{-1}$, $LnGluc_2H_{-3}^{2-}$, and $Ln_2Gluc_2H_{-5}^-$. In all systems, $LnGlucH_{-2}^0$ was identified as the predominant species at pH = 8–10[31].

Table 3. Stability constants of Nd(III)–$Gluc^-$ complexes forming in acidic and neutral media

pH range	I (M)	Composition	lgβ
5.3–8.1	0.2 M	$NdGluc^{2+}$	2.66 ± 0.03[88]
		$NdGluc_2^+$	4.70 ± 0.09[88]
2.5–4.5	1 M ($NaClO_4$)	$NdGluc^{2+}$	2.55 ± 0.05[29]
		$NdGluc_2^+$	4.45 ± 0.05[29]
		$NdGluc_3^0$	5.60 ± 0.15[29]
2.0–8.0	1 M (NaCl)	$NdGluc^{2+}$	2.44 ± 0.02[89]
		$NdGluc_2^+$	4.32 ± 0.02[89]
		$NdGluc_3^0$	5.46 ± 0.02[89]
		$NdH_{-2}Gluc^0$	-9.51 ± 0.02[89]
		$Nd_2H_{-2}Gluc_3^+$	-1.97 ± 0.03[89]
		$Nd_2H_{-2}Gluc_4^0$	-0.85 ± 0.05[89]

An exception among the lanthanide metal ions is Eu(III), which does not have a stable complex with the composition of $LnGluc_2H_{-3}^{2-}$. In addition, there are slight differences between the distribution diagrams of the individual lanthanides. Based on ^{13}C NMR results, their conclusion was that the $LnGluc_2^+$ complex (which is present in significant amounts at pH = 4–5), the ligand coordinates through the carboxylate group but not in a bidentate manner; α–hydroxyl functions also interact with the cation, improving the stability of the complex[31].

CD observations suggested that regarding the $PrGlucH_{-2}^0$ complex, in addition to the deprotonated α–hydroxyl group, a second hydroxyl function, most probably the one in γ–position, also plays a role in the coordination, and loses its proton as pH is increased[47]. This was supported by measurements performed by using other related ligands[31].

Kutus et al. reported the formation of a complex with analogous stoichiometry in the Nd(III)−$Gluc^-$ system (i.e. $NdGlucH_{-2}^0$) at the same pH and detected a precipitate which appears at pH = 8[89]. However, aqueous solutions of Nd(III)−$Gluc^-$ remain clear above pH = 11 if the M:L ratio is held at least at 1:2. This raises concerns of how much the solubility of lanthanide ions can be increased by $Gluc^-$, since the complex formation of lanthanides was scarcely studied in strongly alkaline media[21,90], although it is inherent to radioactive waste storage sites[24] alongside high ionic strength (I = 5.3−7.4 M)[23]. Since two

independent research groups published results suggesting the formation of polynuclear Nd(III)−$Gluc^-$ complexes as pH increases[31,89] the precipitate dissolving in alkaline media implies that polynuclear complexes can be present at pH > 12, causing the solubility to significantly increase.

2.3. Ternary systems of Ca(II), gluconate and actinides/lanthanides

Several processes can induce potential mobilization of actinides in radioactive waste repositories. The main concern is the retention of radionuclides in cement pore water since low- and intermediate-level radioactive wastes are regularly solidified in a cement matrix[15]. Another important condition is how the adjacent geochemical environment of the disposal location is affected upon an incidental water intrusion in the repository.[24]

How the cementitious matrix is altered upon getting in contact with solution (most likely Na(I) or Mg(II) rich brines) is essential to determine the composition of the resulting secondary phase of cement corrosion[15]. Bube et al. found that the erosion of cement by an initially weakly alkaline $MgCl_2$ rich brine results in a strongly alkaline secondary phase charachterized by high $CaCl_2$ and NaCl concentrations[15]. Calcite is also a potential host rock for locations of radioactive waste storage sites, i.e. high Ca(II) concentration is often ensured in surrounding environments.[91]

Tits et al. found that the sorption of Eu(III) and Th(IV) is not only reduced by relatively low concentrations of Isa^- (10^{-5} M) and $Gluc^-$ (10^{-7} M) in artificial cement pore water, but brines containing Ca(II) in large amounts also promote the formation of ternary complexes (Shown in Table 4.) [21].

Table 4. Stability constants of binary and ternary complexes of Isa^- and $Gluc^-$

pH	I (M)	Complex	logβ
10.7–13.3	I → 0	$EuH_{-2}Isa^0$	–31.1 ± 0.2
		$EuH_{-2}Gluc^0$	–28.7 ± 0.1
		$CaThH_{-4}Isa_2^0$	–5.0 ± 0.0
		$CaThH_{-4}Gluc_2^0$	–2.14 ± 0.01

A study published in 1998 showed that periodic flooding of waste storages results in increased mobility of transuranic elements (mostly ^{244}Cm and ^{241}Am) in contrast to the supposed adsorption of low solubility inorganic species of radionuclides onto layer silicates

and mineral oxides[92]. Another study proved that the solubility of U(IV) and Th(IV) increased in presence of cellulose degradation products[22]. This could only be explained by the complexation with organic ligands present in the groundwater used to mimic flooding.[92]

Stepwise studies of small size model systems have to be carried out to understand the complex matrices of complexing agents, radionuclides and the host environment. This way, pathways of migration can be characterized on a predictive level and potential migration of radionuclides can be accurately estimated.[21,93,94] While different host rocks (sand[94], silica[94], clay[95], etc.) and ligands have been studied, little is known about the process of complexation and information is also limited on cement additives[96].

Although Vercammen et al. showed that Eu(III) does not form ternary complexes[97], it has recently been proven that Eu(III) (alongside Sr(II)) incorporates to the solid $CaIsa_2$, which contributes to its immobility[98]. As for Th(IV), it was detected in solution in the form of ternary complexes in cement pore water[97]:

$$ThH_{-4}Isa^{-} + Isa^{-} + Ca(II) \rightleftarrows CaThH_{-4}Isa_2^{0} \quad (12)$$

Tasi et al. studied the Ca(II)–Pu(IV)–Isa^{-} system ($8.0 < pH < 12.5$) and proved the formation of two heteromultinuclear $Ca(II)Pu(IV)(OH)_3H_{-2}Isa(H_2O)_8^{0}$ and $Ca(II)Pu(IV)(OH)_3H_{-1}Isa(H_2O)_8^{+}$ complexes[99]. Acquired solubility data was best simulated by assuming these two complexes in solutions. Other compositions (stoichiometric numbers of Ca(II) and Isa^{-} were varied between 1–2, based on the publication of J. Tits et al.[21]) gave a significant difference between measured and calculated data. DFT calculations were performed to assess whether the hydrolysis of Pu(IV) or the deprotonation of the ligand is preferred in alkaline media. These calculations showed that the $Ca(II)Pu(IV)(OH)_3H_{-2}Isa(H_2O)_8^{0}$ complex is formed via the deprotonation of α– and δ–hydroxyls of isosaccharinate, while three hydroxides and three water molecules are also present in the coordination sphere. The other, positively charged complex is also formed by the deprotonation of either the α– or the δ–hydroxyl of Isa^{-} [99].

Rojo et al. found that in the absence of Ca(II), the solubility of Nd(III) is not affected significantly by the presence of $Gluc^{-}$ (albeit for Cm(III), formation of Cm(III)–$Gluc^{-}$ complexes could be discerned by time-resolved fluorescence spectroscopy measurements). When Ca(II) is present in solution, ternary Ca(II)–Nd(III)–$Gluc^{-}$ complexes are suggested to be formed and to increase the solubility of Nd(III). Based on DFT calculations, $Ca_3Nd(OH)(H_{-3}Gluc)_2^{0}$ is the most likely complex composition[30]. However, their

conclusions regarding Nd(III) are based on solubility measurements, during which Nd(III) was present as $Nd(OH)_3$ solid phase resulting in very low concentrations of Nd(III) in solution. Studying the Nd(III)–$Gluc^-$ and Ca(II)–Nd(III)–$Gluc^-$ systems in more concentrated solutions and by different methods is necessary to devise a chemically more accurate model.

3. Aims of the Thesis

While complexation in systems containing Ln(III) and $Gluc^-$ have been studied in relation to radioactive repositories, our knowledge on their aquatic chemistry in alkaline solutions is far from complete. In particular, high metal ion and ligand concentrations help establish chemical models with higher accuracy which can then be used to model very dilute systems. To this end, Nd(III) is an adequate proxy of actinides, enabling measurements at higher total reactant concentrations and various methods of investigation. The main goal of this work is to understand equilibrium behavior in concentrated solutions of Ca(II), Nd(III) and $Gluc^-$, including possible formation of polynuclear complexes. It is important to perform measurements at high pH and ionic strength which are characteristic to storage sites. Furthermore, the effect of large amounts of Ca(II) present in cement pore water on Nd(III) complexation has been scarcely investigated with regard to complexation equilibria. The results published by far hint on the presence of polynuclear complexes involving Ca(II), hence on the increase of the solubility of Ln(III). Also, structural information concerning ligand coordination sites are limited to quantum chemical modelling.

Accordingly, our main goals were the followings:

- to analyze precipitates forming in binary Nd(III)–$Gluc^-$ and ternary Ca(II)–Nd(III)–$Gluc^-$ systems and to determine their composition and stoichiometry;
- to identify the species forming in Nd(III)–$Gluc^-$ solutions at the pH range of 10–14 and to determine the stability constants of these complexes;
- to pinpoint the most likely hydroxyl functions of $Gluc^-$ that take part in coordination;
- to determine the composition and stability constants of ternary complexes forming in the Ca(II)–Nd(III)–$Gluc^-$ system;
- to model how binary and ternary complexes affect the solubility of Nd(III) when in contact with the $Nd(OH)_3$ solid phase.

4. Experimental part

4.1. Reagents and solutions

4.1.1. Stock solutions

For stock solutions, sodium-D-gluconate (Sigma, ≥ 99%) was accurately weighed and dissolved in deionized water to reach the desired concentration. It was used as received without any further purification. The neodymium(III) solution was prepared by dissolving crystalline neodymium(III) chloride hexahydrate (Alfa Aesar, ≥ 99.9%) in deionized water. This concentrated (≈ 1 M) solution was filtered due to the incidental formation of colloidal $Nd(OH)_3$. Employing methylthymol blue as an indicator, a diluted neodymium(III) solution (~ 0.02 M) was titrated with EDTA using hexamethylene tetramine as buffer (pH ≈ 6). $CaCl_2 \cdot 2H_2O$ (Sigma-Aldrich, > 99 %) was used to prepare $CaCl_2$ stock solutions. Its exact concentration was determined via EDTA titrations using eriochrome black T indicator for endpoint detection and ammonia buffer to set the pH to ~10.

For potentiometric calibrations, the titrant was prepared by diluting freshly filtered ~ 20 M NaOH (made from pellets from Analar Normapur) to approximately 2.0 M. The ionic strength of this stock solution was set to 4.5 M and its precise concentration was determined via titrating standardized HCl solution. 1.0 M stock solution of HCl at 4.5 M ionic strength was prepared for reverse titrations by volumetric dilution of concentrated HCl (ca. 37% w/w, VWR). To determine its accurate concentration, a solution of dried $KHCO_3$ was titrated using methyl orange as indicator. All stock solutions and samples were prepared with deionized water (Merck Millipore Milli-Q), and the ionic strengths were adjusted by NaCl (Acros Organics, ≥ 99%).

4.1.2. Preparation of precipitates

Solid complexes of the Nd(III)–$Gluc^-$ system were prepared via mixing solutions of 25 mL 0.50 M $NdCl_3$ and 25 mL 0.50 M Na-D-gluconate and then adding NaOH solution (~ 1 M) under vigorous stirring until a precipitate formed at pH ≈ 8. We used a calibrated glass electrode to monitor the pH of the solution.

Ternary Ca(II)–Nd(III)–$Gluc^-$ precipitate was prepared by adding ca. 20 mL of 1 M NaOH gradually to a mixture of 25 mL of 0.50 M $NdCl_3$ and 25 mL of 0.50 M sodium D-gluconate under vigorous stirring until pH ≈ 12.0–12.5 was reached. (Binary precipitate appearing at pH ≈ 8 redissolves at ca. pH ≈ 12.0–12.5). 0.5 M $CaCl_2$ solution was slowly

added to this solution until a precipitate occurred. In both cases, the solid phase was washed at least three times with distilled water to get rid of the excess NaCl, then was filtered and dried in a desiccator for 1 week. The dry, purple precipitation was pulverized in an agate mortar and stored in an airtight glass container.

Nd_2O_3 (Merck, 99.9 %), dried $Nd(OH)_3$ (Aldrich, 99.9 %) and Ca-D-gluconate (both Sigma, ≥ 99 %) were used as references during the spectroscopic measurements.

4.1.3. Samples for NMR and CD measurements

Solutions of Na-D-galactonate and Na-L-gulonate acid γ–lactone (Sigma-Aldrich, 95 %) were prepared via dissolving D-galactonic acid γ–lactone (Fluka Chemika, 95%) and L-gulonic acid γ–lactone (Sigma-Aldrich, 95%) in deionized water and adding 1 equivalent of NaOH to ensure the exclusive formation of the respective anions. Samples measured by CD contained 0.02 M Nd(III) at a 1:10 metal to ligand ratio. The same samples were prepared for NMR measurements via adding 10 V/V% D_2O. We investigated the pH dependence of the CD spectra by preparing samples containing 0.05 M Nd(III) and 0.2 M ligand in the Nd(III)–$Gluc^-$/ Gal^-/ Gul^- systems, by setting the pH between 5 and 13 using NaOH. A set of NMR samples were prepared for comparing binary and ternary samples. The former contained 0.050 M Nd(III) and 0.500 M $Gluc^-$ while in case of the latter, Ca(II) concentration was adjusted to 0.200 M for NMR and CD measurements.

4.2. Methods used for the analysis of the precipitates

X-ray diffractograms were obtained in the range of $2\Theta = 5-80°$ with 4°/min scan speed using a Rigaku XRD-6000 diffractometer instrument (CuKα (λ = 1.5418 Å) radiation at 40 kV and at 30 mA).

IR spectra (4 cm^{-1} resolution) were recorded in ATR (attenuated total reflectance) mode by a BIO-RAD Digilab Division FTS-65A/896 FT-IR (Fourier-transform infrared) spectrophotometer. Every spectrum is an average of 256 scans collected in the 4000–600 cm^{-1} wavenumber range.

The diffuse reflectance (DR) spectra of the solid samples were collected in the 230–890 nm wavelength range (resolution 0.2 nm, integration time 0.5 s) using an Ocean Optics UV-Vis USB4000 diode array spectrophotometer. An Ocean Optics DH-2000-BAL (consisting of a deuterium and a halogen lamp) was used as light source; samples were

termostatted at 22 ± 2 °C and the incident angle was set to 45°. MgO was used as reference for white background.

We investigated the morphologies of the precipitates by scanning electron microscopy (SEM-Hitachi S-4700 instrument). Measurements were carried out by placing the samples onto conductive carbon adhesive tapes, and gold-palladium alloy films were condensed onto the surface of the samples (in few nm thickness) to avoid charging. For elemental analysis, we carried out energy dispersive X-ray (EDAX) measurements using a Röntec QX2 spectrometer equipped with Be window and coupled to the SEM.

We carried out thermogravimetric measurements using a Setaram Labsys derivatograph applying constant flow of air at 3 °C/min heating rate to study the thermal properties of the solids. 45–55 mg of the samples were weighed into high-purity alpha alumina crucibles for the analysis between 25 and 1000 °C.

A Perkin Elmer Optima 7000 DV ICP-OES spectrometer was used for carrying out the ICP-OES measurements. We prepared the measured solutions by dissolving exactly known amounts of the dried precipitates in deionized water. Yttrium was added to each measured sample as internal standard (1 mg/L) and three parallel measurements were carried out for each sample.

4.3. Potentiometric titrations

Potentiometric titrations were carried out employing a platinized platinum electrode and a thermodynamic Ag/AgCl reference electrode attached to a Metrohm 888 Titrando instrument.

Constant ionic strength of 4.0 M (NaCl) was set throughout this work. High purity H_2 gas (necessary for the platinum electrode) was bubbled through the titrated solutions and minimized the amount of CO_2 above the liquid. The electrochemical cell was constructed as follows:

$$H_2/Pt \mid \text{test solution, I = 4 M (NaCl)} \parallel \text{4 M NaCl} \mid \text{4 M NaCl, Ag/AgCl} \qquad (12)$$

Cell calibrations were performed in the pH range of 1.0–13.5 (where pH is defined as $-\log([H^+]/c^o$, with c^o being 1 M). The cell response was linear within this range and showed a Nernstian slope of 59.1 ± 0.2 mV. For each calibration, a pair of measurements was carried out, via titrating 0.1 M HCl and 0.05 M malonic acid solutions with 2.0 M NaOH at 4.0 M

ionic strength. The obtained data were evaluated with the pHCali software[100]. The titration cell was thermostatted to 25.0 ± 0.1 °C (Julabo F12-MB thermostat).

Potentiometric titrations for both binary (containing both $NdCl_3$ and NaGluc) and ternary (containing $CaCl_2$, $NdCl_3$ and NaGluc) solutions were performed. The total concentration of $NdCl_3$ (hereafter $[NdCl_3]_T$) was varied between 0.05 and 0.15 M, while the titrations were carried out at 1:2.5–1:4 metal to ligand ratios in the binary, and 1:3–1:5 ratios in the ternary systems. Reverse titrations were carried out using 1.0 M HCl solution as titrant; the initial $[NaOH]_T$ was 0.8 M in each titrated solution. Ionic strength was set to 4.0 M with NaCl in each measurement. Evaluation of obtained data was completed using the program PSEQUAD[101]. The autoprotolysis constant of water was fixed at pK_w = 14.26 at I = 4.0 M ionic strength as previously determined by Buckó et al.[53].

4.4. UV-Vis spectrophotometry

UV-Vis absorption spectra were recorded in the wavelength range of 200–900 nm on an Analytik Jena Specord 210 Plus double-beam spectrophotometer, applying 1 nm optical resolution. (Thus, the uncertainty of a certain wavelength is ± 0.5 nm.) All samples (thermostatted at 25.0 ± 0.1 °C, I = 4.0 M (NaCl)) were measured in a standard quartz cuvette with an optical pathlength of 1 cm. Several sets of binary and ternary samples were measured; $[NdCl_3]_T$ was set to 0.05, 0.10 or 0.15 M, while $[NaOH]_T$ was varied between 0.2 and 1.0 M. The metal to ligand ratio was fixed between 1:2.5–1:5.0. To determine the minimum number of light-absorbing species present in solution, the 445–900 nm range of the recorded spectra were evaluated by Matrix Rank Analysis (MRA)[102]. UV–Vis data together with potentiometric ones were processed by the PSEQUAD software, thereby enabling simultaneous modeling using input from two different experimental methods.

4.5. Freezing-point depression

To corroborate the chemical model obtained via fitting of potentiometric and spectrophotometric data, freezing-point depression measurements were performed using a Testo 735 digital precision thermometer. The accuracy of the probe was ± 0.05 °C. The freezing-point depression values were calculated compared to that of distilled water, and the coolant was 5.0 M NaCl with a temperature of ~ –20 °C. Measured freezing points were corrected by the freezing point of deionized water (used as a reference point). The freezing point was determined by overcooling samples, then promoting nucleation with

mechanical agitation until stable temperature readings were obtained ensuring equilibrium between the solid and liquid phases. The measured samples contained $[NdCl_3]_T$ = 0.050–0.150 M and the metal to ligand ratio was fixed at 1.0:2.5. The contribution of additional NaCl present in the solutions to the freezing-point depression was taken into account using the well-known Blagden's law which relates the depression induced by a species to its molality. (Here, molarity was used as an approximation for molality.)

4.6. Nuclear magnetic resonance (NMR)

^1H and ^{13}C NMR spectra were recorded on a Bruker Avance III HD 500MHz NMR spectrometer employing a 5 mm inverse broadband probe head (CryoProbe™Prodigy) furnished with z-oriented magnetic field-gradient capability. The baseline was subtracted from each spectrum numerically and solvent suppression was not applied. The magnetic field was locked to the 2D signal of the solvent for stabilization at the beginning of every measurement, for which 10% (V/V) D_2O was added to each sample. The temperature was set to 25 ± 1 °C, whereas the ionic strength was not adjusted during measurements.

For the investigation of Nd(III)–$Gluc^-$/Gal^-/Gul^- systems, each sample contained 10% V/V D_2O and 6.5 mM DSS as internal reference, and 128/512 interferograms were collected at (25 ± 1) °C to obtain the $^1H/^{13}C$ NMR spectra. Peaks of the free ligands were assigned based on literature sources referring to $Gluc^-$ [89], Gal^- [103] and Gul^- [104].

4.7. Circular dichroism spectroscopy

CD spectra were recorded on a Jasco J-1500 circular dichroism spectrophotometer in the wavelength ranges of 500–750 and 350–810 nm. Samples containing 0.020 M $NdCl_3$ and 0.200 M ligand were measured in a masked quartz cuvette with 2 cm optical pathlength. Samples that contained 0.05 M of $NdCl_3$ and 4 equiv. $Gluc^-$, Gal^- or Gul^- were measured in a standard quartz cuvette with 1 cm optical pathlength. The pH was adjusted between pH 5 to 13. All measurements were carried out at room temperature (25.0 ± 0.1) °C, the ionic strength was not adjusted.

4.8. Data processing

Formation of Nd(III)−$Gluc^-$ complexes can be generally described as follows:

$$p\mathrm{Nd}^{3+} + q\mathrm{Gluc}^- + r\mathrm{H}^+ \rightleftharpoons \mathrm{Nd}_p\mathrm{Gluc}_q\mathrm{H}_r^{(3p-q+r)} \quad (13)$$

$$\beta_{pqr} = \frac{[M_p L_q H_r]}{[M]^p [L]^q [H^+]^r (c^{\emptyset})^{1-p-q-r}} \quad (14)$$

where $c^{\emptyset}$ is the standard molar concentration of unity, $c^{\emptyset}$ = 1 M. The stability constants and molar abosorptivities of the forming complexes were determined by fitting the measured data with the aid of the PSEQUAD[101] software. During the process of fitting, the aim is to minimalize the fitting parameter (FP):

$$FP = \sum_{q=1}^{n_d} FP_q = \sum_{q=1}^{n_d} \sum_{i=1}^{r_q} \left(\omega_P \sum_{k=1}^{m} \left(\Delta X_k^P\right)^2 + \omega_A \sum_{k=m+1}^{p} \left(\Delta X_k^A\right)^2 \right) \quad (15)$$

where n_d is the number of sets of measurements derived from different types of primary experimental data, r_q is the number of experimental points in the q^{th} set of measurements, ω_1 is the weighting factor of the volume of the titrant or total concentrations, ω_P is the weighting factor for the potential measurements, and ω_A is the weighting factor for the absorbance measurements. During our fitting process, ω_P was set to 1 and ω_A was set to 0.01.

5. Results and discussions

5.1. Preparation and analysis of the binary and ternary solid complexes

5.1.1. Elemental analysis

The solid complexes alongside other inorganic salts used as references were subjected to powder X-ray measurements. The obtained diffractograms (Figure 5) suggest the forming precipitates to be amorphous, thereby completely different from the reflection pattern of either NaGluc, $Nd(OH)_3$, or $Ca(OH)_2$. In conclusion, the thus obtained solids are solid complexes incorporating Ca(II), Nd(III) and $Gluc^-$ ions.

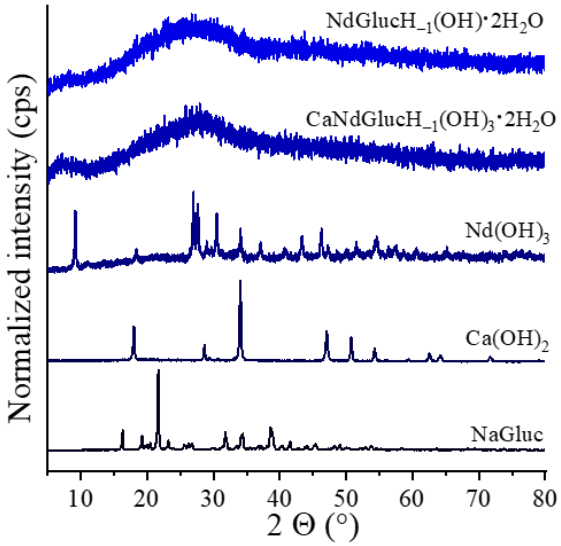

Figure 5. X-Ray powder diffractograms of $NdGlucH_{-1}(OH)\cdot 2H_2O$ and $CaNdGlucH_{-1}(OH)_3\cdot 2H_2O$ (top of the diagram), and $Nd(OH)_3$, $Ca(OH)_2$ and NaGluc as references (bottom of the diagram)[105]

Pulverized solid samples of the Nd(III)–$Gluc^-$ and Ca(II)–Nd(III)–$Gluc^-$ systems were subjected to elemental analysis. An accurately weighed portion of the sample was placed in a furnace at 1000 °C for 24 hours. Based on the weight of the calcined sample assuming complete combustion of $Gluc^-$, the mass percentage of Nd(III) in the original binary sample was calculated to be 37.39 wt%. This was supported by an ICP-OES measurement for the uncalcined precipitate, yielding 38.61 wt% Nd(III) content.

In the case of the ternary solid, an ICP-OES measurement showed the Nd(III) content to be 36.85 wt%. As a next step, similar calcination was performed and the remaining solid was weighed. The Ca(II) content of the sample calculated from the mass balance of the solid

was determined to be 8.00 wt%. These results suggest the Ca(II):Nd(III) stoichiometric ratio to be 1:1. In addition, thermogravimetric curves taken for the uncalcined samples show strong endothermic mass loss up to 200 °C (Figures 6 and 7), indicating the presence of crystalline water in the precipitates which was estimated to be the 8–9 wt% in both cases.

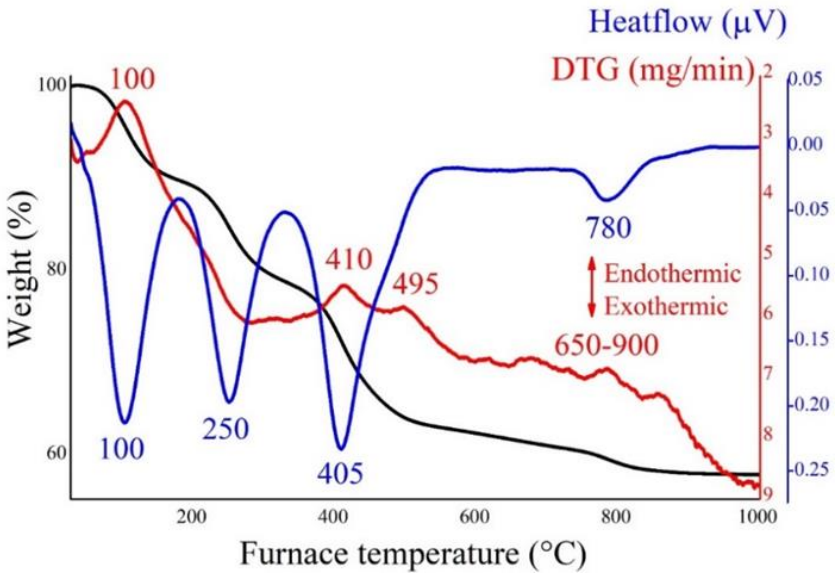

Figure 6. TG/DTG/DTA curves of the binary system $NdGlucH_{-1}(OH)\cdot 2H_2O$. TG : black; DTG: blue; DTA: red[105]

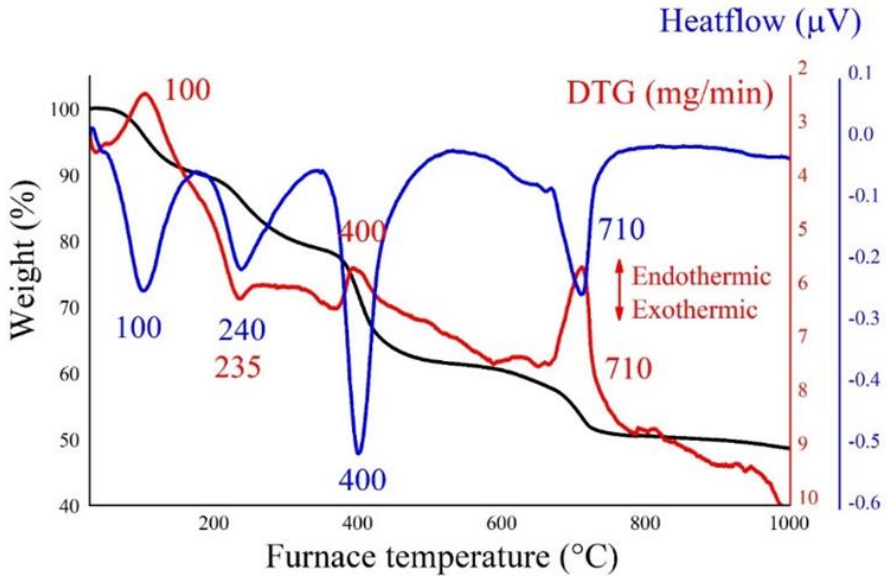

Figure 7. TG/DTG/DTA curves of the binary system $CaNdGlucH_{-1}(OH)_3\cdot 2H_2O$. TG : black; DTG: blue; DTA: red[105]

With the assumption that the unaccounted mass from ICP-OES and TG corresponds to $Gluc^-$ and OH^- ions, the suggested formulae of the solid complexes are as follows:

$NdGlucH_{-1}(OH)\cdot 2H_2O$ – Nd(III): the ideal value of 36.85 wt% is close to the average of the calcination (37.39 wt%) and ICP (38.61 wt%) results with a crystalline water content of 9.20 wt% (concluded from TG).

$CaNdGlucH_{-1}(OH)_3\cdot 2H_2O$ – Nd(III): the ideal value of 30.99 wt% is in agreement with that of 30.0 wt% (ICP-OES) measurements; Ca(II): the calculated value of 8.61 wt% is close to the experimental 8.00 wt% (calcination) with crystalline water present in 7.73 wt% (8–9 wt% based on TG). Water content was rounded off to the closest integer value. While analysis suggested that crystalline water content of the sample was slightly larger than two equivalent, the error presumably corresponds to some remaining moisture.

5.1.2. Structural information on the solid complexes

The morphology of the binary and ternary solid complexes is illustrated by scanning electron microscope images. The simultaneously obtained EDAX pictures show that Ca(II) and Nd(III) are evenly distributed (Figure 8).

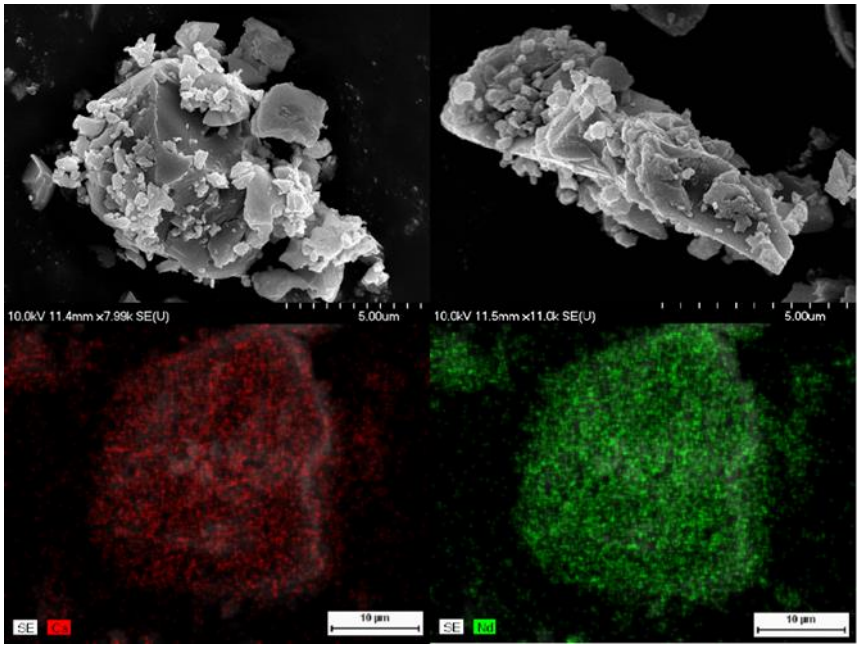

Figure 8. SEM images obtained for $NdGlucH_{-1}(OH)\cdot 2H_2O$ (top, left) and for $CaNdGlucH_{-1}(OH)_3\cdot 4H_2O$ (top, right). On the bottom, the EDX distribution of Ca (left) and Nd (right) of the ternary solid complex is shown[105]

FT-IR spectra of the two complexes were compared to the spectra of $Nd(OH)_3$, Ca-D-Gluconate and Na-D-Gluconate (Figure 9). The data obtained attest that $Gluc^-$ is present in both complexes, since the asymmetric and symmetric (indicated by * and $^+$) carboxylate peaks of $Gluc^-$ (1633 and 1398 cm^{-1}, respectively) appear in the spectrum of $NdGlucH_{-1}(OH)\cdot 2H_2O$ (at 1664 cm^{-1} and at 1498 cm^{-1}) and that of $CaNdGlucH_{-1}(OH)_3\cdot 2H_2O$ (at 1659 cm^{-1} and at 1500 cm^{-1}). The band positions are almost identical in the two complexes, suggesting that the carboxylate moiety coordinates in a similar mode. The possible coordination mode of the carboxylate group can be inferred from the difference Δ [$\Delta = \nu_{asym(COO-)} - \nu_{sym(COO-)}$] between the asymmetric and symmetric carboxylate vibrations. Accordingly, the coordination mode can be monodentate ($\Delta_{complex} > \Delta_{sodium\ salt}$) or bidentate bridging ($\Delta_{complex} \sim \Delta_{sodium\ salt}$) or bidentate chelating ($\Delta_{complex} < \Delta_{sodium\ salt}$)[106]. Regarding NaGluc, the $\Delta_{sodium\ salt}$ is 235 cm^{-1}, and both complexes have a characteristic difference of $\Delta_{complex}$ = 160–170 cm^{-1}. Consequently, the carboxylate group is supposed to be in a chelating bidentate coordination mode in both solid complexes[107–109]. The broad band that occurs in the range of 3700–3000 cm^{-1} with high intensity (not shown) is produced by the stretching vibrations of hydroxyl groups belonging to excess water, indicating that crystalline water is present in the complexes.

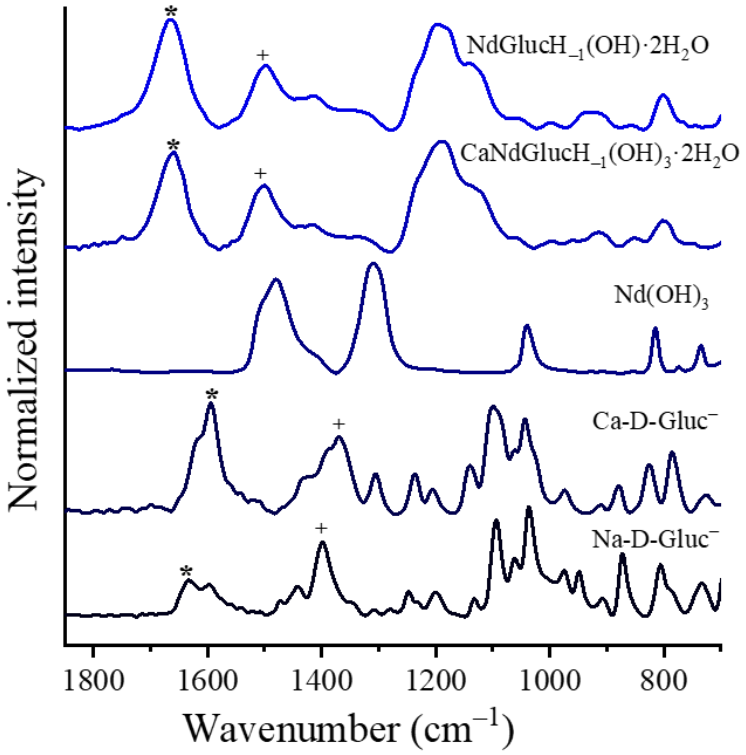

Figure 9. FT-IR spectra of the solid complexes compared to the inorganic and the organic compounds used as references[105]

The difference between the diffuse reflectance spectra of the solid complexes and those of the $Nd(OH)_3$ and Nd_2O_3 references (Figure 10) proves that Nd(III) is not present in its oxide or hydroxide form. On the other hand, the spectra of the two solid complexes differ only slightly, which can be explained by the uncertainty of the measurement. This suggests the chemical environments of the chromphores to be very similar for the binary and in the ternary complexes. Consequently, the ternary complex is a co-precipitate of the binary solid and $Ca(OH)_2$, which is fully supported by the obtained stoichiometry.

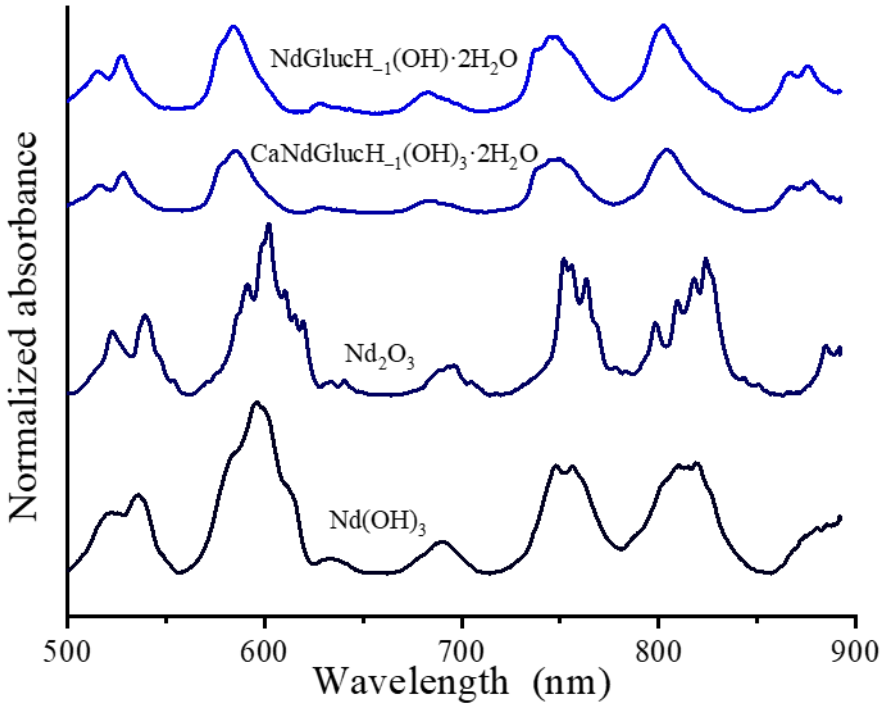

Figure 10. The Vis-DR spectra of the solid complexes compared to the oxide and hydroxide of Nd(III) used as reference[105]

The Nd(III)–$Gluc^-$ system has been previously studied by Kutus et al. who reported the calculated molar absorptivities of the Nd(III)–$Gluc^-$ complexes in solution. Comparing the molar absorption spectrum of the species $NdGlucH_{-2}^0(aq)$[89] that forms at pH = 7 and the DR spectrum of $NdGlucH_{-1}(OH)\cdot 2H_2O$ (Figure 11), the two spectra are very similar (this stands for the whole spectra of these two specimen). This suggests that indeed the charge-neutral solution species precipitates at pH = 8 and its structure remains similar in the solid state.

The most likely scenario is that the $NdGlucH_{-2}^{0}(aq)$ complex, which is present predominantly at pH ≈ 8, reaches its solubility limit and precipitates as $NdGlucH_{-1}(OH)\cdot 2H_2O$. This would mean that this is the least soluble species under the employed experimental conditions.

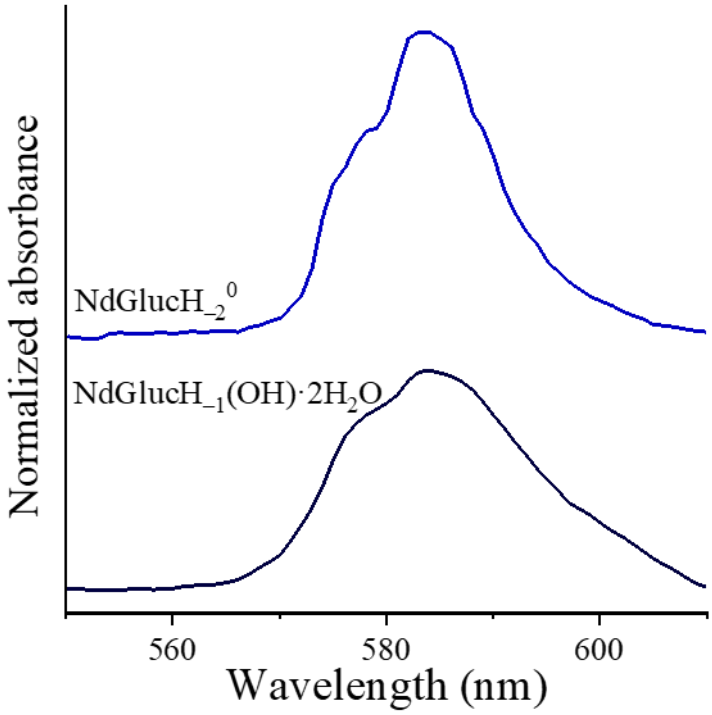

Figure 11. Top spectrum: excerpt from the molar absorbance spectrum of $NdGlucH_{-2}^{0}$ complex in solution. Bottom: excerpt from the diffuse reflectance spectrum of the solid $NdGlucH_{-1}(OH)\cdot 2H_2O$ complex[105]

5.2. Speciation in the Nd(III)–Gluc⁻ system in alkaline medium

5.2.1. Potentiometric and UV-Vis spectrophotometric data analysis

For creating an accurate model for the Nd(III)–Gluc⁻ aqueous equilibria in strongly alkaline solutions, potentiometric titrations and spectrophotometric measurements were carried out.

In general, Nd(III) has two transitions at 585.0 and 805.0 nm ($^4I_{9/2} \rightarrow {}^4G_{5/2}$, $^2G_{7/2}$, depicted in Figure 12) which are routinely studied when coordination compounds are investigated[81,84,110,111]. The former is often referred to as the hypersensitive transition of Nd(III). Both peaks in Figure 12 show a slight redshift with increasing $[NaOH]_T$, indicating weaker f-f transitions. Also, absorbances become weaker, indicative of a decrease in the concentration and/or molar absorptivity of the forming coordination complexes. In this respect, Levitskaia et al. found that the deprotonation of coordinated D-glucosamine is manifested in the spectra of Nd(III) as a significant redshift[81], similar to our observations. Therefore, deprotonation is likely to occur in the present system, too. In addition, there are at least two isobestic points showing the co-existence of at least three Nd(III) bearing species with different protonation states. Evaluation of these spectrophotometric data by matrix rank analysis suggests that minimum three different absorbing species are present (one is the Nd(III) aqua-ion).

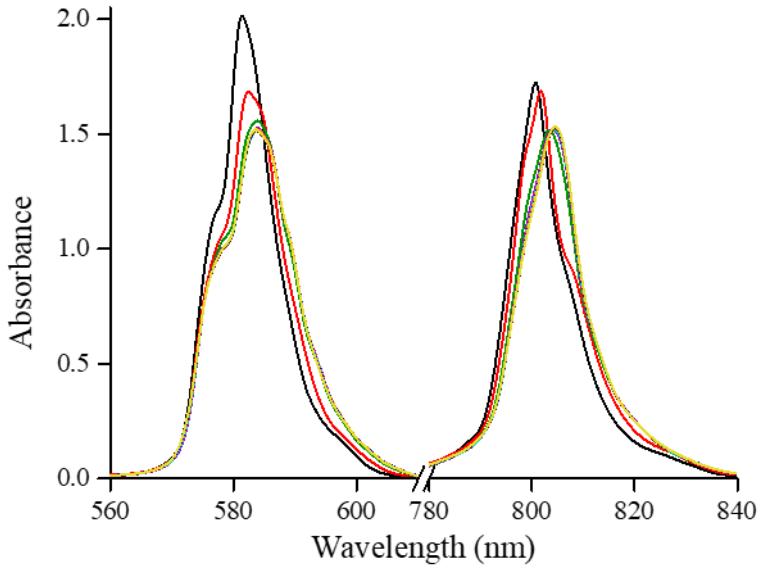

Figure 12. Effect of increasing $[NaOH]_T$ on the visible spectra of the Nd(III)–Gluc⁻ system. Experimental conditions: T = 25 °C, I = 4 M (NaCl); analytical concentrations: $[NdCl_3]_T$ = 0.09910 M, $[NaGluc]_T$ = 0.3000 M, $[NaOH]_T$ changes from 0.1988 M (black spectrum) to 0.9938 M (yellow spectrum) in ca. 0.1 M increments[112]

The titration curves (Figure 13) display pronounced dependence of the pH on the Nd(III) concentration, which suggests the formation of polynuclear complexes. While the potentiometric data indicate that complex formation is highly affected by Nd(III) concentration, the collected Vis spectra show marked pH dependence.

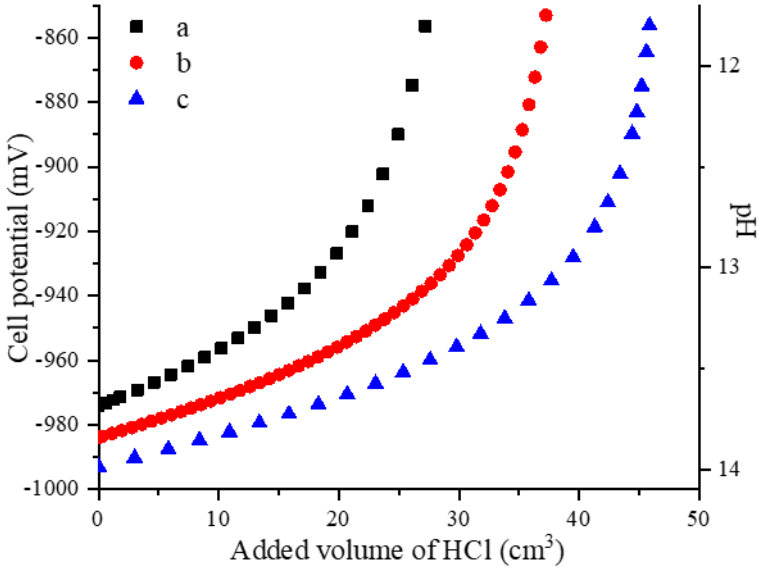

Figure 13. Potentiometric titration data for the Nd(III)–Gluc⁻ system. Symbols denote the measured cell potential values. Experimental conditions: T = 25 °C, I = 4 M (NaCl). Exact reactant concentrations used for the titration curves a, b and c are shown in Table 5[112]

Table 5. Initial total concentrations of titrated samples and the titrant HCl solution corresponding to the graph in Figure 13. Titrated volume was 70 cm^3 in every measurement[112]

Sample	$[NdCl_3]_{T,0}$/M	$[NaGluc]_{T,0}$/M	$[NaOH]_{T,0}$/M	c_{HCl}/M
a	0.1557	0.3908	0.7952	1.009
b	0.1013	0.3053	0.7913	1.009
c	0.04954	0.1483	0.7909	0.9906

To determine the stoichiometry and stability of the forming complexes, a conventional fitting procedure was carried out using the PSEQUAD program. An extended set of chemically meaningful species were fitted in several different combinations and measured data were simulated by testing several hundred different models. First, most probable models were chosen on the basis of fitting of potentiometric data separately, assuming at least three

species as suggested by the MRA results. The second step was to refine these models via simultaneous fitting of the potentiometric and spectrophotometric data.

The first sequence of fitting was based on trivial mononuclear complexes but systematic differences between the collected and calculated data could not be eliminated, especially at higher Nd(III) concentrations. The observation that several plausible combinations of complexes with different Nd(III):$Gluc^{-}$:OH^{-} ratios were not sufficient to accurately describe the entire set of the measured data points to the presence of polynuclear species in solution. Consequently, binuclear Nd(III)–$Gluc^{-}$ complexes were included for further model selection.

Fitting the $Nd_2Gluc_4H_{-6}^{4-}$ complex together with its protonated form, $Nd_2Gluc_4H_{-5}^{3-}$, resulted in an adequate simulation of the experimental data; this is displayed in Figure 14A. The fitting is further improved by adding two other binuclear complexes, $Nd_2G_6H_{-4}^{4-}$ and $Nd_2G_6H_{-5}^{5-}$ to the model (Figure 14B).

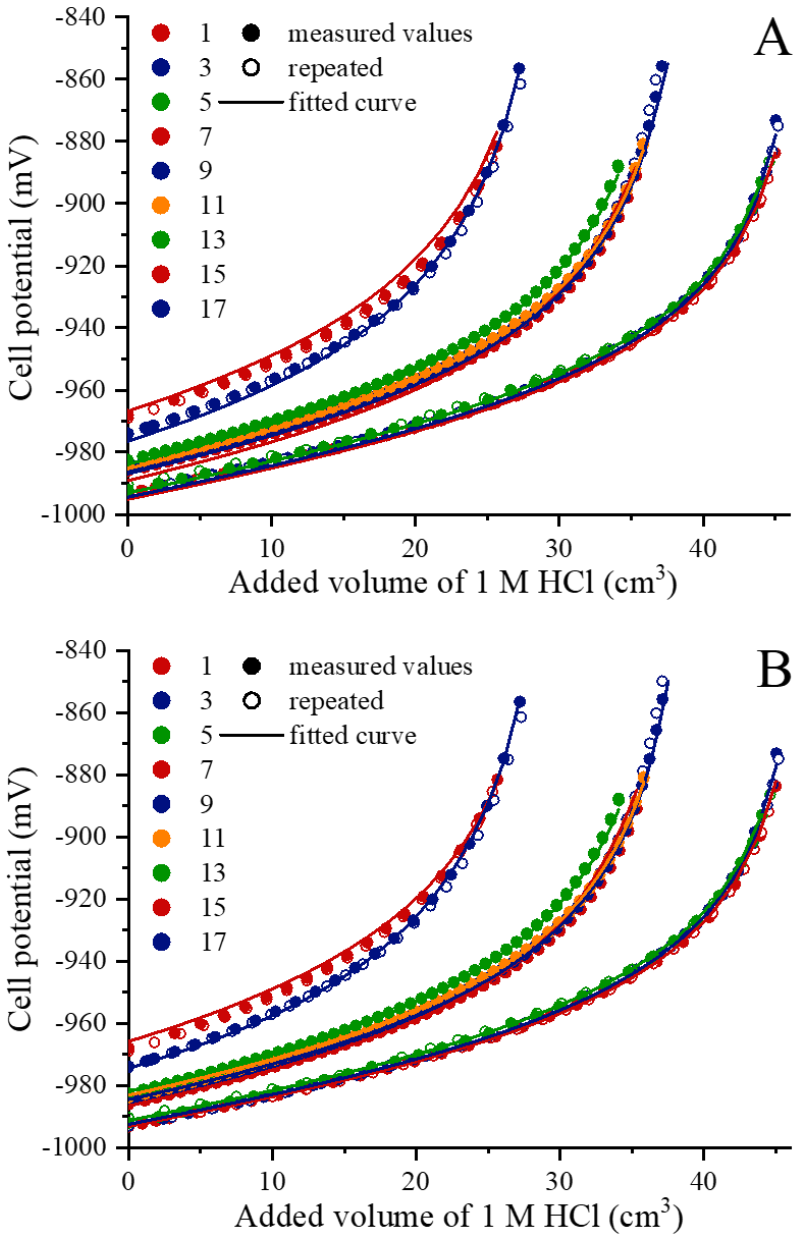

Figure 14. Experimental and simulated data of potentiometric curves in the Nd(III)–$Gluc^{-}$ system. Fitting carried out presuming the formation of the following complexes:

A – $Nd_2G_4H_{-5}^{3-}$ and $Nd_2G_4H_{-6}^{4-}$;

B – $Nd_2G_4H_{-5}^{3-}$, $Nd_2G_4H_{-6}^{4-}$ and $Nd_2G_6H_{-4}^{4-}$, $Nd_2G_6H_{-5}^{5-}$;

Experimental conditions: T = 25 °C, I = 4 M (NaCl); Full and hollow circles denote experimental data collected at the same initial total concentrations (latter are repeated measurements) while continuous lines depict calculated data[112].

Analytical (or total) concentrations of the titrated samples are shown in Table 6

Table 6. Initial total concentrations of samples and titrating HCl solution of all potentiometric measurements[112]

Titration	$[NdCl_3]_{T,0}$/M	$[NaGluc]_{T,0}$/M	$[NaOH]_{T,0}$/M	c_{HCl}/M
1	0.0495	0.125	0.791	1.005
2	0.0495	0.126	0.791	1.005
3	0.0495	0.150	0.791	1.009
4	0.0495	0.148	0.791	1.009
5	0.0495	0.199	0.791	1.009
6	0.0495	0.199	0.791	1.009
7	0.101	0.204	0.791	1.017
8	0.101	0.203	0.791	1.017
9	0.101	0.254	0.791	0.991
10	0.101	0.253	0.791	0.991
11	0.101	0.305	0.791	0.991
12	0.101	0.305	0.791	0.991
13	0.105	0.370	0.797	1.017
14	0.105	0.370	0.797	1.017
15	0.156	0.623	0.795	1.009
16	0.156	0.625	0.795	1.009
17	0.156	0.390	0.795	1.009
18	0.156	0.390	0.795	1.009

Adding one mononuclear complex to the above mentioned four complexes slight and systematic differences between the calculated and experimental curves' improved significantly. As the best result is given when the $NdGluc_2H_{-5}^{4-}$ complex is added to the four binuclear complexes already included in the model, the final model consists of the following complexes: $Nd_2Gluc_4H_{-6}^{4-}$, $Nd_2Gluc_4H_{-5}^{3-}$, $Nd_2Gluc_6H_{-4}^{4-}$, $Nd_2Gluc_6H_{-5}^{5-}$ and $NdGluc_2H_{-5}^{4-}$. The stability constants of these are shown in Table 7 and calculated data based on the final model is shown in Figure 15.

Table 7. Stability constants of the species present in alkaline solutions containing Nd(III) and $Gluc^-$ at T = 25 °C and I = 4 M (NaCl)[112]

Reaction	logβ	standard error
$Nd(III) + 2Gluc^- = NdGluc_2H_{-5}^{4-} + 5H^+$	–58.76	0.03
$2Nd(III) + 4Gluc^- = Nd_2Gluc_4H_{-5}^{3-} + 5H^+$	–47.57	0.07
$2Nd(III) + 4Gluc^- = Nd_2Gluc_4H_{-6}^{4-} + 6H^+$	–60.02	0.07
$2Nd(III) + 6Gluc^- = Nd_2Gluc_6H_{-4}^{4-} + 4H^+$	–35.38	0.07
$2Nd(III) + 6Gluc^- = Nd_2Gluc_6H_{-5}^{5-} + 5H^+$	–46.57	0.07

Figure 15 shows that the structure of potentiometric titration curves is well-reproduced, and the average difference between the fitted and observed data is as low as 1.34 mV.

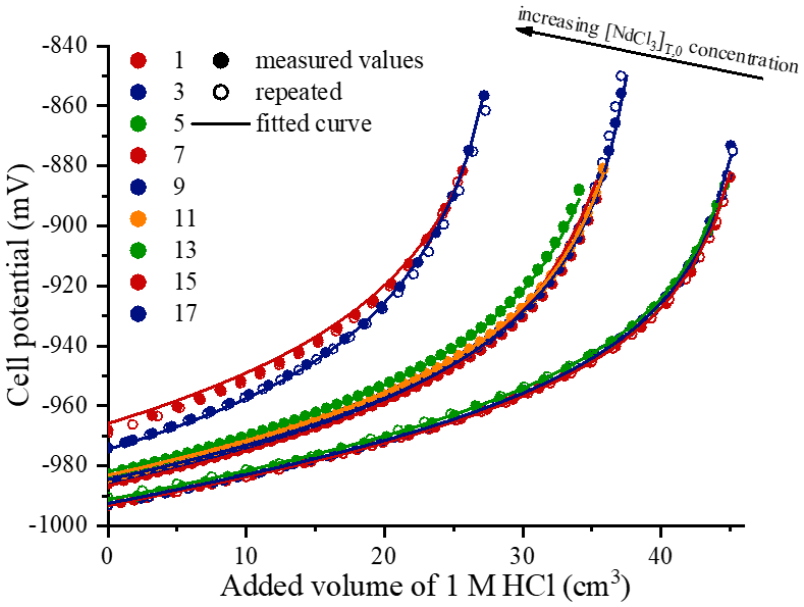

Figure 15. Potentiometric titration curves of the Nd(III)–$Gluc^-$ system. Experimental conditions: T = 25 °C, I = 4 M (NaCl); pH is varied between 12.5 and 13.8. Full and hollow circles denote experimental data collected at the same initial total concentrations (latter are repeated measurements) while continuous lines depict calculated data. Analytical (or total) concentrations of the titrated samples are shown in Table 6[112]

Log β values obtained from the fitting process were used to calculate the distribution diagram of the Nd(III)–Gluc$^-$ system, shown in Figure 16. These experimental data show that the solid $NdGlucH_{-1}OH^0$ complex, precipitating around pH ≈ 8, redissolves at higher pH (which was confirmed by visual inspection too), giving rise to the appearance of the $Nd_2Gluc_6H_{-4}^{4-}$ and $Nd_2Gluc_4H_{-5}^{3-}$ binuclear complexes and their deprotonated forms, $Nd_2Gluc_6H_{-5}^{5-}$ and $Nd_2Gluc_4H_{-6}^{4-}$. The $NdGluc_2H_{-5}^{4-}$ complex forms only at pH > 13.

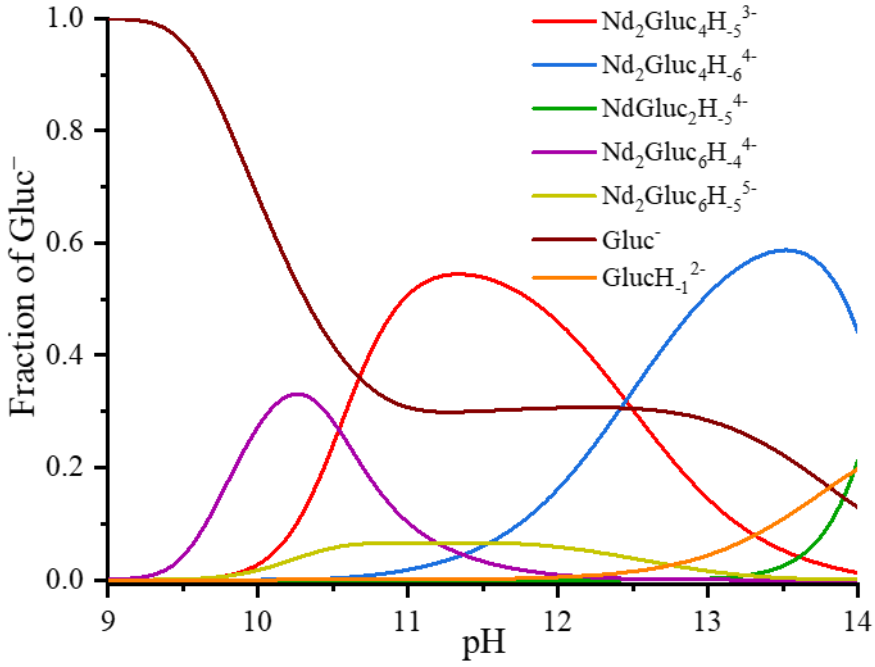

Figure 16. Distribution diagram of the Nd(III)–Gluc$^-$ binary system, presuming $[Nd(III)]_T$=0.100 M and $[Gluc^-]_T$ =0.300 M concentrations[112]

In a publication based on a previous work of our research group, Kutus et al. reported the formation of a complex $Nd_2Gluc_4H_{-2}^0$ at pH = 6.5 having the same M:L ratio as that of $Nd_2Gluc_4H_{-2}^{4-}$ detected in this work. The formation of binuclear complexes at high pH corroborates the dimerization characteristic to lanthanides in alkaline solutions. Giroux et al. found that several lanthanides exhibit this tendency; La(III), Eu(III), Dy(III), Er(III), and Lu(III) cations all form a complex with $M_2L_2H_{-5}^-$ stoichiometry[31]. The notion that Nd(III) tends to dimerize is further supported by the work of Ciavatta et al., who found that in dilute solutions ($[Nd(III)]_T$ < 0.3 M) $Nd_2(OH)_2^{4+}$ hydroxido complexes are formed[79].

Although there are numerous examples of mononuclear Ln(III)–Gluc$^-$ complexes in the literature[29,31,47,85–89], polynuclear complexes have rarely been reported[31,89]. A possible reason for this discrepancy is that measurements in the former systems were usually and

routinely carried out in more dilute solutions, where the formation of multinuclear species is not favorable due to reduced Nd(III) concentrations.

The molar absorptivity values of the complexes included in the final model were calculated using PSEQUAD via simultaneous fitting of potentiometric and Vis spectrofotometric data, shown in Figures 17 and 18. Interestingly, the thus obtained molar absorptivity values show a bathochromic shift upon deprotonation only in the wavelength range of 780–830 nm (Figure 18), while peak positions are not very sensitive to proton dissociation in the hypersensitive range of 560–610 nm. Since this region reports typically on variations in direct metal-ligand interactions[89], the marked changes seen above 700 nm strongly suggest that deprotonation occurs (at least partially) on coordinated water molecules. Furthermore, the molar absorptivity values of binuclear complexes are ca. twice as high as the molar absorptivity values of the mononuclear complex as found earlier[89].

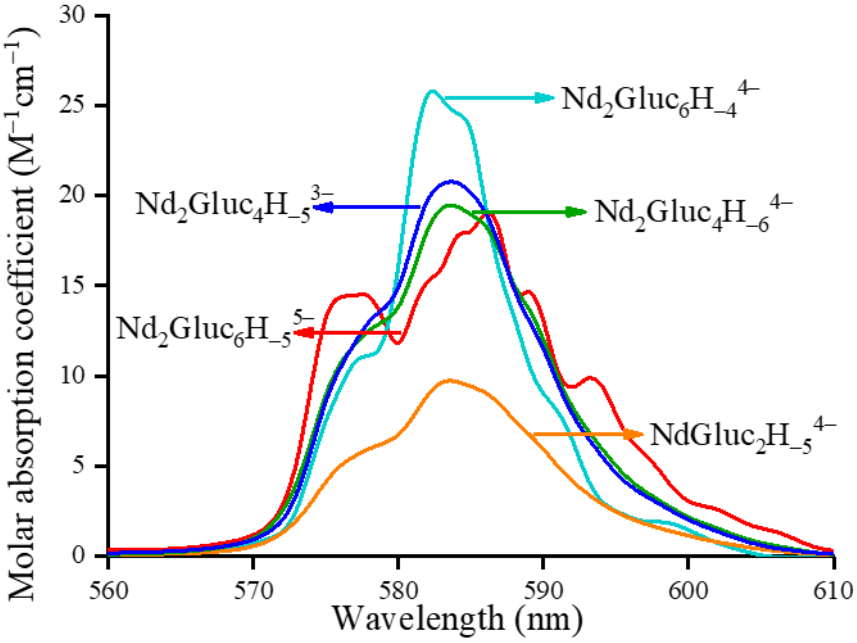

Figure 17. Molar absorption spectra of the mononuclear and binuclear Nd(III) complexes in the range of 560–610 nm[112]

Molar absorption spectra at 805 nm of the five species affirm the bathochromic shift upon further deprotonation as illustrated in Figure 18.

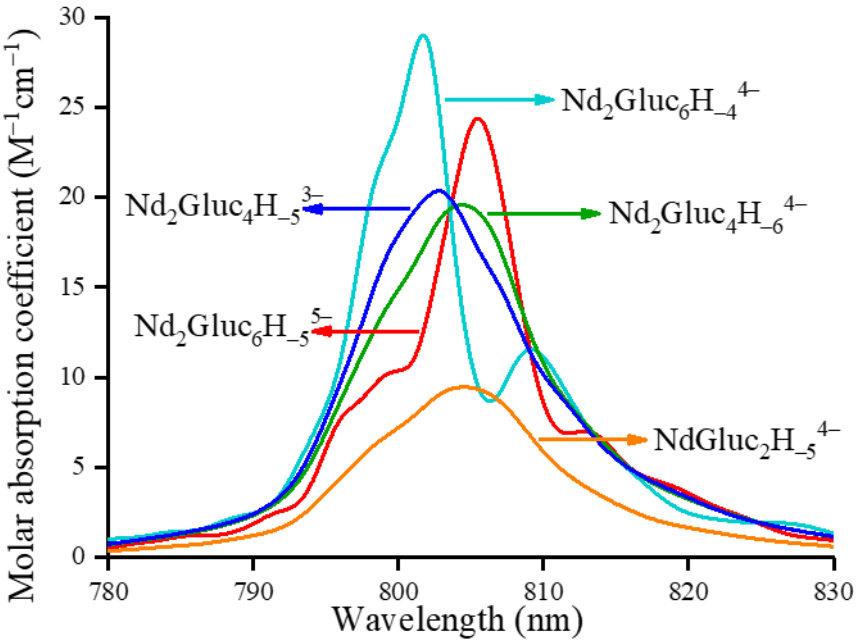

Figure 18. Molar absorption spectra of the mononuclear and binuclear Nd(III) complexes in the range of 780–830 nm.[112]

5.2.2. Model validation via freezing-point depression measurements

Measured and calculated freezing-point depression values of selected solutions (Table 7) were compared to validate the chosen chemical model. The formula of calculation is as follows:

$$\Delta T_f = T_{f(\text{pure solvent})} - T_{f(\text{solution})} = K_f \cdot m_B \quad (16)$$

where theoretical freezing point depression (ΔT_f) is proportional to the concentration of the fully dissociated species, K_f is the cryoscopic constant (1.86 K·kg/mol for water), and m_B is the molality of the solute, which can be replaced by molar concentration values in relatively dilute solutions. Because freezing point depression is a colligative property, it decreases upon complexation as the number of solute particles.

Table 8. Total ion concentration and composition of the samples measured by freezing point depression. ΔT_{meas} is the measured freezing point value, ΔT_{tot} is the simulated freezing point depression assuming total dissociation of used inorganic salts, ΔT_{calc} is the calculated freezing point value based on the model derived from the fitting of the potentiometric and spectrophotometric measurements. The first two solutions were strong electrolytes; therefore, freezing point depressions were not calculated in these cases[112]

Total ion c. /M	**$[Nd^{3+}]_T$ /M**	**$[Gluc^-]_T$**	**$[OH^-]_T$ /M**	**ΔT_{meas}/°C**	**ΔT_{tot}/°C**	**ΔT_{calc}/°C**
0.5914	0.0000	0.0000	0.2957	1.12	1.10	—
0.7886	0.0000	0.0000	0.3943	1.43	1.47	—
1.0426	0.0503	0.1250	0.2957	1.44	1.94	1.41
1.2682	0.0754	0.1875	0.2957	1.52	2.36	1.59
1.4937	0.1006	0.2500	0.2957	1.88	2.78	1.79
1.6909	0.1006	0.2500	0.3943	2.15	3.14	2.11
1.9165	0.1257	0.3125	0.3943	2.41	3.56	2.30
2.1420	0.1509	0.3750	0.3943	2.69	3.98	2.54

The measured freezing point depression values of inorganic salts in solution (ΔT_{meas}) are the same as values calculated by assuming total dissociation (ΔT_{tot}). Every other solution contained Nd(III) and $Gluc^-$ at a pH higher than 12. Based on distribution diagrams, the ratio of complexes to free ions are large enough to explain the difference between measured and theoretical freezing point depression; latter is when total dissociation is assumed (Figure 19).

It is seen in Figure 19 that freezing point depression values of samples containing both Nd(III) and $Gluc^-$ are significantly lower than when total dissociation is assumed; this points to complex formation. Finally, formation constants presented in Table 7 were used to calculate freezing point depression values (ΔT_{calc}) which were found to reasonably agree with observed data, which corroborates our final model.

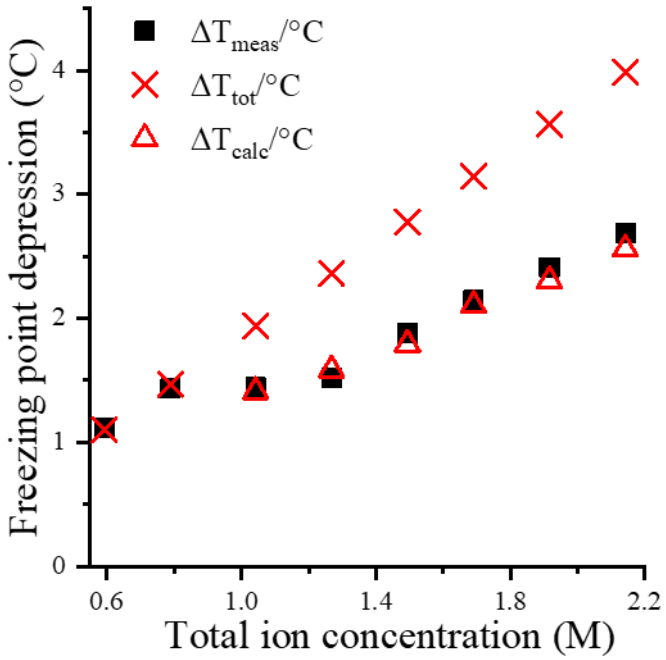

Figure 19. Comparison of the measured and calculated freezing point depression values as a function of total ion concentration to validate the suggested speciation model presented in Table 7[112] . ΔT_{meas}: measured freezing point values; ΔT_{tot}: freezing point depression values calculated by assuming total dissociation; ΔT_{calc}: freezing point depression values calculated based on the created model

5.3. Coordination sites and solution structure of Nd(III) complexes forming with $Gluc^-$ and related ligands

5.3.1. NMR study of the Nd(III)–$Gluc^-$ system

Paramagnetic lanthanide ions affect the NMR spectra upon complexation. As unpaired electrons interact with the NMR active nucleus, NMR peaks might express a large paramagnetic shift and significant broadening. Paramagnetic ions have been extensively studied via NMR (Nd(III)[113], Dy(III)[31], Pr(III)[47], Mn(II) and Co(II)[114]) to determine how the degree of shifting and broadening of certain signals is applicable to identify the binding sites of the ligands. We collected a series of ^1H spectra as a function of $[Nd(III)]_T$ at pH = 13 to gain structural information of the forming complexes. In samples containing 0.100 M $Gluc^-$ as Nd(III) increases from 0.005 to 0.020 M, complexation of Nd(III) by $Gluc^-$ induces a general peak shift and broadening even at the highest ligand to metal ratio (Figure 20).

Because of the fast exchange between complexes and the free ligand, all peaks are shifted and broadened; with the H2 and H3 peaks being the most affected, implying that

hydroxyls attached to the C2 and C3 atoms are most probable binding sites, in addition to the COO^- anchor. (Assigments of the ^1H and ^{13}C peaks of $Gluc^-$ were based on previous publications[49,115].) Giroux et al. reported that the C2 alcoholate group of $Gluc^-$ takes part in coordination when Pr(III) and Dy(III) complexes form[31], while in the case of Eu(III)−$Gluc^-$ [28] and Ca(II)−$Gluc^-$ [49] complexes, also the C3–OH moiety takes part in complexation.

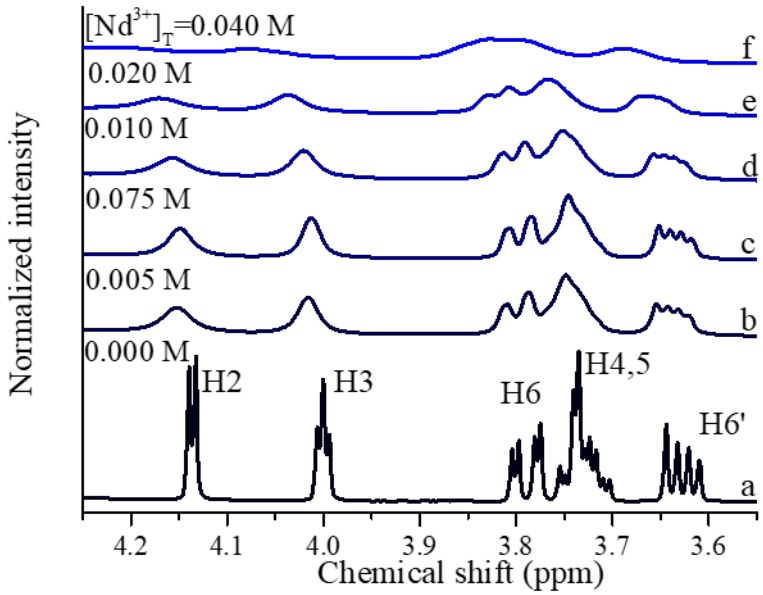

Figure 20. NMR spectra as a function of increasing $[Nd(III)]_T$ at pH = 13. $[Gluc^-]$=0.1000 M was kept constant[112]

5.3.2. The effect of Nd(III) on the ^1H and ^{13}C NMR spectra of $Gluc^-$, Gal^- and Gul^-

To deduce a general coordination manner for the binding of Nd(III) ions by polyhydroxy carboxylate molecules, we studied other anions related to $Gluc^-$, i.e. D-galactonate (Gal^-) and L-gulonate (Gul^-) (Figure 21). To better understand structural variations, not only NMR but also circular dichroism measurements were carried out for the above ligands. $Gluc^-$ has been previously reported to coordinate through the carboxylate (and depending on pH) partially deprotonated C2–OH, C3–OH and C4–OH functional groups in the Cu(II)–, and Al(III)–$Gluc^-$ systems[18,48].

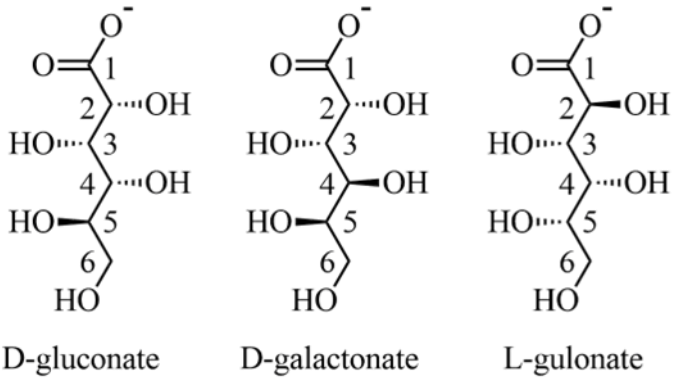

Figure 21. Structure of the studied aldonate anions: D-Gluc$^-$, D-Gal$^-$, L-Gul$^-$[116]

In the ^{1}H NMR spectra of Gluc$^-$ at pH = 7.0 and at a metal to ligand ratio of 1:10, only the group of H4–H6' peaks appears with an upfield shift as compared to the signals of the neat ligand (Figure 22A). Likewise, only the C4, C5 and C6 peaks show up in ^{13}C NMR spectra, with the C4 being broadened due to the proximity of the paramagnetic metal ion (Figure 23a).

The H2, H3, C1, C2 and C3 peaks are so broadened that they essentially merge into the baseline. This points to stronger interaction between the carboxylate and the α– and β–OH groups, suggesting them to be the metal-ion binding sites. Nevertheless, the widening of the C4 peak renders the coordination of the C4–OH group also likely, in line with the finding for the Pr(III)–Gluc$^-$ system at the same pH[47]. As for Gal$^-$, the most displaced peak in the ^{1}H spectra of Gal$^-$ is the H4 signal and the most widened is the H2 (Figure 22B) under the same experimental conditions, suggesting that Gal$^-$ coordinates to Nd(III) mainly via the C2–OH and C4–OH functions. It is noteworthy that the binding of Nd(III) might be weaker than for Gluc$^-$, since also the peak of C2 is well-discernible in the ^{13}C spectra (Figure 23b). In the case of Gul$^-$, ^{1}H and ^{13}C NMR spectra (Figures 22C and 23c) indicate the coordination of COO$^-$, C2–OH and C3–OH groups.

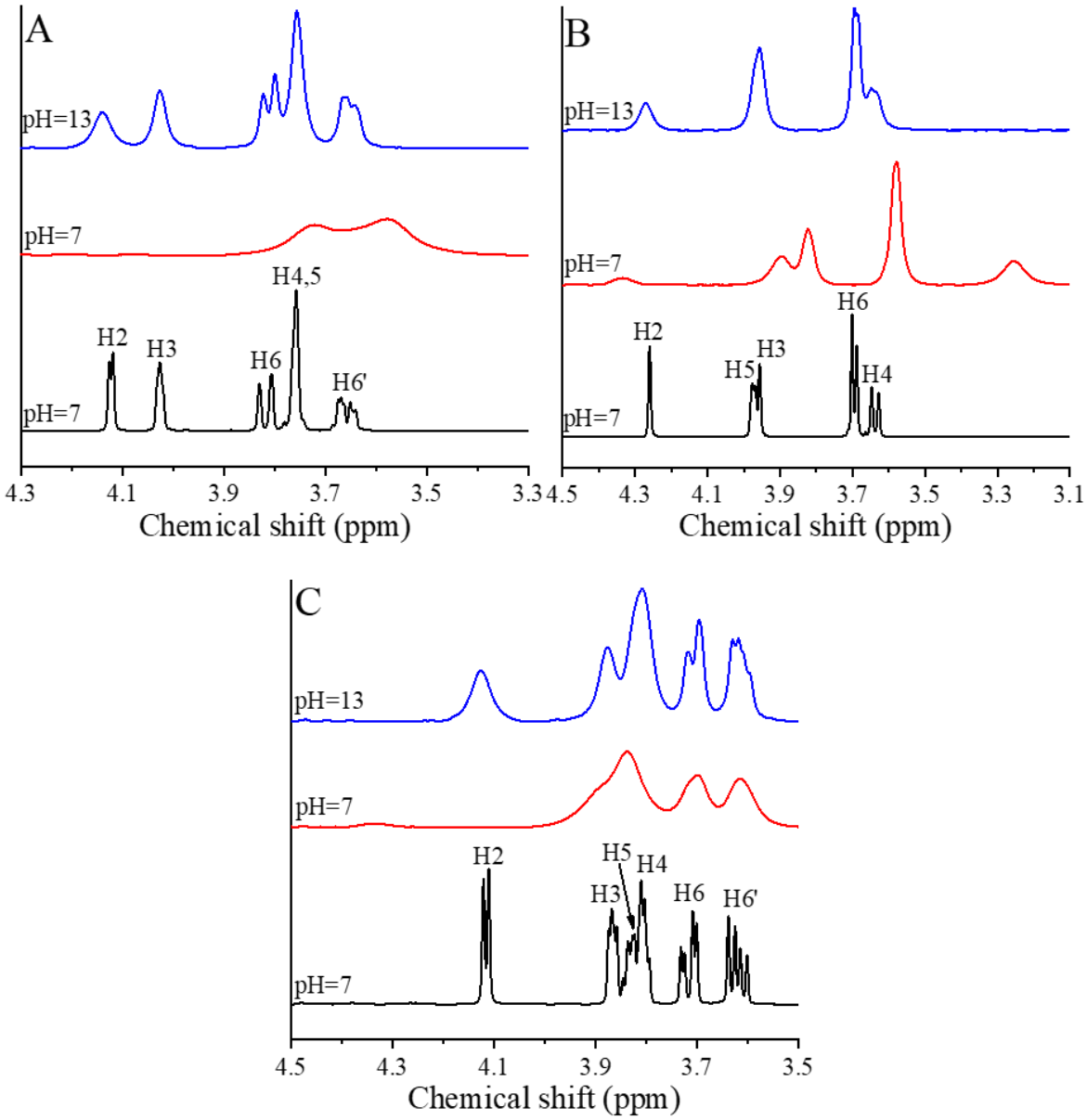

Figure 22. ^{1}H NMR spectra of samples containing 0.02 M Nd(III) and 0.20 M $Gluc^{-}$ (A), Gal^{-} (B) or Gul^{-} (C) at the indicated pH values in the presence of 10% V/V D_2O. Spectra of the neat ligand solutions at pH = 7 are plotted as well (black line) for comparison; the numbering corresponds to the adjacent carbon atoms, shown in Figure 21[116]

In summary, in neutral solutions Nd(III) is always bound by the carboxylate function, while the coordinating hydroxyl moieties differ depending on the ligand (α–hydroxyls take part in metal ion binding for all three ligands, with the additional coordination of the C3–OH ($Gluc^{-}$, Gul^{-}) and C4–OH ($Gluc^{-}$, Gal^{-}) moieties).

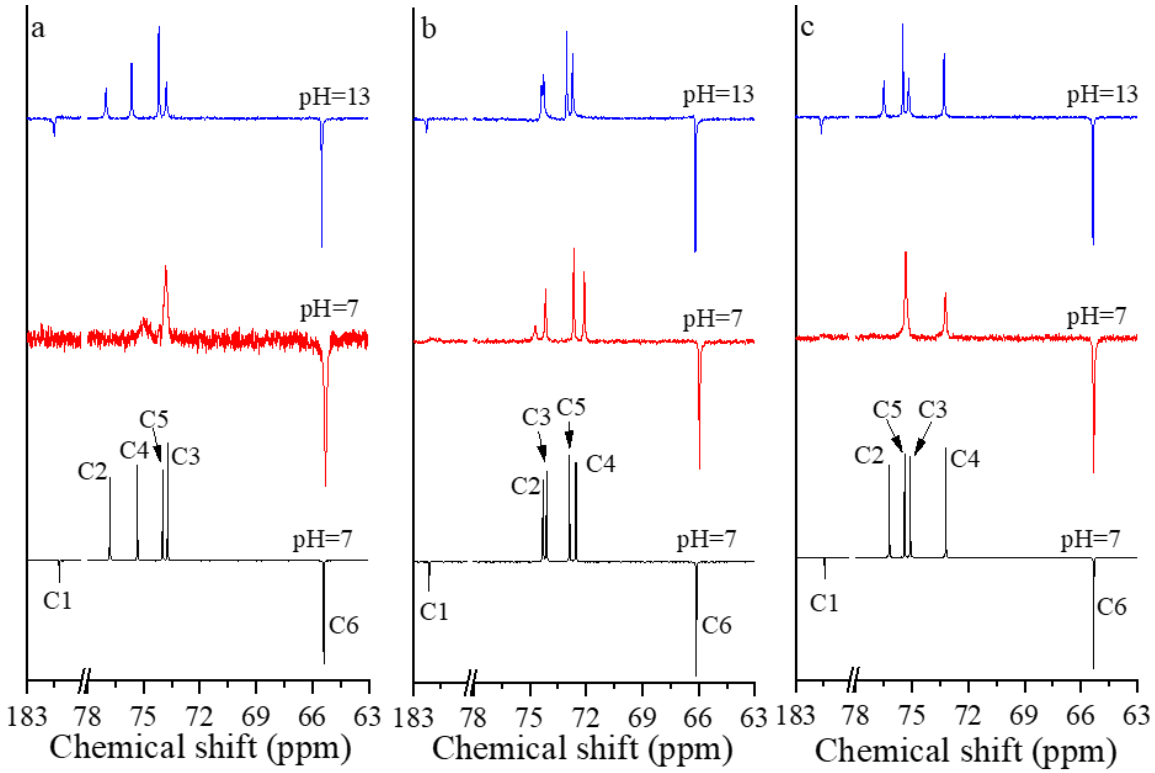

Figure 23. ^{13}C NMR spectra of samples containing 0.02 M Nd(III) and 0.20 M Gluc$^-$ (a), Gal$^-$ (b) or Gul$^-$ (c) at the indicated pH values in the presence of 10% V/V D_2O. Spectra of the neat ligand solutions at pH = 7 are plotted as well (black line) for comparison; the numbering corresponds to the adjacent carbon atoms, shown in Figure 21[116].

Upon increasing the pH to ~13, both the ^{1}H and ^{13}C NMR spectra undergo salient variations, as compared to the ones at pH ~7 (Figures 22 and 23). For instance, ^{13}C NMR spectra of solutions containing 0.020 M Nd(III) and 0.2 M Gluc$^-$ (Figure 24) show that the signals of C1, C2 and C3 appear again in the spectra and the half-width of all peaks decreases at higher pH. Essentially, the same effects are observed as earlier in the case of the Pr(III)–Gluc$^-$ system[31] which suggests that the metal-ligand interactions are significantly weaker, including the coordination of the carboxylate group[81,82].

As explained by Giroux et al., the exchange between the free and coordinated ligand slows down as pH is increased and signals of the free ligand are well-separated from those of complexed ligands which however disappear due to extreme broadening[31]. Assuming the limit of slow exchange, ligand's peak intensities should have the same ratios as those of the bare ligand at the same pH. However, the peak-widths of the ^{1}H signals are widened to a much smaller degree at pH = 13 as compared to neutral solutions, with peak positions similar to those of the neat ligand (see Figure 22). The ^{13}C NMR spectra show for all the three

ligands that the intensities unambiguously increase in the order of C1 < C2 < C3 < C4 < C5 < C6 (see Figures 24 and 25).

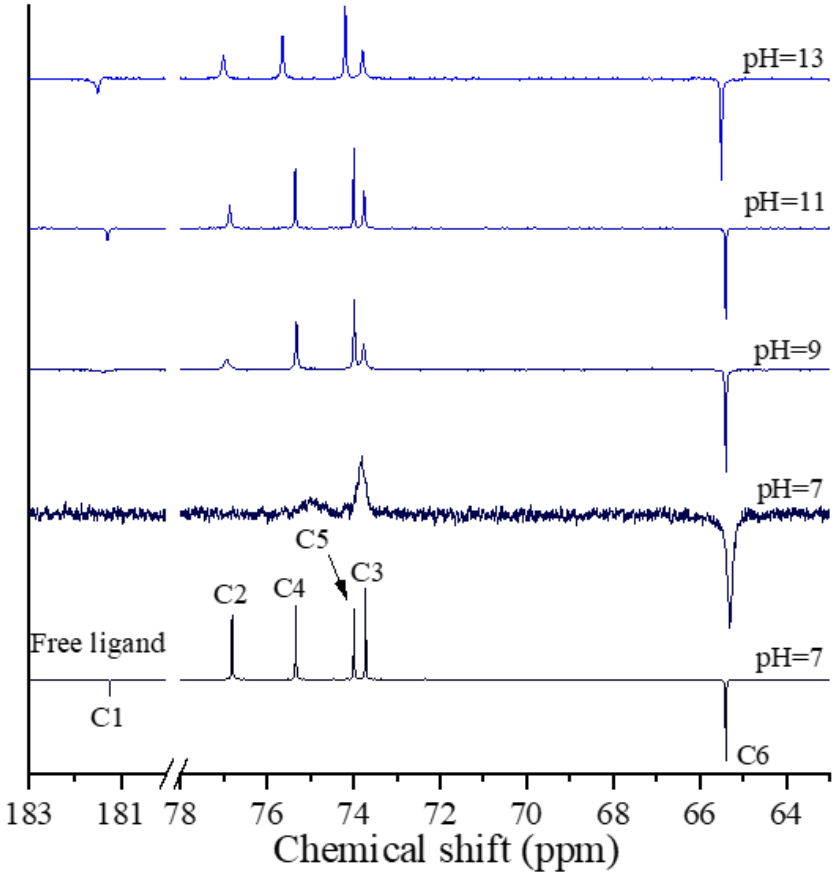

Figure 24. ^{13}C NMR spectra of samples containing 0.020 M Nd(III) and 0.200 M $Gluc^-$ at the indicated pH values (10 %V/V D_2O). The bottom spectrum corresponds to a neat 0.200 M NaGluc solution[116]

These observations strongly indicate that metal ions most likely interact only with the carboxylate group of the ligand, giving rise to the above ordering of intensities. This phenomenon can be elucidated in terms of metal-ligand separation: The further the carbon nucleus is from Nd(III), the higher its intensity becomes owing to the reduced influence of unpaired electrons (i.e. decreased broadening), which is not ligand-specific. (Note that the peak area of C1 is the lowest already for the neat ligand, which arises from the absence of an adjacent proton nucleus, resulting in a slower relaxation and thus lower intensity.)[28]. Likewise, the peaks' chemical shifts are very similar to those of the neat ligand, indicating again rather weak metal-ligand interactions.

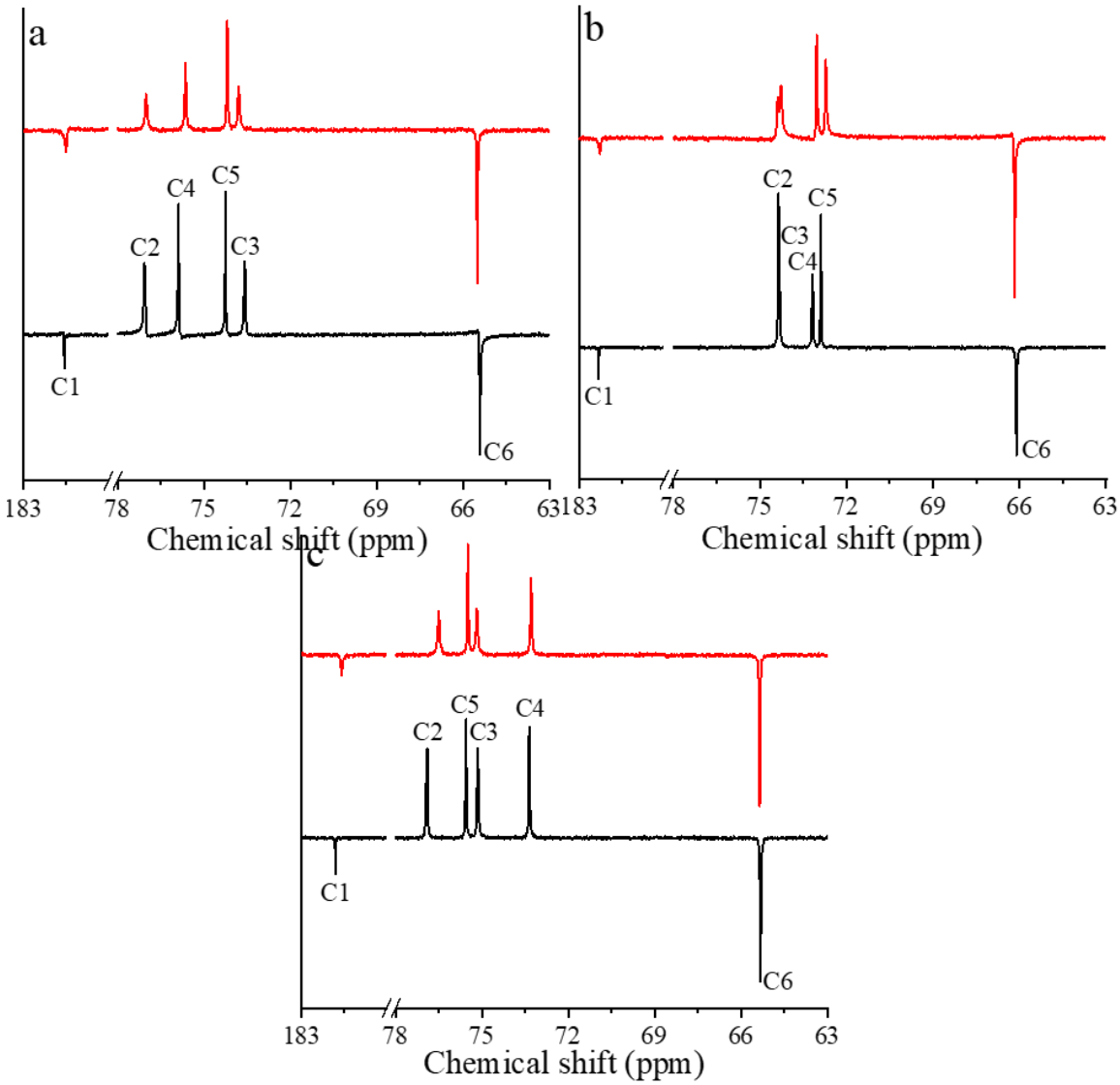

Figure 25. ^{13}C NMR spectra of samples containing 0.20 M $Gluc^-$ (a), Gal^- (b) or Gul^- (c) at pH = 13 in the presence of 10% V/V D_2O. black: the free ligand, red: Nd(III)-complex[116]

The weakening of metal ion coordination upon rising pH is unexpected, since simultaneous ligand deprotonation becomes more favorable. This contradiction can be resolved by assuming that the deprotonation takes place on the Nd(III)-bound water molecules[31,47,112] instead of the OH moieties of the ligand. This hints on that the gradual weakening of coordination is accompanied by the formation of outer-sphere complexes. Namely, the ligand does not coordinate directly to the metal ion but rather interacts with it mainly via electrostatic attraction.

In terms of hydrolysis the existence of these complexes elucidated as follows: even at pH ≈ 8, Nd(III) typically forms hydroxido complexes[117]. Water molecules coordinated to the metal ion undergo hydrolysis as pH increases, thereby weakening the binding between the

metal ion and the ligand. The latter is eventually displaced from the inner shell when pH becomes sufficiently high, resulting in the formation of an outer-sphere complex, which may be viewed as a ligand-stabilized $Nd(OH)_3(aq)$ species (see the proposed structures displayed in Figure 26). Other examples for this type of complex structure in the presence of $Gluc^-$ were proposed for Al(III)[117], Fe(III)[118] and Mg(II)[119].

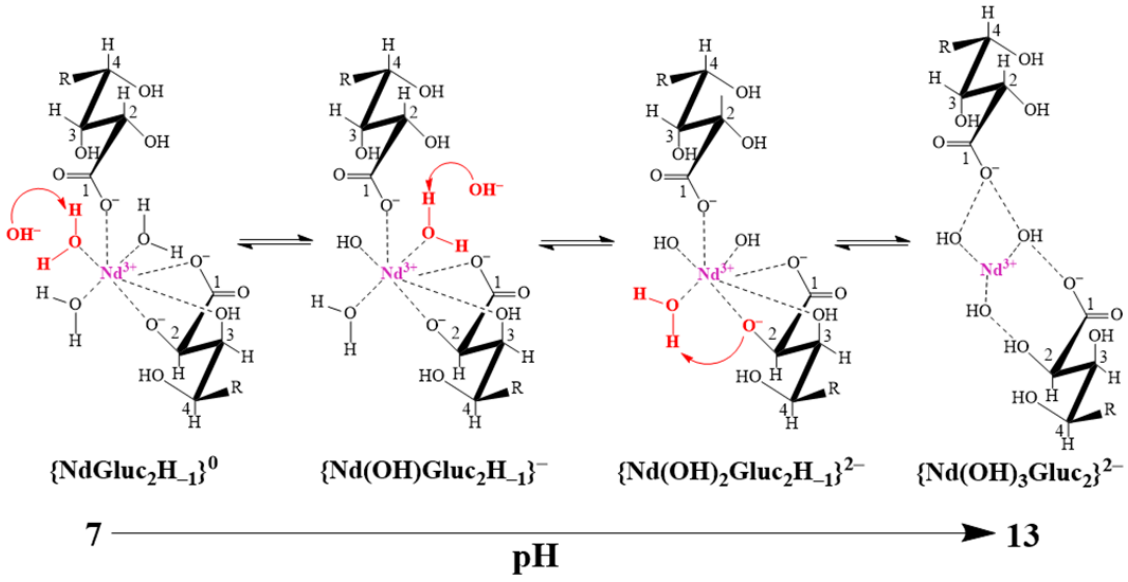

Figure 26. Proposed structure of binary Nd(III)–$Gluc^-$ complexes forming predominantly at pH > 10. Deprotonation and subsequent transition from inner- to outer-sphere complex for the $Nd_2Gluc_4H_{-6}^{4-}$ species. To have a better overview, only the monomeric units, $NdGluc_2H_{-3}^{2-}$ are shown in braces. The sites of proton displacement are highlighted in red and 'R' represents the terminal –C5HOH–C6H2OH moiety[116]

5.3.3. The effect of pH on the CD spectra of Nd(III)–Gluc⁻ complexes

CD spectroscopy is often employed for the investigation of optically active species. In Nd(III)–aldonic acid complexes, the lanthanide ion serves as the chromophore in the visible region (due to f-f transitions), while optical activity is provided by the coordinating ligand. When complexes are formed, intensive CD signals are detected in the UV-Vis region at ca. 350 nm, 520 nm, 580 nm, 670 nm and 740 nm, corresponding to the electronic transitions $^4I_{9/2} \rightarrow [^4D_{5/2}, {}^4D_{3/2}, {}^4D_{1/2}, {}^2I_{11/2}]$, $[^4G_{7/2}, {}^4G_{9/2}]$, $[^2G_{7/2}, {}^4G_{5/2}]$, $[^4F_{9/2}]$ and $[^4F_{7/2}, {}^4S_{3/2}]$, respectively. Among these, the hypersensitive transition of Nd(III) appears at ~570–585 nm, which exhibits high sensitivity to even minute changes in the inner coordination sphere of Nd(III)[120].

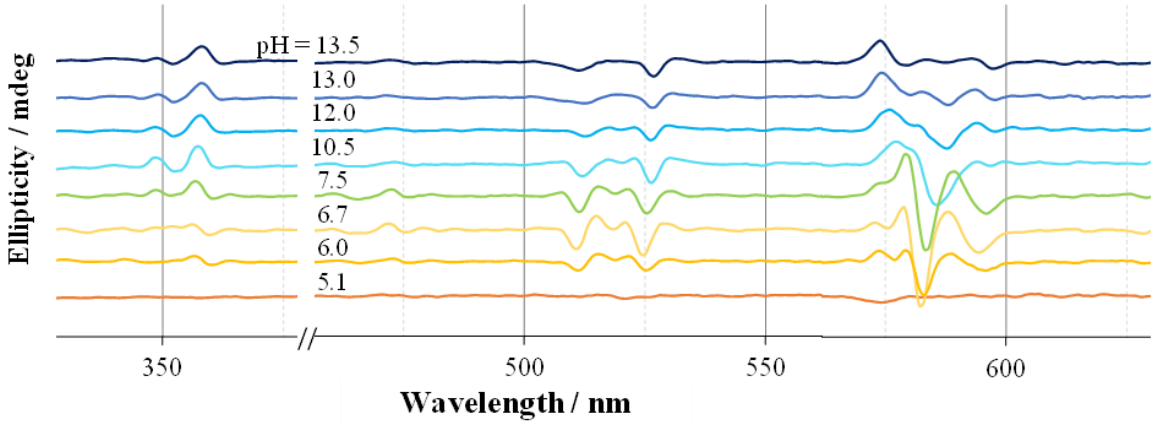

Figure 27. CD spectra of the Nd(III)–Gluc⁻ system containing 0.05 M Nd(III) and 0.20 M Gluc⁻ at the indicated pH values[116]

The first step was to collect CD spectra of solutions containing Nd(III) and Gluc⁻ at several different pHs. CD spectra recorded at fourfold ligand excess relative to metal concentration are shown in Figure 27. The observed CD signals at 575 nm are weak in contrast to strong Cotton effect detectable between pH = 6.0 and 7.5. Precipitation appearing in the pH range of 7.5–10.5 impeded collecting spectra in this region. Above this pH range solutions remain clear and the ellipticity becomes lower, while peaks at 525 and 580 in the negative region express a slight bathochromic shift. These differences attest a marked change in the optical activity affected by the change in chemical speciation induced by the increase in pH. Based on the weak Cotton effect at pH = 5.1, we assume that the hydroxyl moieties coordinating to Nd(III) are still protonated. The relation of the formation constants of Nd(III)-acetate and Nd(III)–Gluc⁻ species confirms this assumption. In spite of Gluc⁻ being

a weaker base than acetate, the mononuclear complexes of the former, $NdGluc^{2+}$, $NdGluc_2^{+}$ and $NdGluc_3^{0}$, are more stable than their acetate congeners; stability products of $Gluc^{-}$ complexes are higher by ca. 0.5 and 1.0 log units (see details in Table 9)[89,121,122]. This enhanced stability can be explained by assuming that in addition to COO^{-}, alcoholic functions also take part in coordination resulting in more stable chelate structures. On the other hand, lactate and α–hydroxy-isobutirate, which are monohydroxy carboxylates, form complexes which have stabilities comparable to their $Gluc^{-}$ analogues (the differences are most likely associated with the difference in ionic strength), in spite of $Gluc^{-}$ having four hydroxyl groups[123]. Therefore, it is not very likely that more than one hydroxyl moiety of $Gluc^{-}$ binds strongly to Nd(III) in the acidic range (pH = 2–5).

Table 9. Stability product (log β) of Nd(III) complexes forming with different hydroxycarboxylic acids (indicated as L^{-}) under the indicated conditions[116].

Ligand	Conditions	Stability products			Ref.
		NdL	**NdL_2**	**NdL_3**	
D-gluconic acid	25 °C, I = 1 M (NaCl)	2.44	4.32	5.46	89
acetic acid[a]	25 °C, I = 0.1 M (NaCl)	2.07	3.51	—	121
lactic acid[b]	25 °C, I = 0.2 M ($NaClO_4$)	2.65	4.44	5.37	122
α–hydroxyisobutiric acid[c]	25 °C, I = 0.2 M ($NaClO_4$)	2.74	4.42	5.98	122

Strong chiral perturbation can be observed in the spectra of the complexes registered at nearly neutral pH. CD bands of similar intensities were published for the Cu(II) and Pr(III)–$Gluc^{-}$ systems at neutral pH[18,47,124] as well. As pH is increased from 5.1 to 8.0, the speciation significantly changes in the Nd(III)–$Gluc^{-}$ system, as shown on the species distribution diagram (Figure 28), simulated based on the stability constants published by Kutus et al[89]).

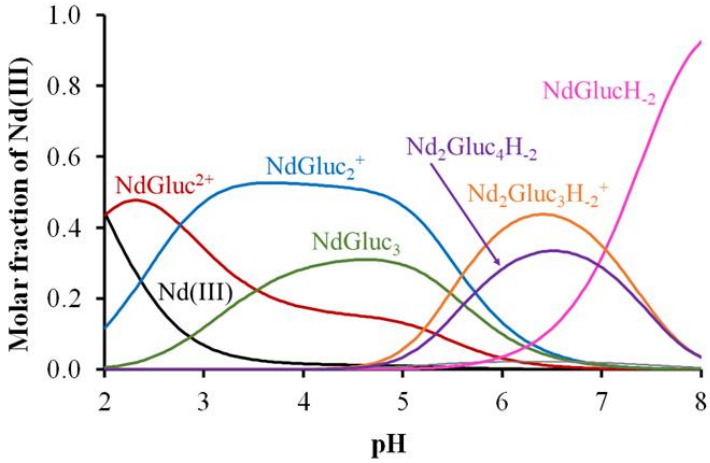

Figure 28. Distribution diagram computed for the Nd(III)–Gluc$^-$ 1 : 4 system on the basis of reported stability constants in Ref. 89. Experimental conditions: $[Nd(III)]_T$ = 0.020 M, l = 2 cm[116]

As the contribution of $NdGluc_2^+$ and $NdGluc_3$ to the Nd(III) speciation decreases above pH ~ 5.5, the $Nd_2Gluc_4H_{-2}^0$ and $Nd_2Gluc_3H_{-2}^+$ deprotonated binuclear species become dominant. Since the first pK_a for the hydrolysis of Nd(III) is ca. 8.0[74], deprotonation occurring on Nd(III)-bound water molecules is unlikely. Consequently, protons are displaced from one or two OH groups induced by metal ion coordination resulting in the formation of alcoholate group(s) which promote stronger interaction between Nd(III) and Gluc$^-$. This stronger interaction can explain the larger Cotton effect observed at neutral pH. In slightly acidic or neutral solutions Gluc$^-$ coordinating through an alkoxide function has been proposed earlier for Cu(II)[18], Al(III)[48] and Pr(III) as well for other lanthanides[124].

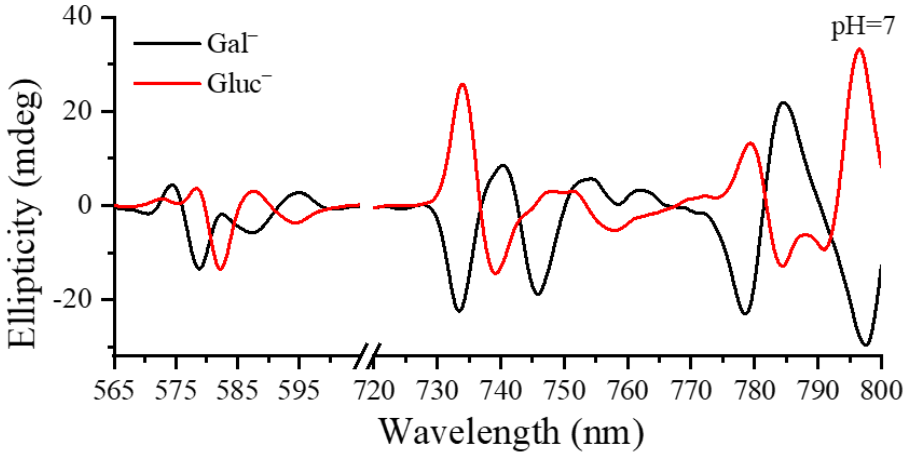

Figure 29. CD spectra of the Nd(III)–Gluc$^-$ and Nd(III)–Gal$^-$ systems containing 0.020 M Nd(III) and 0.200 M Gluc$^-$ or Gal$^-$, respectively, at pH = 7.0[116]

Comparing the spectra of $Gluc^-$ with those of Gal^-at pH = 7, it is seen that they are almost inverse of each other (Figure 29). Since the only difference between the two ligands is the configuration of the C4 carbon atom, the fashion of the two spectra indicates the C4–OH moiety to be involved in coordination[18,124]. It is noteworthy, that the two CD spectra are not identical, which reflects the effect of neighboring groups and differences in metal ion binding. Most importantly, NMR spectra suggest the coordination of the C3–OH group for $Gluc^-$ but not for Gal^- (Figures 22 and 23). As for Gul^-, the spectra are much more different from those of $Gluc^-$ and Gal^- (Figure 30), indicating an altered coordination environment, such as weak binding of the C4–OH of Gul^- moiety.

As pH is further increased from 10.5 to 13.5, the observed Cotton effect for Nd(III) complexation by $Gluc^-$ decreases; thus, chiral carbon moieties are less involved in the binding of Nd(III) ions. This is in line with the outcome of the NMR studies. (Alternatively, the weaker ellipticities may indicate that the newly formed complexes arranged spatially such that their net optical activity is reduced.) For the other two ligands, the observed decrease in ellipticities is similar as compared to that for $Gluc^-$. Moreover, the inversion of the signals for $Gluc^-$ and Gal^- observed at pH = 7 is not discernible in the basic pH range (see Figure 31).

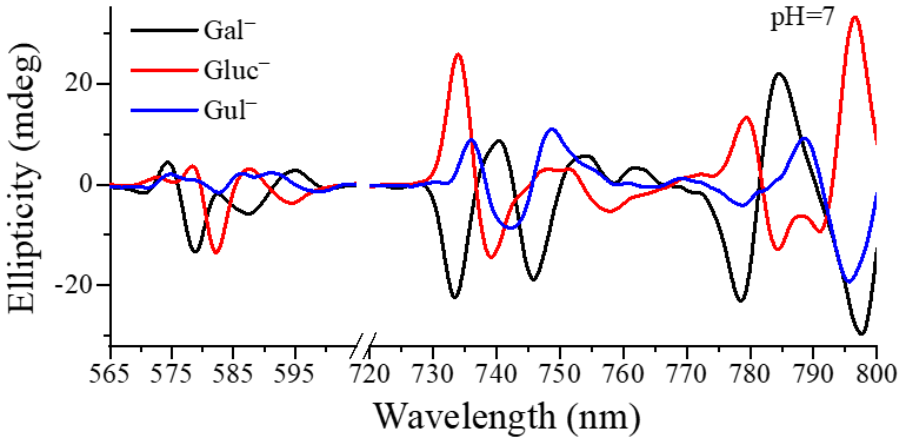

Figure 30. CD spectra of the indicated Nd(III)-aldonic acid 1:4 systems at pH = 7.0 (c_{Nd} = 0.02 M, l = 2 cm)[116]

These findings agree with the interpretation of the NMR spectra, which suggest the weakening of coordination between the metal and ligand (i.e. the increase of distance between Nd(III) and coordinating moieties) as pH is shifted to the strongly alkaline regime. Assuming that carboxylate becomes the main binding moiety, the sensitivity of CD spectra

induced by the coordination of optically active OH functions is largely lost, leading to a decrease in ellipticity.

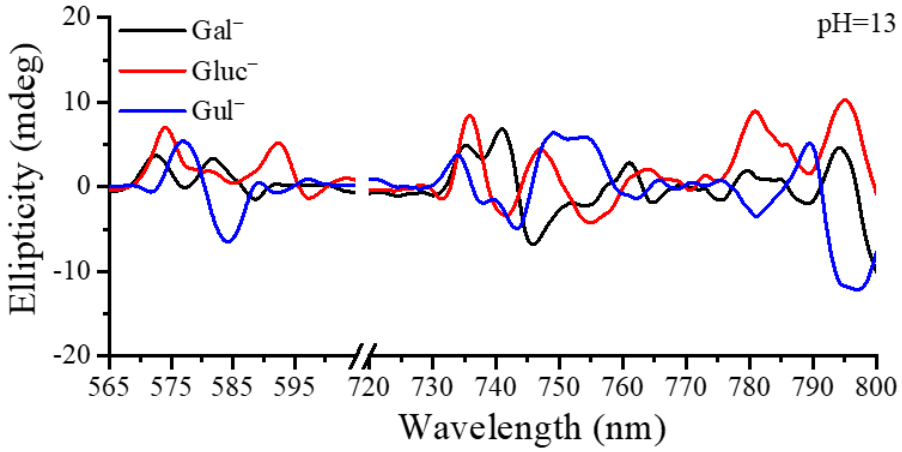

Figure 31. CD spectra of the indicated Nd(III)-aldonic acid 1 : 4 systems at pH = 13.0 (c_{Nd} = 0.02 M, l = 2 cm)[116]

5.4. Formation of Gluc⁻ complexes incorporating Ca(II) and Nd(III) ions

5.4.1. Equilibrium characterization of Ca(II)–Nd(III)–Gluc⁻ ternary complexes

In possession of the stability constants for the aqueous Ca(II)–Gluc⁻ [49,52] and Nd(III)–Gluc⁻ [89,112] complexes, we studied the equilibria in the ternary Ca(II)–Nd(III)–Gluc⁻ system to obtain an appropriate speciation model.

First, as in the case of the binary Nd(III)–Gluc⁻ system, systematic potentiometric measurements were carried out also via reverse titrations. Potentiometric data were collected at 0.05, 0.10 and 0.15 M Nd(III) concentrations while the Ca(II) and Gluc⁻ concentrations were varied (the concentrations are listed in Table 10). Measurements were performed twice; the thus obtained data show excellent reproducibility as demonstrated in Figure 32. It is seen that similarly to the binary system, the titration curves depend heavily on $[Nd(III)]_{T,0}$, while they can be further separated by $[Ca(II)]_{T,0}$ and $[Gluc^-]_{T,0}$, except for the lowest concentration of $NdCl_3$ (0.05 M).

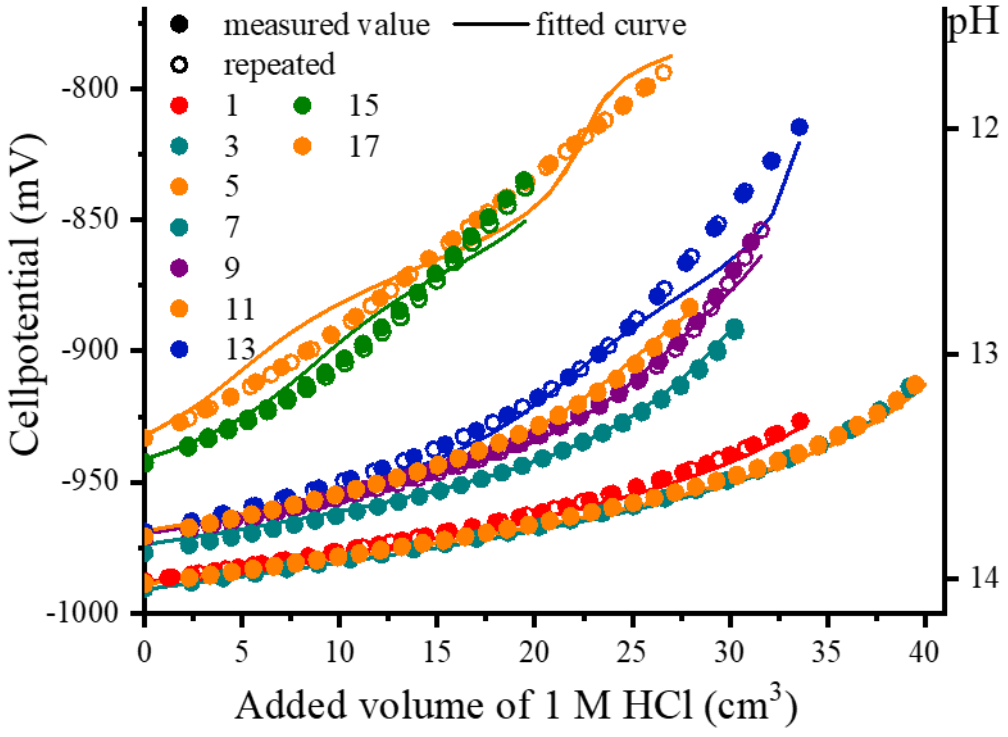

Figure 32. Titration curves of ternary Ca(II)–Nd(III)–Gluc⁻ systems fitted assuming only binary complex formation. Full circles indicate measured data, hollow ones are repetetion of measurements at the same initial total concentrations. Continuous lines are fitted data. Initial total concentrations of titrated samples and titrating HCl solution are shown in Table 10

This is well-reflected by simulation of the potentiometric data, assuming first only the formation of binary Nd(III)–Gluc$^-$ (Table 7) and Ca(II)–Gluc$^-$ complexes: Figure 32 demonstrates that this binary model describes the titrations satisfactorily at $[Nd(III)]_{T,0}$ = 0.05 M. At higher concentrations, however, the curves exhibit significant deviations between the measured and simulated data, especially below pH = 13. These differences are significantly larger than the expected experimental uncertainty of the measurements, providing sound evidence that complexes incorporating both Nd(III) and Ca(II) are formed.

Table 10. Initial total concentrations of samples and titrating HCl solution of all potentiometric measurements. Titrated volume was 70 mL in every case.

Sample	$[NdCl_3]_{T,0}$/M	$[NaGluc]_{T,0}$/M	$[CaCl_2]_{T,0}$/M	$[NaOH]_{T,0}$/M	c_{HCl}/M
1	0.0503	0.251	0.0761	0.802	1.007
2	0.0503	0.251	0.0761	0.802	1.007
3	0.0503	0.200	0.0406	0.802	1.007
4	0.0503	0.200	0.0406	0.802	1.007
5	0.0508	0.0150	0.0202	0.791	1.007
6	0.0508	0.0150	0.0202	0.791	1.007
7	0.101	0.300	0.0508	0.793	1.007
8	0.101	0.300	0.0508	0.793	1.007
9	0.101	0.400	0.0761	0.793	1.007
10	0.101	0.400	0.0761	0.793	1.007
11	0.101	0.402	0.102	0.803	1.007
12	0.101	0.402	0.102	0.803	1.007
13	0.101	0.500	0.127	0.793	1.007
14	0.101	0.500	0.127	0.793	1.007
15	0.152	0.600	0.156	0.789	1.007
16	0.152	0.600	0.156	0.789	1.007
17	0.151	0.750	0.203	0.7929	1.007
18	0.151	0.750	0.203	0.7929	1.007

To elucidate the stability and stoichiometry of such solution species, nonlinear fitting of potentiometric data was carried out using PSEQUAD, via including ternary complexes in the speciation model in addition to the binary ones. Nearly six hundred different complexes were tested during the fitting process in various combinations. It was found that complexes with a Ca(II):Nd(III) stoichiometric ratio of 3:1 provided very good description of all

titrations. In the next step, the model was further refined with the inclusion of the photometric spectra to obtain the simplest model with the least number of metal complexes.

To this end, matrix rank analysis calculations were performed on the spectrophotometric data, which resulted in a minimum number of ternary species of three. With the aid of this information, assuming the formation of the $Ca_3NdGlucH_{-6}^{2+}$, $Ca_3NdGluc_2H_{-7}^{0}$ and $Ca_3NdGluc_4H_{-4}^{+}$ complexes (in addition to the binary ones) was chosen as the final speciation model to describe strongly alkaline solutions containing Ca(II), Nd(III) and $Gluc^-$ ions. The fit is shown in Figure 33, whereas the corresponding stability constants are listed in Table 11.

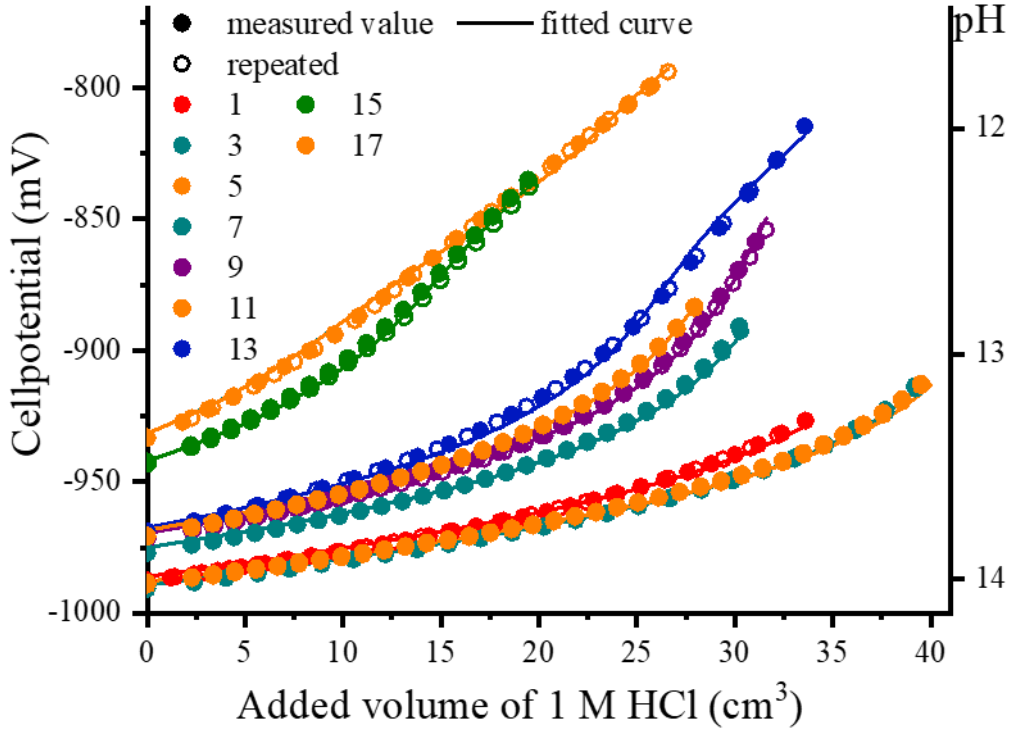

Figure 33. Titration curves of ternary Ca(II)–Nd(III)–$Gluc^-$ systems fitted assuming ternary complexes present

Table 11. Formation and stability constants of ternary Ca(II)–Nd(III)–$Gluc^-$ complexes.

Reaction	logβ	std. dev.
$3Ca(II) + Nd(III) + Gluc^- = Ca_3NdGlucH_{-6}^{2+} + 6H^+$	–59.75	0.01
$3Ca(II) + Nd(III) + 2Gluc^- = Ca_3NdGluc_2H_{-7}^{0} + 7H^+$	–72.09	0.02
$3Ca(II) + Nd(III) + 4Gluc^- = Ca_3NdGluc_4H_{-4}^{+} + 4H^+$	–34.99	0.02

While the hypersensitive transition of Nd(III) at 585 nm was found to be the most altered at pH = 8, it seems to be much less affected by complexation in strongly alkaline solutions. However, another peak at ~804 nm shifts to higher wavelengths significantly and its absorbance also increases as indicated in Figure 34. Given this sharp difference from the hypersensitive range sensitive to variations in the vicinity of Nd(III), the changes seen above 700 nm suggest the alteration of the outer coordination sphere of Nd(III). Molar absorption coefficients generated by PSEQUAD (Figure 35) show that the spectrum of $Ca_3NdGlucH_{-6}^{2}$ changes markedly upon binding of an additional ligand and simultaneous deprotonation yielding $Ca_3NdGluc_2H_{-7}^{0}$. It has to be noted that the $Ca_3NdGluc_4H_{-4}^{+}$ complex forms in higher amounts only below pH = 12 (see the distribution diagram in Figure 36), where only few data points could be collected due to precipitation. Therefore, the absorbance spectrum of this species could not be fitted with acceptable accuracy, hence it was treated as 'non-absorbing' complex.

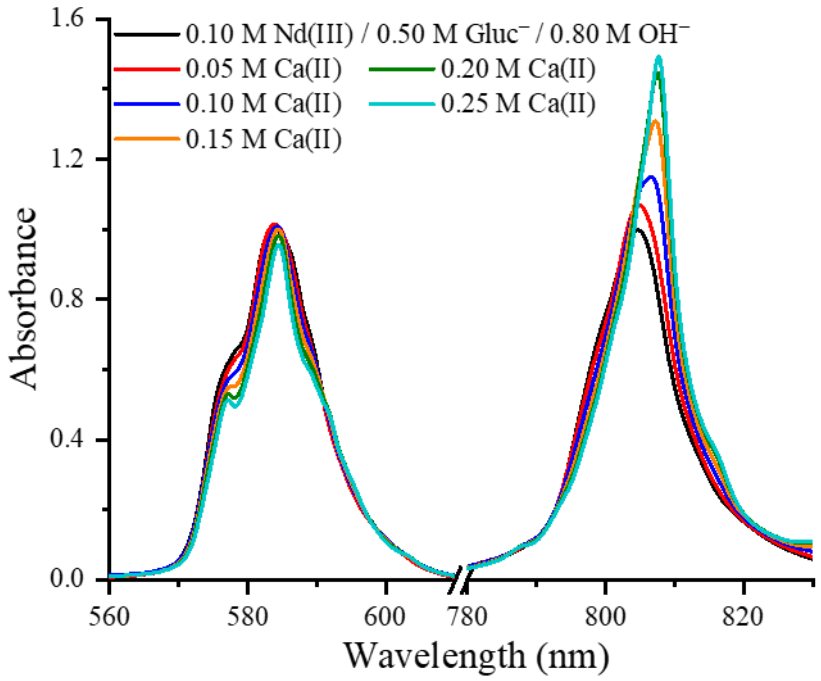

Figure 34. Visible spectra of ternary complexes increasing Ca(II) concentration

The distribution diagram based on the proposed model shows that at $[Nd(III)]_T$ = 0.050 M, $[Ca(II)]_T$ = 0.075 M and $[Gluc^-]_T$ = 0.250 M , ternary complexes are formed to a significant degree above pH ~ 11.5, reaching as high as 45% of $[Nd(III)]_T$ (Figure 36). As for the composition, the characteristic 3:1 Ca(II):Nd(III) molar ratio was previously found for the formation of the aqueous $Ca_3Nd(OH)_6^{3+}$ species, based on solubility

measurements[14]. Addition of a $Gluc^-$ yields the complex proposed in this work. It is likely that this species is formed via the binding of $Gluc^-$ to $Ca_3Nd(OH)_6^{3+}$.

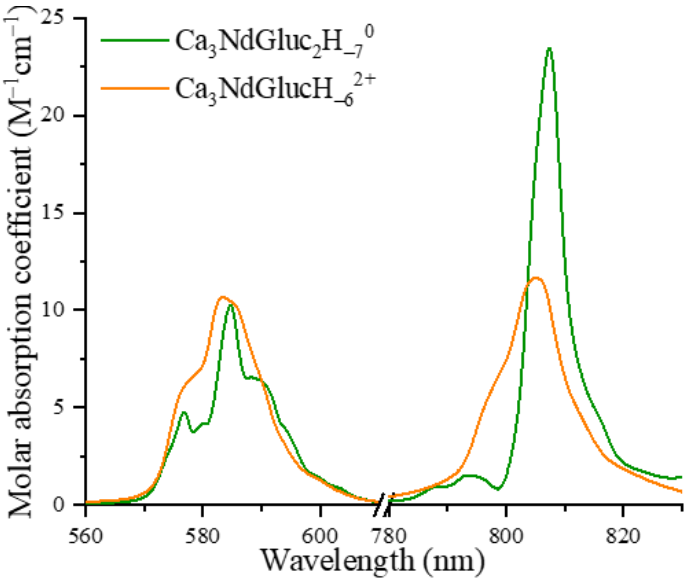

Figure 35. Molar absorptivities of species $Ca_3NdGluc^{2+}$ and $Ca_3NdGluc_2^0$

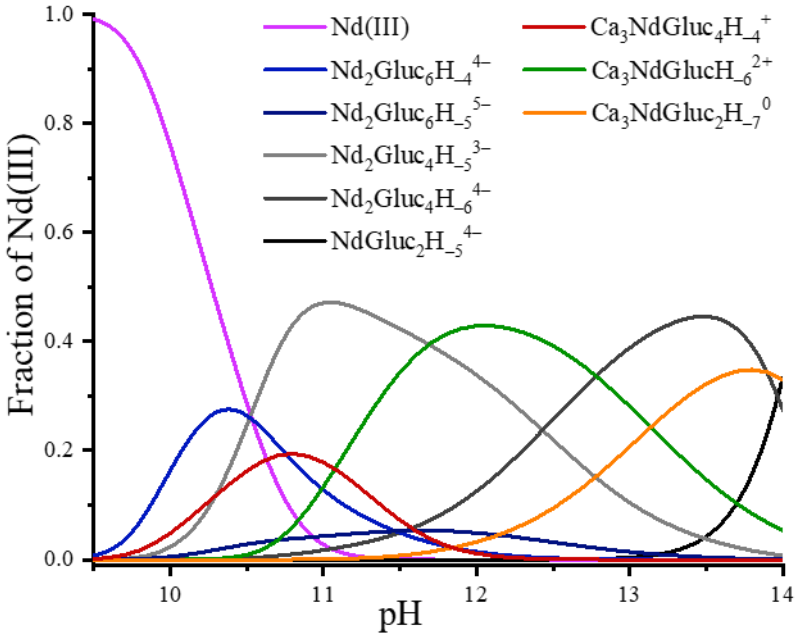

Figure 36. Distribution diagram of binary and ternary complexes in solution, at I = 4 M (NaCl) and 25 °C 0.050 Nd(III), 0.075 Ca(II), 0.250 $Gluc^-$

5.4.2. The effect of ternary complexes on the spectra of Gluc⁻

To gain structural information on the ternary complexes forming in strongly alkaline media, ^{1}H NMR spectra were recorded for solutions containing Gluc⁻ only and those containing Gluc⁻ and Nd(III); Gluc⁻ and Ca(II) or Gluc⁻, Nd(III) and Ca(II) at 0.5 M NaOH (Figure 37a). In the presence of Nd(III), the signals of the ligand are broadened owing to the vicinity of unpaired electrons. In the presence of Ca(II), however, peaks are not only broadened (arising from interactions with quadrupole Ca(II) nuclei), but there is another peak appearing at ca. 4.4 ppm. This additional signal appears as a result of the formation of Ca(II) complexes and the associated slowdown of ligand exchange. Such reduction of complexation dynamics stems most probably from metal ion induced deprotonation, where complex dissociation is slow due to metal ion alcoholate coordinative bonds.

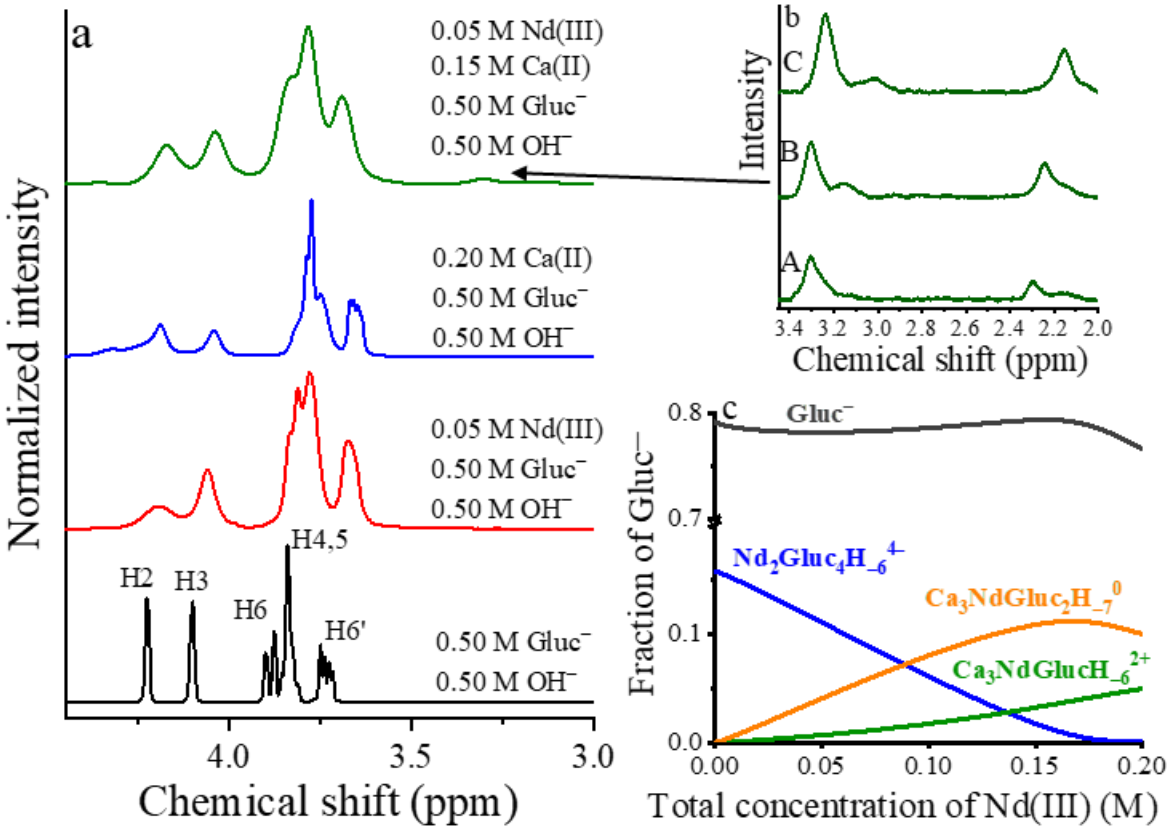

Figure 37. NMR spectra (a) of Ca(II)–Nd(III)–Gluc⁻, Ca(II)–Gluc⁻, Nd(III)–Gluc⁻ and Gluc⁻ solutions for comparison at ca. pH = 13.

Spectra A, B and C in the top right corner (b) belong to 0.100, 0.150 and 0.200 M Ca(II) concentrations. Distribution diagram of Gluc⁻ (bottom right, c) was generated assuming concentrations 0.050 M Nd(III), 0.500 M Gluc⁻, and 0.500 M OH⁻

When both metal ions are present, new peaks, different from those in the Ca(II)–$Gluc^-$ binary spectrum, show up between 2.0 and 3.4 ppm, indicating the formation of ternary Ca(II)–Nd(III)–$Gluc^-$ complexes. Upon increasing $[Ca(II)]_T$ from 0.10 to 0.20 M, the peak areas also increase (Figure 37b), consistent with slow chemical exchange between the free ligand and complex(es). This is indicative of slow ligand exchange, which is probably associated with the formation of strong metal ion alcoholate bonds as in the case of the Ca(II)–$Gluc^-$ binary system. These spectral variations are probably due to the formation of the $Ca_3NdGlucH_{-6}^{2+}$, $Ca_3NdGluc_2H_{-7}^{0}$ complexes, demonstrated by the distribution diagram in Figure 37c. Moreover, these 'ternary' signals are rather weak which is reflected by their low degree of formation, ca. 15% at $[Ca(II)]_T = 0.2$ M (Figure 37c). Nevertheless, the diagram suggests the absence of any binary Ca(II)–$Gluc^-$ complex which explains why its characteristic peak at ~4.4 ppm (Figure 37a) cannot be detected when Nd(III) is present.

Finally, it should be noted that the slow exchange is only discernible when Ca(II) ions are present, indicating that the alcoholate moieties formed are bound primarily to the Ca(II) ions, while the hydroxide complexes of Nd(III) ions are weekly interacting with the Ca(II)–$Gluc^-$ unit, in line with the results of NMR studies for the binary Nd(III)–$Gluc^-$ system. The assumption of the presence of deprotonated Nd(III) aqua ions is based on the fact that while $Gluc^-$ can only be twofold deprotonated when bound to Ca(II), the compositions of the ternary species suggest deprotonation to occur also on water molecules attached to Nd(III).

Comparing the ^{13}C and ^{1}H NMR spectra as a function of pH in both binary and ternary systems (Figure 38) shows that at pH = 8, all peaks but C1 appear in the presence of fourfold $CaCl_2$, contrary to Ca(II)-free solutions. This indicates the formation of Nd(III)–$Gluc^-$ binary species to be less pronounced, due to the high excess of Ca(II) ions forming binary Ca(II)–$Gluc^-$ rather than ternary species, such as $CaGluc^+$ and $CaGluc_2^0$ [16]. Upon increasing the pH, the differences become reversed: while all signals show up in the spectra of the binary system, C1 and C2 merge into the baseline while C3 is very broad for the ternary system, suggesting stronger interactions between Ca(II) and $Gluc^-$ ions. (Note that with Nd(III), only weak $Gluc^-$ bound metal-hydroxido species formed, see Chapter 5.3). In conclusion, the possible binding sites are the COO^-, C2–OH and the C3–OH (albeit to a lesser extent) moieties, as in the case for e.g. the trinuclear $Ca_3Gluc_2(OH)_4^0$ complex[52].

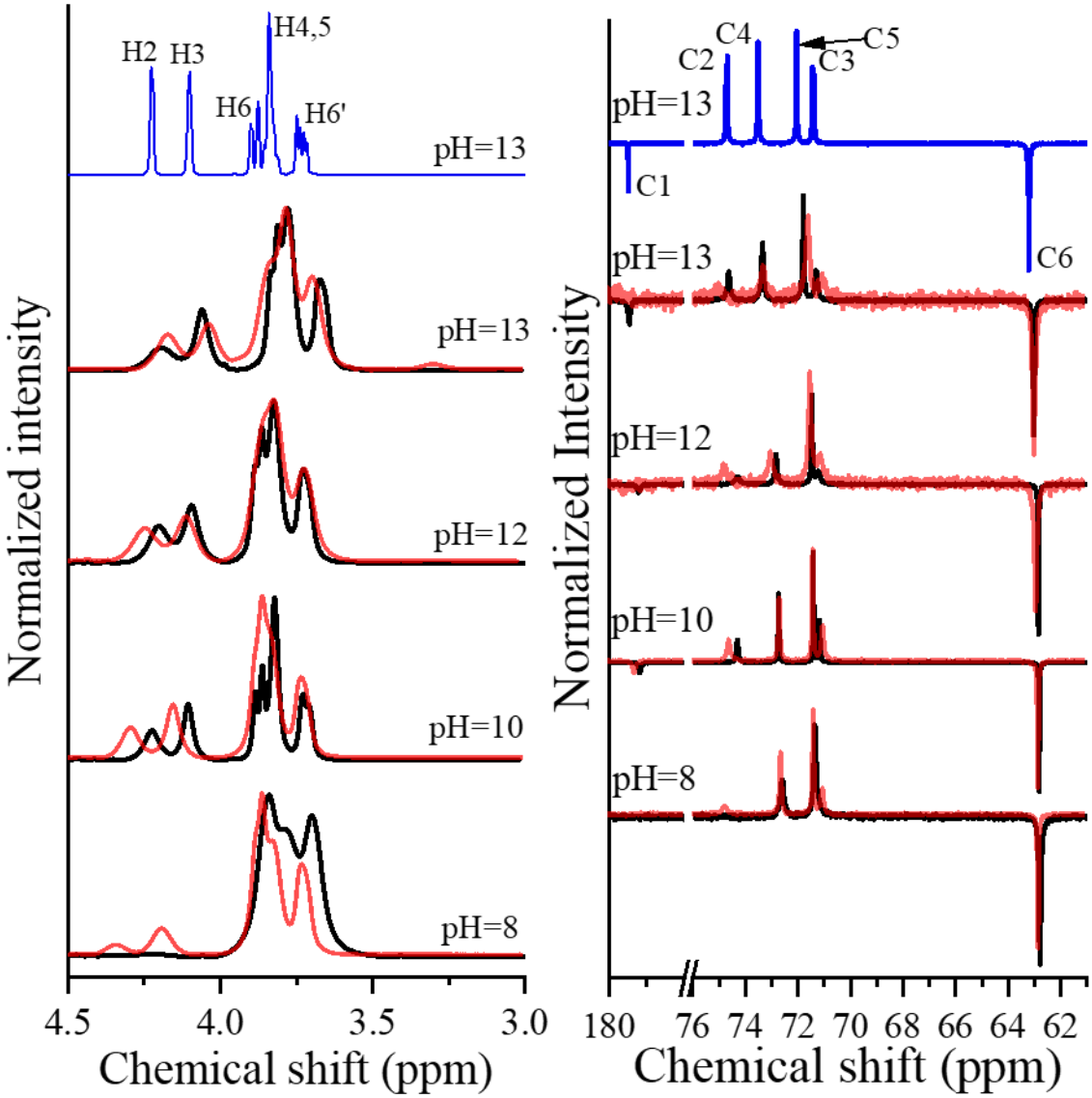

Figure 38. pH-dependent ^{1}H and ^{13}C NMR spectra of samples containing 0.050 M Nd(III) and 0.500 M $Gluc^{-}$ (black spectra) and 0.200 M Ca(II), 0.050 M Nd(III) and 0.500 M $Gluc^{-}$ (red spectra) at various pH values

Coordination of the OH groups are supported by the CD spectra too, since ellipticities are not expected to be as intense as those in Figure 39 when assuming coordination only through the carboxylate. Increasing $[Ca(II)]_T$ from 0.05 to 0.20 M, salient variations can be observed both in shape and magnitude, mostly above 700 nm, supporting the previous assumption that complexation mostly affects the outer-sphere of the coordination environment of Nd(III).

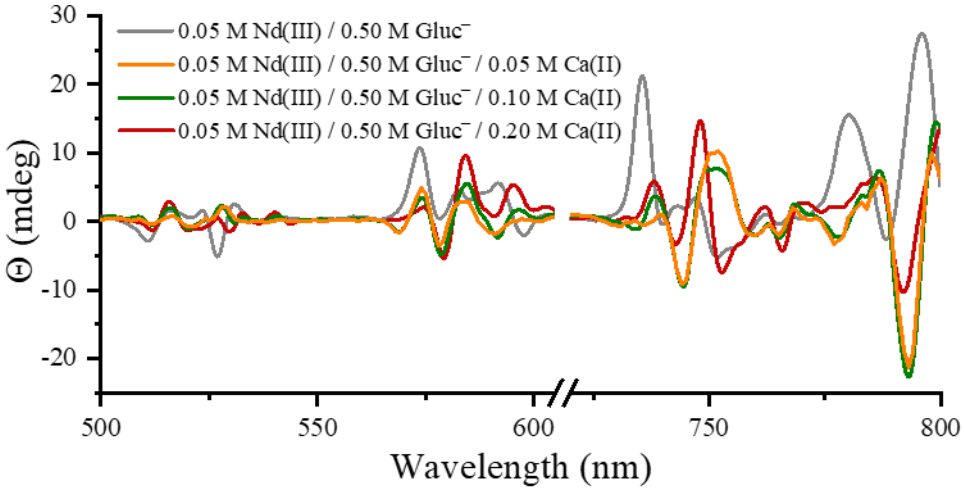

Figure 39. 0.050 M Nd(III), 0.500 M $Gluc^-$, and 0.500 M NaOH while Ca(II) concentration is increased. All samples have a pH of approximately 13.0

Interestingly, when $[Nd(III)]_T$ is increased, the shape of the spectra change only to a minor extent, while their magnitude increases proportionally to the Nd(III) concentration (Figure 40). This is demonstrated by the speciation diagram in Figure 41: albeit the fraction of $Ca_3NdGlucH_{-6}^{2+}$, $Ca_3NdGluc_2H_{-7}^{0}$ varies with $[Nd(III)]_T$, their sum remains ~100%.

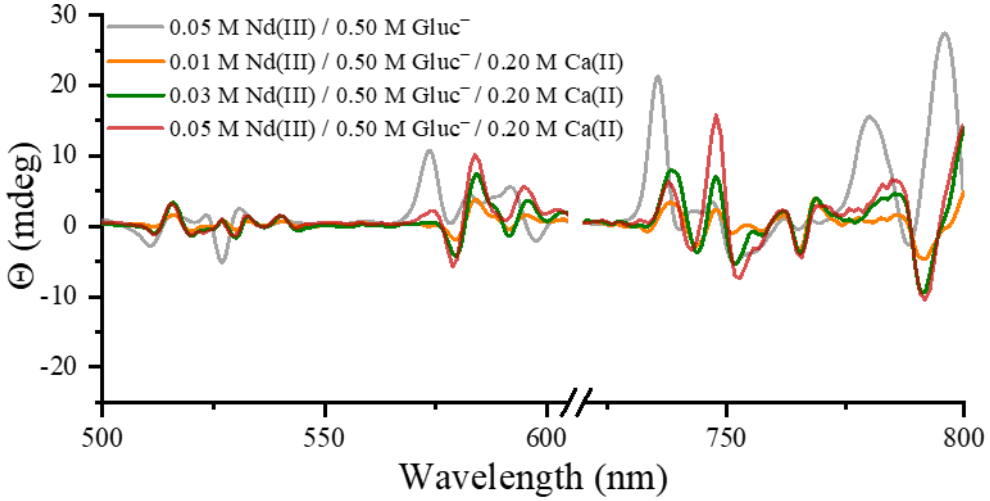

Figure 40. 0.200 M Ca(II), 0.500 M $Gluc^-$, and 0.500 M NaOH, the concentration of Nd(III) was increased. All samples have a pH of approximately 13.0

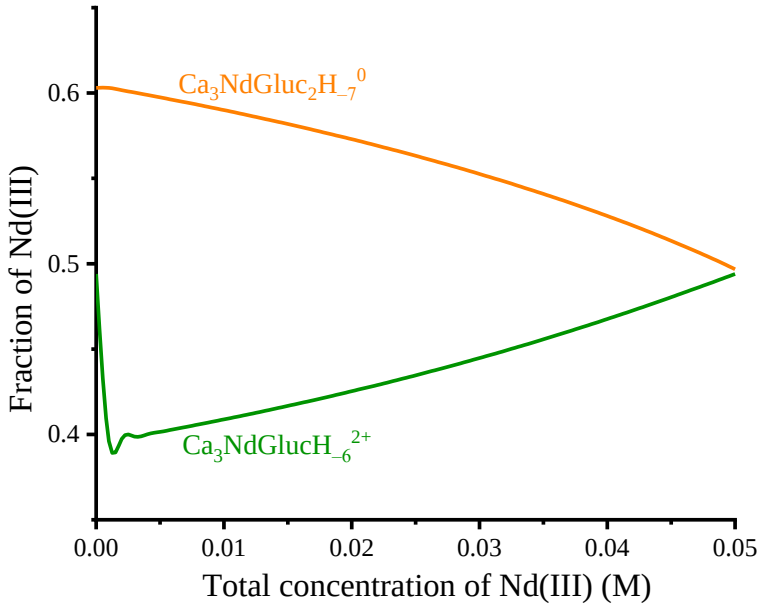

Figure 41. Distribution diagram of Nd(III) as a function of total concentration of Nd(III) at total concentrations 0.200 M Ca(II), 0.500 M $Gluc^-$, 0.500 M OH^-

In conclusion, based on NMR and CD results, we propose that concerning Nd(III) binding, the same process takes place in the ternary system as in the binary one in alkaline media. Nd(III) is likely to be kept in solution in its hydroxide form, via $Gluc^-$ coordinating through primarily its carboxylate moiety, and its OH groups to a lesser extent. We hypothesize that either the Ca(II)–$Gluc^-$ complexes described by Pallagi et al.[52] sequester Nd(III) (at a pH high enough, partially present in hydroxide form, $NdOH^{2+}$ or $Nd(OH)_2^+$), or $Gluc^-$ coordinates to a mixed hydroxide, such as $Ca_3Nd(OH)_6^{3+}$ as reported by Neck et al.[30]), which eventually inhibits the precipitation of $Nd(OH)_3$.

5.4.3. How solubility of Nd(III) is affected by complexation of $Gluc^-$ in conditions characteristic to radioactive repositories

Having both the binary and ternary systems characterized, the obtained thermodynamic models were applied to simulate the complex formation in conditions characteristic to radioactive waste disposals, assuming $Nd(OH)_3$ as the solid phase. In Figure 42 it is seen that addition of 0.01 M $Gluc^-$ barely alters the solubility of Nd(III). Conversely large increase in the solubility occurs in the presence of 0.25 M Ca(II), due to the formation of Ca(II)–Nd(III)–OH^- hydroxide complexes. When again 0.01 M $Gluc^-$ is added, the changes are minor, which is due to the exclusive formation of Ca(II)–$Gluc^-$ binary complexes: at a molar ratio of Ca(II):$Gluc^-$ = 25:1 and still very low $[Nd(III)]_T$ of ~10^{-6} M, $Gluc^-$ is almost exclusively bound by Ca(II) ions, as depicted in the corresponding speciation diagram in Figure 43.

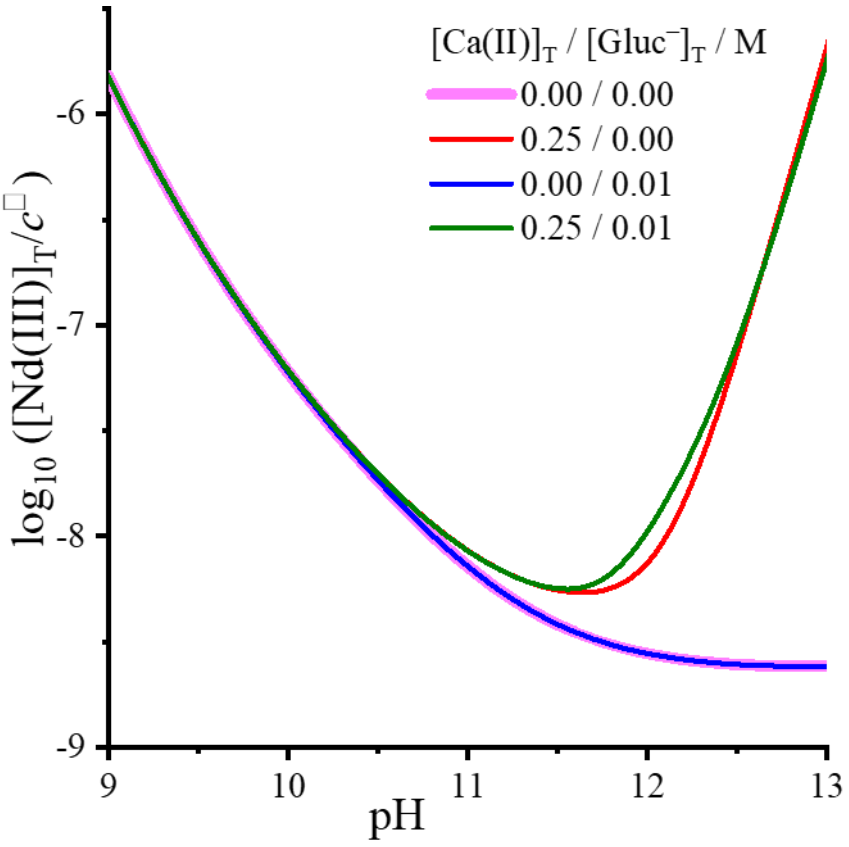

Figure 42. Simulated solubility curves of total dissolved Nd(III) showing the logarithm base ten of the total concentration of Nd(III) in solution in the presence of Ca(II) and $Gluc^-$ in concentrations typical to radioactive repositories compared to when only Nd(III) is present in the system (depicted in magenta)

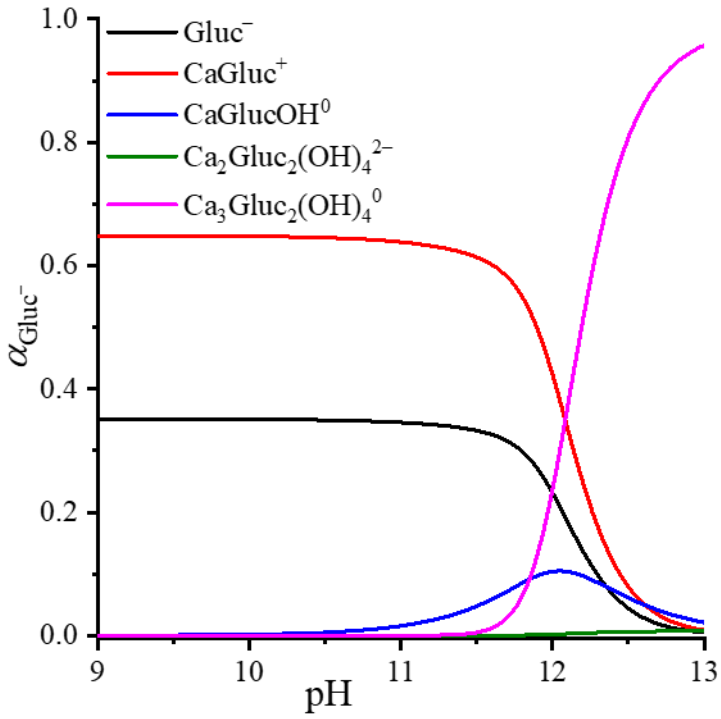

Figure 43. Distribution diagram of Ca(II)–$Gluc^-$ complexes forming in a ternary system when assumed concentrations are characteristic to radioactive disposal sites (high Ca(II) and low $Gluc^-$ concentration in alkaline media)

In conclusion, although Ca(II) itself can enhance the solubility of Nd(III) and related actinides markedly, the presence of $Gluc^-$ seems not to alter the solubility of Nd(III) under the conditions as a result of negligible formation of Nd(III)–$Gluc^-$ binary and Ca(II)–Nd(III)–$Gluc^-$ ternary complexes.

6. Conclusion

Precipitates appearing in the binary Nd(III)–$Gluc^-$ and ternary Ca(II)–Nd(III)–$Gluc^-$ systems have been isolated and investigated. Based on elemental analysis their composition and stoichiometry were determined as follows:

$$NdGlucH_{-1}(OH)\cdot 2H_2O \text{ and } CaNdGlucH_{-1}(OH)3\cdot 2H_2O$$

FT-IR and Vis-DRS measurements point out that there is no significant structural difference between the structure of the ternary and binary solids. This suggests that Nd(III) is bound by the carboxylate moiety while hydroxyl functions are more likely to coordinate to Ca(II) when it is present. Comparison between the molar absorptivity spectrum of the solvated $NdGlucH_{-2}(aq)$ complex and the Vis-DR spectrum of the $NdGlucH_{-1}(OH)\cdot 2H_2O$ precipitate shows that the chemical environment of Nd(III) is identical in these two complexes. Kutus et al. reported that in the forming $NdGlucH_{-2}(aq)$ complex Nd(III) is bound by the β–alcoholate and by the carboxylate of $Gluc^-$. Further six water molecules coordinate to Nd(III) one of which is deprotonated, meaning that the water soluble species $NdGlucH_{-2}(aq)$ is a mixed-hydroxo complex of Nd(III). We assume that upon precipitation the structure does not change significantly resulting in the solid complex having an identical structure, except that IR-spectra suggest the binding mode of the carboxylate is likely to be bidentate, while monodentate coordination was assumed for the solution species based on DFT calculations.

Collected spectra attest to the coordination sphere being very similar in the two solid complexes $NdGlucH_{-1}(OH)\cdot 2H_2O$ and $CaNdGlucH_{-1}(OH)_3\cdot 2H_2O$ suggesting that the binding of Ca(II) takes place remotely from the Nd(III) center. This provides explanation for how the presence of Ca(II) in the complex has only a slight influence on the DR spectra. It is likely that Ca(II) forms an outer-sphere complex with the $NdGlucH_{-1}(OH)\cdot 2H_2O$ and is bound by deprotonated alcoholic functions.

While precipitation occurs in pH = 8–10 range even at metal to ligand ratios as high as 1:5, at pH > 10 Nd(III)–$Gluc^-$ aqueous solutions remain clear, precipitate free. For this reason, reverse potentiometric titrations were performed and pH of samples for spectrophotometry were adjusted as required. However, depending on the total concentrations the pH limit of solubility varies, and samples close to pH = 10 often became cloudy therefore spectrophotometric data is absent in this narrow range because these

measurements were omitted during evaluation. Matrix Rank Analysis of Vis spectra suggest that at least three colored species exist in the binary system.

The Vis spectra of the Nd(III)–$Gluc^-$ samples do not express significant shifts in highly alkaline media but when spectrophotometric and potentiometric data are evaluated together, complex formation in the Nd(III)–$Gluc^-$ system can be accurately described. Simultaneous fitting of collected Vis spectra and potentiometric curves was carried out using PSEQUAD. Several complexes with various stoichiometries were tried in different combinations; however, employing only mononuclear complexes never resulted in an adequate fit. On the contrary, simulating measured data using a model containing only the two binuclear $Nd_2Gluc_4H_{-5}^{3-}$ and $Nd_2Gluc_4H_{-6}^{4-}$ complexes provided minimal deviations between measured and simulated data. The final model suggests the formation of four binuclear and one mononuclear species ($Nd_2Gluc_4H_{-5}^{3-}$, $Nd_2Gluc_4H_{-6}^{4-}$, $Nd_2Gluc_6H_{-4}^{4-}$, $Nd_2Gluc_6H_{-5}^{5-}$ and $NdGluc_2H_{-5}^{4-}$) confirming the presence of polynuclear complexes.

Further measurements were carried out to investigate the coordination properties of $Gluc^-$ towards Nd(III). For this, Gul^- and Gal^- were investigated alongside $Gluc^-$ since they are stereoisomers of each other (Gal^- being an enantiomer pair of $Gluc^-$ having a different configuration at C4 and Gul^- having opposite configuration on C2 and C5 compared to $Gluc^-$). Coordination characteristics were studied *via* NMR and CD measurements. While these results show that the carboxylate group plays an essential role in complexation, further coordination of hydroxyl or alkoxide groups at pH $\geq$ 5 can not entirely be excluded. While NMR spectra firmly suggest coordination between the carboxylate moiety and not negligible coordination of other hydroxyl functions, CD results attest to the coordination of C4–OH is predominant in the case of $Gluc^-$ and Gal^- to other hydroxyl moieties in neutral solutions. Based on NMR and CD results we propose that as pH increases the carboxylate function becomes the main binding site and water molecules coordinated to Nd(III) go through stepwise deprotonation eventually resulting in a complex in which mixed hydroxides of Nd(III) or $Nd(OH)_3$ itself are kept in solution by coordinating $Gluc^-$.

Similarly to the binary system a model for Ca(II)–Nd(III)–$Gluc^-$ aqueous equilibria was constructed based on potentiometric and spectrophotometric data. First, only potentiometric curves were simulated by PSEQUAD, taking into consideration the results of the Matrix Rank Analysis that suggested at least three ternary complexes in the system. Then, a few models chosen via fitting of potentiometric data were evaluated together with Vis spectra. While a few models were equally adequate to describe the system we chose the one which was chemically most reasonable. Because three to one ratio of Ca(II):Nd(III) was

a recurring attribute to complexes during evaluation the final model consists of $Ca_3NdGluc^{2+}$, $Ca_3NdGluc_2^{0}$ and $Ca_3NdGluc_4^{+}$ complexes and data simulated using this model are in good agreement with experimental values. NMR and CD results support the formation of ternary complexes in the system and suggest a tendency similar to what was observed in the case of binary complexes. Based on ^{13}C and ^{1}H NMR results, the possible binding sites of $Gluc^-$ in ternary complexes are the COO^-, C2–OH and the C3–OH moieties.

Constructed models of the Ca(II)–$Gluc^-$, Nd(III)–$Gluc^-$ and Ca(II)–Nd(III)–$Gluc^-$ systems were utilized in a simulation of complex formation assuming conditions characteristic to radioactive waste repositories. The results show that $Gluc^-$, typically present in low concentration is not a high risk factor since both the formation of Nd(III)–$Gluc^-$ and Ca(II)–Nd(III)–$Gluc^-$ complexes fall behind the formation of Ca(II)–$Gluc^-$ ones. Interestingly, in the absence of $Gluc^-$ Ca(II) does increase the solubility of Nd(III) probably through the formation of mixed hydroxides. In conclusion, while binuclear Nd(III)–$Gluc^-$ complexes and ternary Ca(II)–Nd(III)–$Gluc^-$ complexes do form in more concentrated solutions, in matrices characteristic to radioactive waste disposal sites their existence does not mean a significant risk.

7. Összefoglalás

A Nd(III)–Gluc$^-$ és a Ca(II)–Nd(III)–Gluc$^-$ rendszerekben képződő csapadékokat reprodukálhatóan leválasztottuk és jellemzésükre további méréseket végeztünk. Elemanalízis alapján a csapadékok összetételét és sztöchiometriáját meghatároztuk, és alább összefoglaltuk:

$$NdGlucH_{-1}(OH)\cdot 2H_2O \text{ és } CaNdGlucH_{-1}(OH)_3\cdot 2H_2O$$

Az FT-IR és DR mérések alapján nincs jelentős szerkezeti különbség a terner és a biner rendszerekből leváló szilárd anyagok között. Ez arra utal, hogy a Gluc$^-$ elsődlegesen a karboxilát csoportján keresztül koordinálódik a Nd(III)-hoz, míg a Ca(II) jelenléte esetén a hidroxil funkciók a Ca(II)-hoz koordinálódnak. Az oldatban képződő $NdGlucH_{-2}(aq)$ komplex látható moláris abszorbancia spektrumának és a $NdGlucH_{-1}(OH)\cdot 2H_2O$ csapadék diffúz-reflektancia spektrumának hasonlósága azt mutatja, hogy a két komplexben a Nd(III) kémiai környezete azonos. Kutus és munkatársai által közölt publikáció szerint a $NdGlucH_{-2}(aq)$ komplexben a Nd(III) a β–alkoholát funkciós csoporthoz és a Gluc$^-$ karboxilátjához kötődik. Ezen felül hat vízmolekula koordinálódik a Nd(III)-hoz, amelyek közül az egyik deprotonált, ami azt jelenti, hogy a vízoldható $NdGlucH_{-2}(aq)$ a Nd(III) vegyes hidroxido-komplexe. Feltételezhető, hogy a kicsapódáskor a komplex szerkezete nem változik jelentősen, vagyis a szilárd komplex közel azonos szerkezetű azzal a kivétellel, hogy az IR-spektrumok alapján a karboxilát kötési módja valószínűleg bidentát, míg az oldatban monodentát koordinációt feltételeztünk a DFT-számítások alapján.

A felvett spektrumok alapján a koordinációs szféra nagyon hasonló a két szilárd $NdGlucH_{-1}(OH)\cdot 2H_2O$ és $CaNdGlucH_{-1}(OH)_3\cdot 2H_2O$ komplexben, ami arra utal, hogy a ligandum a Ca(II)-ot a Nd(III)-tól távolabb köti meg. Ez magyarázat arra, hogy a Ca(II) jelenléte miért csak csekély mértékben befolyásolja a DR spektrumot. Valószínű, hogy a Ca(II) az $NdGlucH_{-1}(OH)\cdot 2H_2O$ szilárd komplexszel külsőszférás komplexet képez, és alkoholát funkciós csoportokhoz kötődik.

Míg a pH = 8–10 tartományban még 1:5 fém-ligandum arány esetén is megjelenik a csapadék, addig, ha fennáll a pH > 10 feltétel, a Nd(III)–Gluc$^-$ vizes oldatok csapadékmentesek maradnak. Ezért a potenciometriás titrálásokat visszatitrálásos módszerrel végeztük el, és a spektrofotometriás minták pH-ját szintén szükség szerint állítottuk be. Az oldhatóság pH-határa azonban a teljes koncentrációktól függően változik, és a pH = 10 közelében lévő minták gyakran zavarossá váltak, ezért ebben a szűk

tartományban hiányoznak a spektrofotometriai adatok - ezeket az eredményeket az értékelés során elhagytuk. A látható spektrumok mátrixrang-analízise arra utal, hogy legalább három színes részecske van jelen a biner oldatokban.

Az Nd(III)–$Gluc^-$ minták látható spektrumain a csúcsok nem tolódnak el jelentősen erősen lúgos közegben, de ha a spektrofotometriai és potenciometriás adatokat együttesen értékeljük, a komplexképződés az Nd(III)–$Gluc^-$ rendszerben pontosan leírható. Az összegyűjtött látható spektrumok és potenciometriás görbék egyidejű illesztését a PSEQUAD segítségével végeztük el. Számos különböző sztöchiometriájú komplexet próbáltunk ki különböző kombinációkban; azonban csak egymagvú komplexek illesztése nem eredményezett megfelelő egyezést a mért és számolt adatsorok között. Ezzel szemben a mért adatok szimulálása egy olyan modellel, amely csak a két kétmagvú $Nd_2Gluc_4H_{-5}^{3-}$ és $Nd_2Gluc_4H_{-6}^{4-}$ komplexet tartalmazta, minimális eltérést mutatott a mért és a szimulált adatok között. A végső modell négy kétmagvú és egy egymagvú részecske ($Nd_2Gluc_4H_{-5}^{3-}$, $Nd_2Gluc_4H_{-6}^{4-}$, $Nd_2Gluc_6H_{-4}^{4-}$, $Nd_2Gluc_6H_{-5}^{5-}$ és $NdGluc_2H_{-5}^{4-}$) képződését feltételezi, megerősítve a korábbi tanulmányokban feltételezett többmagvú komplexek jelenlétét.

További méréseket végeztünk, hogy tanulmányozzuk a $Gluc^-$ hogyan képes koordinálódni a Nd(III)-hoz. Ehhez a $Gluc^-$ mellett a Gul^- és Gal^- ligandumokkal is végeztünk méréseket, mivel ezek egymás sztereoizomerjei (a Gal^- a $Gluc^-$ enantiomer párja, amelynek C4-es konfigurációja eltérő, a Gul^- esetében pedig a C2-es és C5-ös konfiguráció ellentétes a $Gluc^-$-éhoz képest). A koordinációs jellemzőket NMR és CD mérésekkel tanulmányoztuk. Bár ezek az eredmények azt mutatják, hogy a karboxilátcsoport alapvető szerepet játszik a komplexképződésben, a hidroxil- vagy alkoxidcsoportok további koordinációja pH ≥ 5 esetén nem zárható ki teljesen. Míg az NMR spektrumok egyértelműen arra utalnak, hogy a karboxilátcsoport játszik jelentős szerepet a koordinációban és a hidroxil funkciók koordinációja sem elhanyagolható, addig a CD eredmények azt igazolják, hogy semleges oldatokban a C4–OH koordinációja dominál a $Gluc^-$ és Gal^- esetében a többi hidroxilhoz képest. Az NMR és CD eredmények alapján azt feltételezzük, hogy a pH növekedésével a karboxilát funkció válik a fő kötőhellyé, és a Nd(III)-hoz koordinált vízmolekulák fokozatos deprotonálódáson mennek keresztül, ami végül egy olyan komplexet eredményez, ahol az Nd(III) vegyes hidroxidjait vagy maga az $Nd(OH)_3$-ot a koordinálódó $Gluc^-$ tartja oldatban.

A biner rendszerhez hasonlóan a Ca(II)–Nd(III)–$Gluc^-$ rendszerben lejátszódó egyensúlyok modelljét potenciometriás és spektrofotometriás adatok alapján állítottuk fel. Először csak a potenciometriás görbéket szimuláltuk a PSEQUAD segítségével, figyelembe

véve a mátrixrang analízis eredményeit, amelyek szerint legalább három terner komplex van a rendszerben. Ezután a potenciometriás adatok illesztésével kiválasztott néhány modellt a látható spektrumokkal együtt értékeltük. Bár néhány modell egyformán alkalmas volt a rendszer leírására, azt választottuk ki, amelyik kémiailag a legindokoltabb volt. Mivel a Ca(II):Nd(III) 3:1 egy arány a komplexek visszatérő jellemzője volt az értékelés során, a végső modell $Ca_3NdGlucH_{-6}^{2+}$, $Ca_3NdGluc_2H_{-7}^{0}$ and $Ca_3NdGluc_4H_{-4}^{+}$ komplexeket tartalmazza és az ezzel a modellel szimulált adatok jó összhangban vannak a kísérleti értékekkel. Az NMR és CD eredmények alátámasztják a terner komplexek képződését és a bináris komplexek esetében megfigyelt tendenciához hasonló folyamatok lejátszódására utalnak. A ^{13}C és ^{1}H NMR spektrumok hasonló tendenciára utalnak, mint ami a biner komplexek esetében volt megfigyelhető. ^{13}C and ^{1}H NMR eredmények alapján a legvalószínűbb $Gluc^-$ kötőhelyek a terner komplexekben a COO^-, C2–OH és a C3–OH funkciós csoportok.

A Ca(II)–$Gluc^-$, Nd(III)–$Gluc^-$ és Ca(II)–Nd(III)–$Gluc^-$ rendszerek meghatározott modelljeit felhasználtuk komplexképződés szimulációjához, a radioaktív hulladéktárolókra jellemző körülményeket feltételezve. Az eredmények azt mutatják, hogy a tipikusan alacsony koncentrációban jelenlévő $Gluc^-$ nem jelent nagy kockázati tényezőt, mivel mind a Nd(III)–$Gluc^-$, mind a Ca(II)–Nd(III)–$Gluc^-$ komplexek stabilitása elmarad a Ca(II)–$Gluc^-$ komplexekétől. Érdekes módon $Gluc^-$ hiányában a Ca(II) növeli a Nd(III) oldhatóságát, valószínűleg vegyes hidroxidok képződése révén. Összefoglalva, bár töményebb oldatokban kétmagvú Nd(III)–$Gluc^-$ komplexek és hárommagvú Ca(II)–Nd(III)–$Gluc^-$ komplexek képződnek, a radioaktív hulladéktárolókra jellemző mátrixokban ezek létezése nem jelent jelentős kockázatot.

8. References

(1) Seymour, D. J.; Sanz-Fernandez, M. V.; Daniel, J. B.; Martín-Tereso, J.; Doelman, J. Effects of Supplemental Calcium Gluconate Embedded in a Hydrogenated Fat Matrix on Lactation, Digestive, and Metabolic Variables in Dairy Cattle. *J. Dairy Sci.* **2021**, *104* (7), 7845–7855. https://doi.org/10.3168/jds.2020-20003.

(2) Faghfouri, A. H.; Khabbazi, A.; Baradaran, B.; Khajebishak, Y.; Baghbani, E.; Noorolyai, S.; Rahmani, S.; Seyyed Shoura, S. M.; Alipour, M.; Alipour, B. Immunomodulatory and Clinical Responses to Zinc Gluconate Supplementation in Patients with Behçet's Disease: A Double-Blind, Randomized Placebo-Controlled Clinical Trial. *Clin. Nutr.* **2022**, *41* (5), 1083–1092. https://doi.org/10.1016/j.clnu.2022.03.019.

(3) Haddadian-Khouzani, S.; Shahidi, S.; Askari, G.; Clark, C. C. T.; Rouhani, M. H. The Efficacy and Safety of Zinc Gluconate Supplementation on Quality of Life, Sleep Quality, and Serum Albumin in Hemodialysis Patients: A Randomized Clinical Trial. *Eur. J. Integr. Med.* **2022**, *55*, 102183. https://doi.org/10.1016/j.eujim.2022.102183.

(4) Abdelileh, M.; Manian, A. P.; Rhomberg, D.; Ben Ticha, M.; Meksi, N.; Aguiló-Aguayo, N.; Bechtold, T. Calcium-Iron-D-Gluconate Complexes for the Indirect Cathodic Reduction of Indigo in Denim Dyeing: A Greener Alternative to Non-Regenerable Chemicals. *J. Clean. Prod.* **2020**, *266*, 121753. https://doi.org/10.1016/j.jclepro.2020.121753.

(5) Ma, S.; Li, W.; Zhang, S.; Ge, D.; Yu, J.; Shen, X. Influence of Sodium Gluconate on the Performance and Hydration of Portland Cement. *Constr. Build. Mater.* **2015**, *91*, 138–144. https://doi.org/10.1016/j.conbuildmat.2015.05.068.

(6) dos Santos, T.; Pereira, C. I.; Gonçalves, R.; Salvini, V. R.; Zetterström, C.; Wöhrmeyer, C.; Parr, C.; Pandolfelli, V. C. Gluconate Action in the Hydration of Calcium Aluminate Cements: Theoretical Study, Processing of Aqueous Suspensions and Hydration Reactivation. *J. Eur. Ceram. Soc.* **2019**, *39* (8), 2748–2759. https://doi.org/10.1016/j.jeurceramsoc.2019.03.007.

(7) Mota, B.; Matschei, T.; Scrivener, K. Impact of Sodium Gluconate on White Cement-Slag Systems with Na_2SO_4. *Cem. Concr. Res.* **2019**, *122*, 59–71. https://doi.org/10.1016/j.cemconres.2019.04.008.

(8) Zou, D.; Zhang, Z.; Wang, D. Influence of Citric Acid and Sodium Gluconate on Hydration of Calcium Sulfoaluminate Cement at Various Temperatures. *Constr. Build. Mater.* **2020**, *263*, 120247. https://doi.org/10.1016/j.conbuildmat.2020.120247.

(9) Cañete-Rodríguez, A. M.; Santos-Dueñas, I. M.; Jiménez-Hornero, J. E.; Ehrenreich, A.; Liebl, W.; García-García, I. Gluconic Acid: Properties, Production Methods and Applications—An Excellent Opportunity for Agro-Industrial by-Products and Waste Bio-Valorization. *Process Biochem.* **2016**, *51* (12), 1891–1903. https://doi.org/10.1016/j.procbio.2016.08.028.

(10) Climent, M. J.; Corma, A.; Iborra, S. Converting Carbohydrates to Bulk Chemicals and Fine Chemicals over Heterogeneous Catalysts. *Green Chem.* **2011**, *13* (3), 520–540. https://doi.org/10.1039/C0GC00639D.

(11) Zhang, Q.; Wan, Z.; Yu, I. K. M.; Tsang, D. C. W. Sustainable Production of High-Value Gluconic Acid and Glucaric Acid through Oxidation of Biomass-Derived Glucose: A Critical Review. *J. Clean. Prod.* **2021**, *312*, 127745. https://doi.org/10.1016/j.jclepro.2021.127745.

(12) Aggarwal, N.; Aadil Yatoo, M.; Saravanamurugan, S. Chapter 2 - Glucose Oxidation to Carboxylic Products with Chemocatalysts. In *Biomass, Biofuels, Biochemicals*; Saravanamurugan, S., Pandey, A., Li, H., Riisager, A., Eds.; Biomass, Biofuels, Biochemicals; Elsevier, 2020; pp 33–60. https://doi.org/10.1016/B978-0-444-64307-0.00002-0.

(13) Zhang, X.; He, Y.; Lu, C.; Huang, Z. Effects of Sodium Gluconate on Early Hydration and Mortar Performance of Portland Cement-Calcium Aluminate Cement-Anhydrite Binder. *Constr. Build. Mater.* **2017**, *157*, 1065–1073. https://doi.org/10.1016/j.conbuildmat.2017.09.153.

(14) Neck, V.; Altmaier, M.; Rabung, T.; Lützenkirchen, J.; Fanghänel, T. Thermodynamics of Trivalent Actinides and Neodymium in NaCl, $MgCl_2$, and $CaCl_2$ Solutions: Solubility, Hydrolysis, and Ternary Ca-M(III)-OH Complexes. *Pure Appl. Chem.* **2009**, *81* (9), 1555–1568. https://doi.org/10.1351/PAC-CON-08-09-05.

(15) Bube, C.; Metz, V.; Bohnert, E.; Garbev, K.; Schild, D.; Kienzler, B. Long-Term Cement Corrosion in Chloride-Rich Solutions Relevant to Radioactive Waste Disposal in Rock Salt – Leaching Experiments and Thermodynamic Simulations. *Phys. Chem. Earth* **2013**, *Complete* (64), 87–94. https://doi.org/10.1016/j.pce.2012.11.001.

(16) Kutus, B.; Gaona, X.; Pallagi, A.; Pálinkó, I.; Altmaier, M.; Sipos, P. Recent Advances in the Aqueous Chemistry of the Calcium(II)-Gluconate System – Equilibria, Structure

and Composition of the Complexes Forming in Neutral and in Alkaline Solutions. *Coord. Chem. Rev.* **2020**, *417*, 213337. https://doi.org/10.1016/j.ccr.2020.213337.

(17) Mishelevich, A.; Apelblat, A. Solubilities of Magnesium-l-Ascorbate, Calcium-l-Ascorbate, Magnesium-l-Glutamate, Magnesium-d-Gluconate, Calcium-d-Gluconate, Calcium-d-Heptagluconate, l-Aspartic Acid, and 3-Nitrobenzoic Acid in Water. *J. Chem. Thermodyn.* **2008**, *40* (5), 897–900. https://doi.org/10.1016/j.jct.2007.12.006.

(18) Gajda, T.; Gyurcsik, B.; Jakusch, T.; Burger, K.; Henry, B.; Delpuech, J.-J. Coordination Chemistry of Polyhydroxy Acids: Role of the Hydroxy Groups. *Inorganica Chim. Acta* **1998**, *275–276*, 130–140. https://doi.org/10.1016/S0020-1693(97)06108-2.

(19) Escandar, G. M.; Sala, L. F.; Gonzalez Sierra, M. Complexes of Cobalt(II) and Nickel(II) with d-Aldonic and d-Alduronic Acids in Aqueous Solution. *Polyhedron* **1994**, *13* (1), 143–150. https://doi.org/10.1016/S0277-5387(00)86650-4.

(20) Roos, J. T. H.; Williams, D. R. Formation Constants for Citrate-, Folic Acid-, Gluconate- and Succinate-Proton, -Manganese(II), and -Zinc(II) Systems: Relevance to Absorption of Dietary Manganese, Zinc and Iron. *J. Inorg. Nucl. Chem.* **1977**, *39* (2), 367–369. https://doi.org/10.1016/0022-1902(77)80036-5.

(21) Tits, J.; Wieland, E.; Bradbury, M. H. The Effect of Isosaccharinic Acid and Gluconic Acid on the Retention of Eu(III), Am(III) and Th(IV) by Calcite. *Appl. Geochem.* **2005**, *20* (11), 2082–2096. https://doi.org/10.1016/j.apgeochem.2005.07.004.

(22) Felipe-Sotelo, M.; Hinchliff, J.; Field, L. P.; Milodowski, A. E.; Preedy, O.; Read, D. Retardation of Uranium and Thorium by a Cementitious Backfill Developed for Radioactive Waste Disposal. *Chemosphere* **2017**, *179*, 127–138. https://doi.org/10.1016/j.chemosphere.2017.03.109.

(23) Schramke, J. A.; Santillan, E. F. U.; Peake, R. T. Plutonium Oxidation States in the Waste Isolation Pilot Plant Repository. *Appl. Geochem.* **2020**, *116*, 104561. https://doi.org/10.1016/j.apgeochem.2020.104561.

(24) Kim, J. I.; Grambow, B. Geochemical Assessement of Actinide Isolation in a German Salt Repository Environment. *Eng. Geol.* **1999**, *52* (3), 221–230. https://doi.org/10.1016/S0013-7952(99)00007-1.

(25) Rai, D.; Kitamura, A. Thermodynamic Equilibrium Constants for Important Isosaccharinate Reactions: A Review. *J. Chem. Thermodyn.* **2017**, *114*, 135–143. https://doi.org/10.1016/j.jct.2017.02.012.

(26) Diakonov, I. I.; Ragnarsdottir, K. V.; Tagirov, B. R. Standard Thermodynamic Properties and Heat Capacity Equations of Rare Earth Hydroxides:: II. Ce(III)-, Pr-, Sm-, Eu(III)-, Gd-, Tb-, Dy-, Ho-, Er-, Tm-, Yb-, and Y-Hydroxides. Comparison of Thermochemical and Solubility Data. *Chem. Geol.* **1998**, *151* (1), 327–347. https://doi.org/10.1016/S0009-2541(98)00088-6.

(27) Panak, P. J.; Geist, A. Complexation and Extraction of Trivalent Actinides and Lanthanides by Triazinylpyridine N-Donor Ligands. *Chem. Rev.* **2013**, *113* (2), 1199–1236. https://doi.org/10.1021/cr3003399.

(28) Taga, T.; Kuroda, Y.; Ohashi, M. Structures of Lanthanoid Complexes of Glyceric Acid, Gluconic Acid, and Lactobionic Acid from the Lanthanoid-Induced 1H NMR Shifts: PH Dependence of the Lanthanoid-Substrate Equilibria. *Bull. Chem. Soc. Jpn.* **1978**, *51* (8), 2278–2282. https://doi.org/10.1246/bcsj.51.2278.

(29) Zhang, Z.; Bottenus, B.; Clark, S. B.; Tian, G.; Zanonato, P.; Rao, L. Complexation of Gluconic Acid with Nd(III) in Acidic Solutions: A Thermodynamic Study. *J. Alloys Compd.* **2007**, *444–445*, 470–476. https://doi.org/10.1016/j.jallcom.2007.01.034.

(30) Rojo, H.; Gaona, X.; Rabung, T.; Polly, R.; García-Gutiérrez, M.; Missana, T.; Altmaier, M. Complexation of Nd(III)/Cm(III) with Gluconate in Alkaline NaCl and $CaCl_2$ Solutions: Solubility, TRLFS and DFT Studies. *Appl. Geochem.* **2021**, *126*, 104864. https://doi.org/10.1016/j.apgeochem.2020.104864.

(31) Giroux, S.; Aury, S.; Henry, B.; Rubini, P. Complexation of Lanthanide(III) Ions with Polyhydroxy Carboxylic Acids in Aqueous Solutions. *Eur. J. Inorg. Chem.* **2002**, *2002* (5), 1162–1168. https://doi.org/10.1002/1099-0682(200205)2002:5<1162::AID-EJIC1162>3.0.CO;2-O.

(32) Pal, P.; Kumar, R.; Banerjee, S. Manufacture of Gluconic Acid: A Review towards Process Intensification for Green Production. *Chem. Eng. Process. Process Intensif.* **2016**, *104*, 160–171. https://doi.org/10.1016/j.cep.2016.03.009.

(33) IUPAC, I. Compendium of Chemical Terminology. *"Gold Book" Blackwell Sci. Publ. Oxf.* **1997**.

(34) Sartori, S. K.; Diaz, M. A. N.; Diaz-Muñoz, G. Lactones: Classification, Synthesis, Biological Activities, and Industrial Applications. *Tetrahedron* **2021**, *84*, 132001. https://doi.org/10.1016/j.tet.2021.132001.

(35) Şardan, M.; Sezer, S.; Günel, A.; Akkaya, M.; Tanyeli, C. Synthesis and Biological Evaluation of Optically Active Conjugated γ- and δ-Lactone Derivatives. *Bioorg. Med. Chem. Lett.* **2012**, *22* (18), 5814–5818. https://doi.org/10.1016/j.bmcl.2012.07.090.

(36) Zhang, Z.; Gibson, P.; Clark, S. B.; Tian, G.; Zanonato, P. L.; Rao, L. Lactonization and Protonation of Gluconic Acid: A Thermodynamic and Kinetic Study by Potentiometry, NMR and ESI-MS. *J. Solut. Chem.* **2007**, *36* (10), 1187–1200. https://doi.org/10.1007/s10953-007-9182-x.

(37) Mitchell, R. e.; Duke, F. r. Kinetics and Equilibrium Consents of the Gluconic Acid-Gluconolactone System*. *Ann. N. Y. Acad. Sci.* **1970**, *172* (7), 131–138. https://doi.org/10.1111/j.1749-6632.1970.tb34970.x.

(38) Jermyn, M. A. Studies on the Glucono-δ-Lactonase of Psudomonas Fluorescens. *Biochim. Biophys. Acta* **1960**, *37* (1), 78–92. https://doi.org/10.1016/0006-3002(60)90081-0.

(39) Shimahara, K.; Takahashi, T. An Infrared Spectrophotometric Study on the Interconversion and Hydrolysis of D-Glucono-γ- and -δ-Lactone in Deuterium Oxide. *Biochim. Biophys. Acta BBA - Gen. Subj.* **1970**, *201* (3), 410–415. https://doi.org/10.1016/0304-4165(70)90159-5.

(40) Williams, M. *The Merck Index - An Encyclopedia of Chemicals, Drugs, and Biologicals*; 2006.

(41) Riddick, J. A.; Bunger, W. B.; Sakano, T. K. *Techniques of Chemistry 4th Ed., Volume II. Organic Solvents*; 1985.

(42) Zubiaur, J.; Castaño, R.; Etxebarria, N.; Fernández, L. A.; Madariaga, J. M. Potentiometric Study of the Protonation and Distribution Equilibria of D-Gluconic-δ-Lactone Acid in Sodium Perchlorate Solutions at 25°C and Construction of a Thermodynamic Model. *Talanta* **1998**, *45* (5), 1007–1014. https://doi.org/10.1016/S0039-9140(97)00207-5.

(43) Bretti, C.; Cigala, R. M.; De Stefano, C.; Lando, G.; Sammartano, S. Acid–Base and Thermodynamic Properties of d-Gluconic Acid and Its Interaction with Sn^{2+} and Zn^{2+}. *J. Chem. Eng. Data* **2016**, *61* (6), 2040–2051. https://doi.org/10.1021/acs.jced.5b00993.

(44) Pocker, Y.; Green, Edmond. Hydrolysis of D-Glucono-δ-Lactone. I. General Acid-Base Catalysis, Solvent Deuterium Isotope Effects, and Transition State Characterization. *J. Am. Chem. Soc.* **1973**, *95* (1), 113–119. https://doi.org/10.1021/ja00782a019.

(45) Escandar, G. M.; Sala, L. F. Complexes of Cu(II) with D -Aldonic and D -Alduronic Acids in Aqueous Solution. *Can. J. Chem.* **1992**, *70* (7), 2053–2057. https://doi.org/10.1139/v92-259.

(46) Best, W. M.; Harrowfield, J. M.; Shand, T. M.; Stick, R. V. Aluminum(III) Coordination to Hydroxy Carboxylates: The Influence of Hydroxy Substituents Enabling Tridentate Binding. *Aust. J. Chem.* **1994**, *47* (11), 2023–2031. https://doi.org/10.1071/ch9942023.

(47) Giroux, S.; Rubini, P.; Henry, B.; Aury, S. Complexes of Praseodymium(III) with D-Gluconic Acid. *Polyhedron* **2000**, *19* (13), 1567–1574. https://doi.org/10.1016/S0277-5387(00)00422-8.

(48) Lakatos, A.; Kiss, T.; Bertani, R.; Venzo, A.; Di Marco, V. B. Complexes of Al(III) with d-Gluconic Acid. *Polyhedron* **2008**, *27* (1), 118–124. https://doi.org/10.1016/j.poly.2007.08.035.

(49) Pallagi, A.; Sebők, P.; Forgó, P.; Jakusch, T.; Pálinkó, I.; Sipos, P. Multinuclear NMR and Molecular Modelling Investigations on the Structure and Equilibria of Complexes That Form in Aqueous Solutions of Ca^{2+} and Gluconate. *Carbohydr. Res.* **2010**, *345* (13), 1856–1864. https://doi.org/10.1016/j.carres.2010.05.009.

(50) Coccioli, F.; Vicedomini, M. On the Protonation of Gluconate Ions and the Complex Formation with Lead(II) in Acid Solution. *J. Inorg. Nucl. Chem.* **1978**, *40* (12), 2103–2105. https://doi.org/10.1016/0022-1902(78)80215-2.

(51) Zhang, Z.; Clark, S. B.; Tian, G.; Zanonato, P. L.; Rao, L. Protonation of D-Gluconate and Its Complexation with Np(V) in Acidic to Nearly Neutral Solutions. *Radiochim. Acta* **2006**, *94* (9–11), 531–536. https://doi.org/10.1524/ract.2006.94.9-11.531.

(52) Pallagi, A.; Bajnóczi, É. G.; Canton, S. E.; Bolin, T.; Peintler, G.; Kutus, B.; Kele, Z.; Pálinkó, I.; Sipos, P. Multinuclear Complex Formation between Ca(II) and Gluconate Ions in Hyperalkaline Solutions. *Environ. Sci. Technol.* **2014**, *48* (12), 6604–6611. https://doi.org/10.1021/es501067w.

(53) Buckó, Á.; Kutus, B.; Peintler, G.; Pálinkó, I.; Sipos, P. Temperature Dependence of the Acid–Base and Ca^{2+}-Complexation Equilibria of d-Gluconate in Hyperalkaline Aqueous Solutions. *Polyhedron* **2019**, *158*, 117–124. https://doi.org/10.1016/j.poly.2018.10.034.

(54) Gyurcsik, B.; Nagy, L. Carbohydrates as Ligands: Coordination Equilibria and Structure of the Metal Complexes. *Coord. Chem. Rev.* **2000**, *203* (1), 81–149. https://doi.org/10.1016/S0010-8545(99)00183-6.

(55) van Duin, M.; Peters, J. A.; Kieboom, A. P. G.; van Bekkum, H. A General Coordination-Ionization Scheme for Polyhydroxy Carboxylic Acids in Water. *Recl. Trav. Chim. Pays-Bas* **1989**, *108* (2), 57–60. https://doi.org/10.1002/recl.19891080204.

(56) Sawyer, D. T. Metal-Gluconate Complexes. *Chem. Rev.* **1964**, *64* (6), 633–643. https://doi.org/10.1021/cr60232a003.

(57) Pecsok, R. L.; Juvet, R. S. Jr. The Gluconate Complexes. I. Copper Gluconate Complexes in Strongly Basic Media1. *J. Am. Chem. Soc.* **1955**, *77* (1), 202–206. https://doi.org/10.1021/ja01606a076.

(58) Escandar, G. M.; Salas Peregrin, J. M.; Gonzalez Sierra, M.; Martino, D.; Santoro, M.; Frutos, A. A.; Garci´a, S. I.; Labadie´, G.; Sala, L. F. Interaction of Divalent Metal Ions Withd-Gluconic Acid in the Solid Phase and Aqueous Solution. *Polyhedron* **1996**, *15* (13), 2251–2261. https://doi.org/10.1016/0277-5387(95)00478-5.

(59) Szorcsik, A.; Nagy, L.; Gyurcsik, B.; Vankó, Gy.; Krämer, R.; Vértes, A.; Yamaguchi, T.; Yoshida, K. Organotin(IV) Complexes of Polyhydroxyalkyl Carboxylic Acids and Some Related Ligands. *J. Radioanal. Nucl. Chem.* **2004**, *260* (3), 459–469. https://doi.org/10.1023/B:JRNC.0000028203.06936.39.

(60) Kobayashi, T.; Teshima, T.; Sasaki, T.; Kitamura, A. Thermodynamic Model for Zr Solubility in the Presence of Gluconic Acid and Isosaccharinic Acid. *J. Nucl. Sci. Technol.* **2017**, *54* (2), 233–241. https://doi.org/10.1080/00223131.2016.1255573.

(61) Daniele, P. G.; Foti, C.; Gianguzza, A.; Prenesti, E.; Sammartano, S. Weak Alkali and Alkaline Earth Metal Complexes of Low Molecular Weight Ligands in Aqueous Solution. *Coord. Chem. Rev.* **2008**, *252* (10), 1093–1107. https://doi.org/10.1016/j.ccr.2007.08.005.

(62) Yuan, T.; Wang, J.; Li, Z. Measurement and Modelling of Solubility for Calcium Sulfate Dihydrate and Calcium Hydroxide in NaOH/KOH Solutions. *Fluid Phase Equilibria* **2010**, *297* (1), 129–137. https://doi.org/10.1016/j.fluid.2010.06.012.

(63) Johnston, John.; Grove, Clinton. The Solubility of Calcium Hydroxyde in Aqueous Solutions. *J. Am. Chem. Soc.* **1931**, *53* (11), 3976–3991. https://doi.org/10.1021/ja01362a009.

(64) Seewald, J. S.; Seyfried, W. E. Experimental Determination of Portlandite Solubility in H_2O and Acetate Solutions at 100–350 °C and 500 Bars: Constraints on Calcium Hydroxide and Calcium Acetate Complex Stability. *Geochim. Cosmochim. Acta* **1991**, *55* (3), 659–669. https://doi.org/10.1016/0016-7037(91)90331-X.

(65) Angyal, S. J. Complexes of Metal Cations with Carbohydrates in Solution. In *Advances in Carbohydrate Chemistry and Biochemistry*; Tipson, R. S., Horton, D., Eds.; Academic Press, 1989; Vol. 47, pp 1–43. https://doi.org/10.1016/S0065-2318(08)60411-4.

(66) Cannan, R. K.; Kibrick, A. Complex Formation between Carboxylic Acids and Divalent Metal Cations. *J. Am. Chem. Soc.* **1938**, *60* (10), 2314–2320. https://doi.org/10.1021/ja01277a012.

(67) Schubert, J.; Lindenbaum, A. Stability of Alkaline Earth—Organic Acid Complexes Measured by Ion Exchange1. *J. Am. Chem. Soc.* **1952**, *74* (14), 3529–3532. https://doi.org/10.1021/ja01134a021.

(68) Haas, J. W. Complexation of Calcium and Copper with Carbohydrates: Implications for Seawater Speciation. *Mar. Chem.* **1986**, *19* (4), 299–304. https://doi.org/10.1016/0304-4203(86)90051-4.

(69) Van Loon, L. R.; Glaus, M. A.; Vercammen, K.; Ghosh, S.; Andersson, P. G.; Møller, J.; Senning, A.; Yao, X.-K.; Wang, H.-G.; Tuchagues, J.-P.; Ögren, M. Solubility Products of Calcium Isosaccharinate and Calcium Gluconate. *Acta Chem. Scand.* **1999**, *53*, 235–240. https://doi.org/10.3891/acta.chem.scand.53-0235.

(70) Bouzouaid, L.; Lothenbach, B.; Fernandez-Martinez, A.; Labbez, C. Portlandite Solubility and Ca2+ Activity in Presence of Gluconate and Hexitols. *Cem. Concr. Res.* **2021**, *149*, 106563. https://doi.org/10.1016/j.cemconres.2021.106563.

(71) Choppin, G. R.; Rizkalla, E. N. Chapter 128 Solution Chemistry of Actinides and Lanthanides. In *Handbook on the Physics and Chemistry of Rare Earths*; Lanthanides/Actinides: Chemistry; Elsevier, 1994; Vol. 18, pp 559–590. https://doi.org/10.1016/S0168-1273(05)80051-0.

(72) Chen, Y.-M.; Wang, C.-Z.; Wu, Q.-Y.; Lan, J.-H.; Chai, Z.-F.; Nie, C.-M.; Shi, W.-Q. Complexation of Trivalent Lanthanides and Actinides with Diethylenetriaminepentaacetic Acid: Theoretical Unraveling of Bond Covalency. *J. Mol. Liq.* **2020**, *299*, 112174. https://doi.org/10.1016/j.molliq.2019.112174.

(73) Paulenova, A. Physical and Chemical Properties of Actinides in Nuclear Fuel Reprocessing. *Adv. Sep. Tech. Nucl. Fuel Reprocess. Radioact. Waste Treat.* **2011**, 23–57. https://doi.org/10.1533/9780857092274.1.23.

(74) Kragten, J.; Decnop-Weever, L. G. Hydroxide Complexes of Lanthanides—VII: Neodymium(III) in Perchlorate Medium. *Talanta* **1984**, *31* (9), 731–733. https://doi.org/10.1016/0039-9140(84)80161-7.

(75) Orhanović, Z.; Pokrić, B.; Furedi, H.; Branica, M. Precipitation and Hydrolysis of Metallic Ions. III. Studies on the Solubility of Yttrium and Some Rare Earth Hydroxides. *Croat. Chem. Acta* **1966**, *38* (4), 269–276.

(76) Rao, L.; Rai, D.; Felmy, A. R. Solubility of $Nd(OH)_3(c)$ in 0.1 M NaCl Aqueous Solution at 25°C and 90°C. *Radiochim. Acta* **1996**, *72* (3), 151–156. https://doi.org/10.1524/ract.1996.72.3.151.

(77) Tobias, R. S.; Garrett, A. B. The Thermodynamic Properties of Neodymium Hydroxide Nd(OH)3, in Acid, Neutral and Alkaline Solutions at 25°; the Hydrolysis of the Neodymium and Praseodymium Ions, Nd^{3+}, Pr^{3+}. *J. Am. Chem. Soc.* **1958**, *80* (14), 3532–3537. https://doi.org/10.1021/ja01547a011.

(78) Furia, E.; Porto, R. 2-Hydroxybenzamide as a Ligand. Complex Formation with Dioxouranium(VI), Aluminum(III), Neodymium(III), and Nickel(II) Ions. *J. Chem. Eng. Data* **2008**, *53* (12), 2739–2745. https://doi.org/10.1021/je800142f.

(79) Ciavatta, L.; Porto, R.; Vasca, E. The Hydrolysis of the Neodymium(III) Ion, Nd^{3+}, in 3 M LiClO4 Medium at 60 °C. *Polyhedron* **1989**, *8* (22), 2701–2707. https://doi.org/10.1016/S0277-5387(00)80442-8.

(80) Rabung, T.; Altmaier, M.; Neck, V.; Fanghänel, T. A TRLFS Study of Cm(III) Hydroxide Complexes in Alkaline CaCl2 Solutions. *Radiochim. Acta* **2008**, *96* (9–11), 551–560. https://doi.org/10.1524/ract.2008.1536.

(81) Levitskaia, T. G.; Chen, Y.; Fulton, J. L.; Sinkov, S. I. Neodymium(III) Complexation by Amino-Carbohydrates via a Ligand-Controlled Hydrolysis Mechanism. *Chem. Commun.* **2011**, *47* (28), 8160–8162. https://doi.org/10.1039/C1CC11871D.

(82) Bentouhami, E.; Bouet, G. M.; Meullemeestre, J.; Vierling, F.; Khan, M. A. Physicochemical Study of the Hydrolysis of Rare-Earth Elements (III) and Thorium (IV). *Comptes Rendus Chim.* **2004**, *7* (5), 537–545. https://doi.org/10.1016/j.crci.2004.01.008.

(83) Orlov, Yu. F.; Maslov, E. I.; Belkina, E. I. Solubilities of Metal Hydroxides. *Russ. J. Inorg. Chem.* **2013**, *58* (11), 1306–1314. https://doi.org/10.1134/S0036023613110168.

(84) Zanonato, P.; Di Bernardo, P.; Bismondo, A.; Rao, L.; Choppin, G. R. Thermodynamic Studies of the Complexation between Neodymium and Acetate at Elevated Temperatures. *J. Solut. Chem.* **2001**, *30* (1), 1–18. https://doi.org/10.1023/A:1005227108686.

(85) Kostromina, N. A. Comparative Stabilities of the Gluconate Complexes of Rare Earth Metals. *Ukr. Khemichnii Zhurnal* **1960**, *26*, 299–304.

(86) Kostromina, N. A. Complex Compounds of Cerium, Neodymium, and Samarium with Gluconic Acid. *Zhurnal Neorganicheskoi Khimii* **1960**, *5*, 95–101.

(87) Kostromina, N. A. Study of Complex Formation of Lanthanum with Gluconic Acid by the Ion-Exchange Method. *Zhurnal Neorganicheskoi Khimii* **1962**, *7* (1559–1564), 651–657.

(88) Kostromina, N. A. Spectrophotometric and Potentiometric Determination of Acid Dissociation Constants of Some Rare Earth Element Gluconates. *Zhurnal Neorganicheskoi Khimii* **1966**, *11* (1), 381–385.

(89) Kutus, B.; Varga, N.; Peintler, G.; Lupan, A.; Attia, A. A. A.; Pálinkó, I.; Sipos, P. Formation of Mono- and Binuclear Neodymium(III)–Gluconate Complexes in Aqueous Solutions in the PH Range of 2–8. *Dalton Trans.* **2017**, *46* (18), 6049–6058. https://doi.org/10.1039/C7DT00909G.

(90) Warwick, P.; Evans, N.; Hall, T.; Vines, S. Stability Constants of Uranium(IV)-α-Isosaccharinic Acid and Gluconic Acid Complexes. *Radiochim. Acta* **2004**, *92* (12), 897–902. https://doi.org/10.1524/ract.92.12.897.55106.

(91) Tits, J.; Bradbury, M.; Eckert, P.; Schaible, A.; Wieland, E. *The Uptake of Eu(III) and Th(IV) by Calcite under Hyperalkaline Conditions: The Influence of Gluconic and Isosaccharinic Acid*; 1015–2636; Switzerland, 2002; p 106.

(92) McCarthy, J. F.; Czerwinski, K. R.; Sanford, W. E.; Jardine, P. M.; Marsh, J. D. Mobilization of Transuranic Radionuclides from Disposal Trenches by Natural Organic Matter. *J. Contam. Hydrol.* **1998**, *30* (1), 49–77. https://doi.org/10.1016/S0169-7722(97)00032-6.

(93) Zhang, W.; Wang, J. Leaching Performance of Uranium from the Cement Solidified Matrices Containing Spent Radioactive Organic Solvent. *Ann. Nucl. Energy* **2017**, *101*, 31–35. https://doi.org/10.1016/j.anucene.2016.09.055.

(94) Reinoso-Maset, E.; Worsfold, P. J.; Keith-Roach, M. J. The Effect of EDTA, NTA and Picolinic Acid on Th(IV) Mobility in a Ternary System with Natural Sand. *Environ. Pollut.* **2012**, *162*, 399–405. https://doi.org/10.1016/j.envpol.2011.11.038.

(95) Fralova, L.; Lefèvre, G.; Madé, B.; Marsac, R.; Thory, E.; Dagnelie, R. V. H. Effect of Organic Compounds on the Retention of Radionuclides in Clay Rocks: Mechanisms and Specificities of Eu(III), Th(IV), and U(VI). *Appl. Geochem.* **2021**, *127*, 104859. https://doi.org/10.1016/j.apgeochem.2020.104859.

(96) Keith-Roach, M. J. The Speciation, Stability, Solubility and Biodegradation of Organic Co-Contaminant Radionuclide Complexes: A Review. *Sci. Total Environ.* **2008**, *396* (1), 1–11. https://doi.org/10.1016/j.scitotenv.2008.02.030.

(97) Vercammen, K. Complexation of Calcium, Thorium and Europium by α-Isosaccharinic Acid under Alkaline Conditions. Doctoral Thesis, ETH Zurich, 2000. https://doi.org/10.3929/ethz-a-003861976.

(98) Chen, S.; Abdel-Magied, A. F.; Fu, L.; Jonsson, M.; Forsberg, K. Incorporation of Strontium and Europium in Crystals of α-Calcium Isosaccharinate. *J. Hazard. Mater.* **2019**, *364*, 309–316. https://doi.org/10.1016/j.jhazmat.2018.10.001.

(99) Tasi, A.; Gaona, X.; Fellhauer, D.; Böttle, M.; Rothe, J.; Dardenne, K.; Polly, R.; Grivé, M.; Colàs, E.; Bruno, J.; Källstrom, K.; Altmaier, M.; Geckeis, H. Thermodynamic Description of the Plutonium – α–d–Isosaccharinic Acid System II: Formation of Quaternary Ca(II)–Pu(IV)–OH–ISA Complexes. *Appl. Geochem.* **2018**, *98*, 351–366. https://doi.org/10.1016/j.apgeochem.2018.06.014.

(100) Peintler, G.; Kormányos, B.; Gyurcsik, B. PHCali, A Program for Accurate Calibration of PH-Metric Instruments, Versions 1.00–1.32, 2007.

(101) Zékány, L.; Nagypál, I.; Peintler, G. Manual for PSEQUAD, 2018.

(102) Peintler, G.; Nagypál, I.; Jancsó, A.; Epstein, I. R.; Kustin, K. Extracting Experimental Information from Large Matrixes. 1. A New Algorithm for the Application of Matrix Rank Analysis. *J. Phys. Chem. A* **1997**, *101* (43), 8013–8020. https://doi.org/10.1021/jp970136s.

(103) Wehrli, S. L.; Berry, G. T.; Palmieri, M.; Mazur, A.; Elsas, L.; Segal, S. Urinary Galactonate in Patients with Galactosemia: Quantitation by Nuclear Magnetic Resonance Spectroscopy. *Pediatr. Res.* **1997**, *42* (6), 855–861. https://doi.org/10.1203/00006450-199712000-00022.

(104) Kutus, B.; Peintler, G.; Buckó, Á.; Balla, Z.; Lupan, A.; Attia, A. A. A.; Pálinkó, I.; Sipos, P. The Acidity and Self-Catalyzed Lactonization of L-Gulonic Acid: Thermodynamic, Kinetic and Computational Study. *Carbohydr. Res.* **2018**, *467*, 14–22. https://doi.org/10.1016/j.carres.2018.07.006.

(105) Böszörményi, É.; Lado, J.; Dudás, C.; Kutus, B.; Szabados, M.; Varga, G.; Pálinkó, I.; Sipos, P. The Structure and Composition of Solid Complexes Comprising of Nd(III), Ca(II) and D-Gluconate Isolated from Solutions Relevant to Radioactive Waste Disposal. *Pure Appl. Chem.* **2020**, *92* (10), 1709–1715. https://doi.org/10.1515/pac-2019-1010.

(106) Papageorgiou, S. K.; Kouvelos, E. P.; Favvas, E. P.; Sapalidis, A. A.; Romanos, G. E.; Katsaros, F. K. Metal–Carboxylate Interactions in Metal–Alginate Complexes

Studied with FTIR Spectroscopy. *Carbohydr. Res.* **2010**, *345* (4), 469–473. https://doi.org/10.1016/j.carres.2009.12.010.

(107) Boyd, S. A.; Sommers, L. E.; Nelson, D. W. Copper(II) and Iron(III) Complexation by the Carboxylate Group of Humic Acid. *Soil Sci. Soc. Am. J.* **1981**, *45* (6), 1241–1242. https://doi.org/10.2136/sssaj1981.03615995004500060048x.

(108) Swamy, S. J.; Reddy, E. R.; Raju, D. N.; Jyothi, S. Synthesis and Spectral Investigations of Manganese(II), Cobalt(II), Nickel(II), Copper(II) and Zinc(II) Complexes of New Polydentate Ligands Containing a 1,8-Naphthyridine Moiety. *Molecules* **2006**, *11* (12), 1000–1008. https://doi.org/10.3390/11121000.

(109) Zeleňák, V.; Vargová, Z.; Györyová, K. Correlation of Infrared Spectra of Zinc(II) Carboxylates with Their Structures. *Spectrochim. Acta. A. Mol. Biomol. Spectrosc.* **2007**, *66* (2), 262–272. https://doi.org/10.1016/j.saa.2006.02.050.

(110) Wang, Z.-M.; van de Burgt, L. J.; Choppin, G. R. Spectroscopic Study of Lanthanide(III) Complexes with Aliphatic Dicarboxylic Acids. *Inorganica Chim. Acta* **2000**, *310* (2), 248–256. https://doi.org/10.1016/S0020-1693(00)00259-0.

(111) Mondry, A.; Starynowicz, P. Ten-Coordinate Neodymium(III) Complexes with Triethylenetetraaminehexaacetic Acid. *Eur. J. Inorg. Chem.* **2006**, *2006* (9), 1859–1867. https://doi.org/10.1002/ejic.200501023.

(112) Böszörményi, É.; Kása, Z.; Varga, G.; Kele, Z.; Kutus, B.; Peintler, G.; Pálinkó, I.; Sipos, P. Formation of Mono- and Binuclear Complexes of Nd^{3+} with d-Gluconate Ions in Hyperalkaline Solutions – Composition, Equilibria and Structure. *J. Mol. Liq.* **2022**, *346*, 117047. https://doi.org/10.1016/j.molliq.2021.117047.

(113) Mullica, D. F.; Wilson, G. A.; Lok, C. K. C. An Investigation of the Hypersensitive Pseudo-Quadrupole Transitions of Neodymium(III) Complexes and Their Induced NMR Chemical Shifts. *Inorganica Chim. Acta* **1989**, *156* (2), 159–161. https://doi.org/10.1016/S0020-1693(00)83490-8.

(114) Carper, W. R.; Coffin, D. B. NMR Studies of Paramagnetic Metal Ion Interactions with Gluconate and 1,5-Gluconolactone. *Inorganica Chim. Acta* **1990**, *167* (2), 261–264. https://doi.org/10.1016/S0020-1693(00)80507-1.

(115) Akhmetov, M. M.; Gumarov, G. G.; Petukhov, V. Yu.; Volkov, M. Yu. NMR Study of Sodium Gluconate Solutions. *J. Mol. Struct.* **2019**, *1193*, 373–377. https://doi.org/10.1016/j.molstruc.2019.05.061.

(116) Böszörményi, É.; Dömötör, O.; Kutus, B.; Varga, G.; Peintler, G.; Sipos, P. Coordination Motifs of Binary Neodymium(III) D-Gluconate, D-Galactonate and L-

Gulonate Complexes and the Transition from Inner- to Outer-Sphere Coordination in Neutral to Strongly Alkaline Medium. *J. Mol. Struct.* **2022**, *1261*, 132894. https://doi.org/10.1016/j.molstruc.2022.132894.

(117) Buckó, Á.; Kutus, B.; Peintler, G.; Kele, Z.; Pálinkó, I.; Sipos, P. Stability and Structural Aspects of Complexes Forming between Aluminum(III) and D-Heptagluconate in Acidic to Strongly Alkaline Media: An Unexpected Diversity. *J. Mol. Liq.* **2020**, *314*, 113645. https://doi.org/10.1016/j.molliq.2020.113645.

(118) Sipos, P.; Berkesi, O.; Tombácz, E.; St. Pierre, T. G.; Webb, J. Formation of Spherical Iron(III) Oxyhydroxide Nanoparticles Sterically Stabilized by Chitosan in Aqueous Solutions. *J. Inorg. Biochem.* **2003**, *95* (1), 55–63. https://doi.org/10.1016/S0162-0134(03)00068-0.

(119) Kutus, B.; Dudás, C.; Orbán, E.; Lupan, A.; Attia, A. A. A.; Pálinkó, I.; Sipos, P.; Peintler, G. Magnesium(II) D-Gluconate Complexes Relevant to Radioactive Waste Disposals: Metal-Ion-Induced Ligand Deprotonation or Ligand-Promoted Metal-Ion Hydrolysis? *Inorg. Chem.* **2019**, *58* (10), 6832–6844. https://doi.org/10.1021/acs.inorgchem.9b00289.

(120) Bünzli, J.-C. G.; Eliseeva, S. V. Basics of Lanthanide Photophysics. In *Lanthanide Luminescence: Photophysical, Analytical and Biological Aspects*; Hänninen, P., Härmä, H., Eds.; Springer Series on Fluorescence; Springer: Berlin, Heidelberg, 2011; pp 1–45. https://doi.org/10.1007/4243_2010_3.

(121) Wood, S. A.; Wesolowski, D. J.; Palmer, D. A. The Aqueous Geochemistry of the Rare Earth Elements: IX. A Potentiometric Study of Nd^{3+} Complexation with Acetate in 0.1 Molal NaCl Solution from 25°C to 225°C. *Chem. Geol.* **2000**, *167* (1), 231–253. https://doi.org/10.1016/S0009-2541(99)00210-7.

(122) Deelstra, H.; Verbeek, F. The Determination of the Stability Constants of the Lanthanide α-Hydroxyisobutyrate and Lactate Complexes by Potentiometric Titration. *Anal. Chim. Acta* **1964**, *31*, 251–257. https://doi.org/10.1016/S0003-2670(00)88816-9.

(123) Tajmir-Riahi, H. A. Carbohydrate Complexes with Alkaline Earth Metal Ions. Interaction of D-Glucono-1,5-Lactone with the Mg(II), Ca(II), Sr(II), and Ba(II) Cations in the Crystalline Solid and Aqueous Solution. *J. Inorg. Biochem.* **1990**, *39* (1), 33–41. https://doi.org/10.1016/0162-0134(90)80013-N.

(124) Katzin, L. I. Absorption Spectral and Circular Dichroic Studies of Complexes of Hydroxy Acids with Praeseodymium Ion. *Inorg. Chem.* **1968**, *7* (6), 1183–1191. https://doi.org/10.1021/ic50064a027.

9. Acknowledgement

I would like to express my gratitude to Prof. Dr. Pál Sipos for offering an oppurtinity to work in the Material and Solution Structure Research Group (MASOST) and also thank him for his patience and guidence during the process of writing my dissertation. I am also thankful for Dr. Gábor Peintler, who provided tremendous help for computational calculations. I am grateful for the help of all senior and junior members of our research group, who aided me many times. I would like to thank especially Dr. Kutus Bence for his advice and supervision of my dissertation. Special thanks go to Ilona Halasiné-Varga for her help in the laboratory. Last but not least, I express my gratitude to my mother and sister for encouriging me in pursuing a career in chemistry and for my boyfriend for his support during my studies.

I would like to commemorate Prof. Dr. István Pálinkó who aided my progress among many other students but sadly can not witness the result of his efforts.